NASA Technical Memorandum 107300

Structures Division 1995 Annual Report

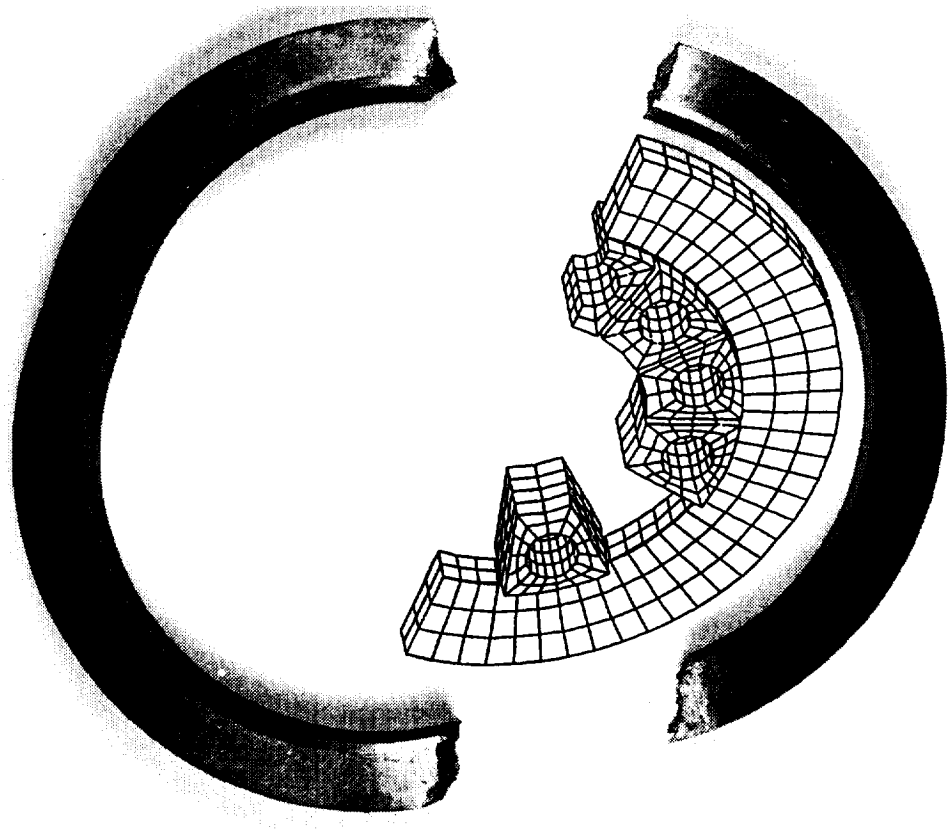

National Aeronautics and
Space Administration

July 1997
Lewis Research Center

Introduction

The 1995 Annual Report of the Structures Division reflects the work areas performed by the Division staff during the 1995 calendar year. This publication covers 54 separate topics. Its purpose is to give a brief, but comprehensive review of the Division's technical accomplishments. As with the reports for the previous years, the report is organized topically. The descriptions of the research reflect work that has been reported in the open literature during the year. A bibliography containing 132 citations is provided to the reader.

The Structures Division comprises a staff of approximately 68 engineers and scientists plus administrative and support personnel. The work areas comprise but are not limited to composite mechanisms, fatigue, fracture, and dynamics with emphasis on life and reliability. Additional work in future years will include mechanical component technologies and acoustics. The Division works cooperatively with both industry and universities to develop the technology necessary for state-of-the-art advancement in aeronautical and space propulsion systems. In the future, propulsion systems will need to be lighter, to operate at higher temperatures and to be more reliable in order to achieve higher performance. Achieving these goals is complex and challenging. If you need additional information, please do not hesitate to contact me or the appropriate Division staff contact provided in this publication.

L. James Kiraly

Acting Chief, Structures Division

Contents

Structures Division

Structural Mechanics

Fatigue and Fracture

Structural Dynamics

Structural Integrity

Structures Division

Soft Computing Methods in Design of Superalloys

In this research, done under contract with the University of Toledo in Ohio, neural networks and genetic algorithms were used to design superalloys. The cyclic oxidation attack parameter Ka was modeled using a backpropagation neural network as a function of the superalloy chemistry and the test temperature. This model was then used in unison with a genetic algorithm to obtain an optimized superalloy composition, which resulted in low values of Ka. The key feature of our approach was employing the neural network to model the material properties and genetic algorithms that were used for optimizing the objective function values provided as the outputs of the neural network.

Lewis contact: Laszlo Berke (216) 433–5648

Fuzzy and Neural Net Approach to Tolerance Level Uncertainty

Under a small disadvantaged business (SDB) 8(a) contract, the practical special case of only tolerance level input uncertainty was examined for structural analysis and optimization. Also assumed was that precise information concerning the distribution of uncertainty within a small tolerance level was not known. One can view such a case through fuzzy techniques and its definitions of "membership functions" as an alternative to detailed probability distributions, with accuracy depending on the quality of available statistical data. The simplest case is to be concerned only with the possible tolerance range defined by minimum and maximum input values and to examine methods for their efficient mapping into possible minimum and maximum output values. The obvious approach is to perform analyses of all combinations of such input values, but that is efficient for only a very small number of variables. One can define various membership functions between the extremes and perform conventional Monte Carlo experiments capturing the extreme tails produced. The neural network models allow a very large number of samplings. As is well known, the tails increase asymptotically towards the extreme values obtainable by exhaustive combinatorial exploration. This operation is made efficient by first generating a fast-executing neural network model for the ranges in question. One may also surmise that the extreme output values do not belong to some combination of extreme input values but that some intermediate input values are also involved in producing them. When a fast-executing neural network model is available, optimization iterations can be run to minimize and maximize output values. Monte Carlo experimentation also can capture such cases. Finally, one can apply "interval equation" techniques of fuzzy sets generated by considering "alpha cuts" of input membership functions, again just the extreme values in the simplest case. These equations can be solved with about twice the computations required by a conventional solution and can produce extreme values that closely match the values generated by the above methods but only for small (tolerance) differences between minimum and maximum input values. For large ranges, over a few percent of mean values, this approach becomes unreliable. Because of the computational advantage, this approach warrants further development to achieve accuracy for larger ranges of uncertainty. This project is nearing completion.

Lewis contact: Laszlo Berke (216) 433–5648

Effect of Cyclic Thermal Loads on Fatigue Reliability in Polymer Matrix Composites

Under the NASA High Speed Research (HSR) Program, technological solutions that will ensure the economic viability and environmental compatibility of a future High Speed Civil Transport (HSCT) aircraft are currently being sought. Concepts for both lighter airframe primary structures and engine structural components are being investigated. It is envisioned that such objectives can be achieved through the use of high-temperature composites and other conventional lighter weight alloys. One of the prime issues for these structural components is assured long-term behavior with a specified reliability.

An investigation was conducted to develop a computational simulation methodology that would predict the fatigue life (fig. 1), reliability, and probabilistic long-term behavior of polymer matrix composites (PMC's). A unified time-, stress-, and load-dependent MultiFactor Interaction Equation (MFIE) model developed at the NASA Lewis Research Center was used to simulate the long-term behavior of polymer matrix composites.

Although the methodology can be applied to other types of PMC's, a typical composite system consisting of graphite fibers in epoxy matrix was chosen to illustrate the application of the methodology. The layup of the composite system was chosen to be $[0/\pm45/90]_s$. The cumulative probability distribution functions (CDF's) for the fatigue life cycles were computed for different thermal cycle rates and constant applied stress. The

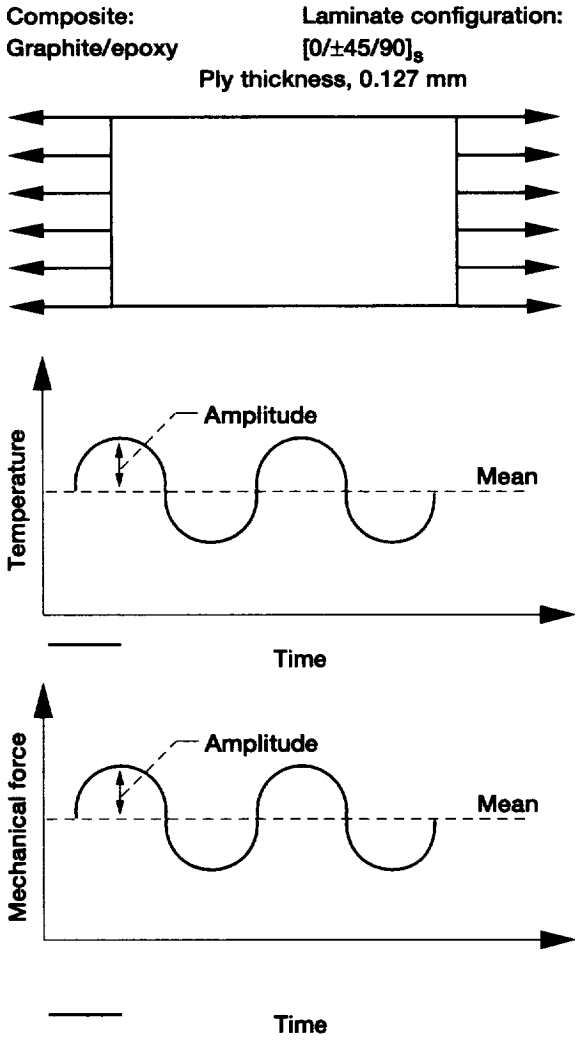

Figure 1.—Thermomechanical cyclic load.

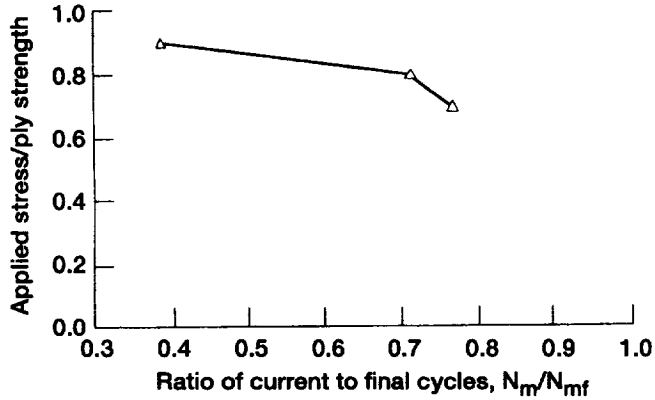

Figure 2.—Fatigue life variation resulting from thermomechanical cyclic load. Mean applied load, 50 percent of ply strength; mean temperature, 65.5 °C; cyclic temperature 51.7 °C.

laminate strength was evaluated on the basis of the first ply failure criteria (hereinafter referred to as laminate strength). First ply failure criteria assumes that the laminate has failed when any stress component in a ply exceeds its respective allowable. Using these CDF's, a fatigue life cycle curve for a reliability of 0.999 was obtained (fig. 2). The results show that at low mechanical cyclic loads and low thermal cyclic amplitudes, the fatigue life for 0.999 reliability is most sensitive to matrix compressive strength, matrix modulus, thermal expansion coefficient, and ply thickness. However, at high mechanical cyclic loads and high thermal cyclic amplitudes, the fatigue life at 0.999 reliability is more sensitive to the shear strength of the matrix, the longitudinal fiber modulus, the matrix modulus, and the ply thickness.

Lewis contact: Christos C. Chamis, (216) 433–3252

T/BEST: Technology Benefit Estimator Select Features and Applications

Progress in aerospace propulsion necessitated an assessment of the benefits to be gained by interfacing advanced technologies. These benefits will be used as guidelines to identify and prioritize high-payoff research areas, to manage research with limited resources, and to demonstrate the link between advanced and basic concepts. An effort was undertaken at the NASA Lewis Research Center to develop a formal computational method, T/BEST (Technology Benefit Estimator), to assess advanced

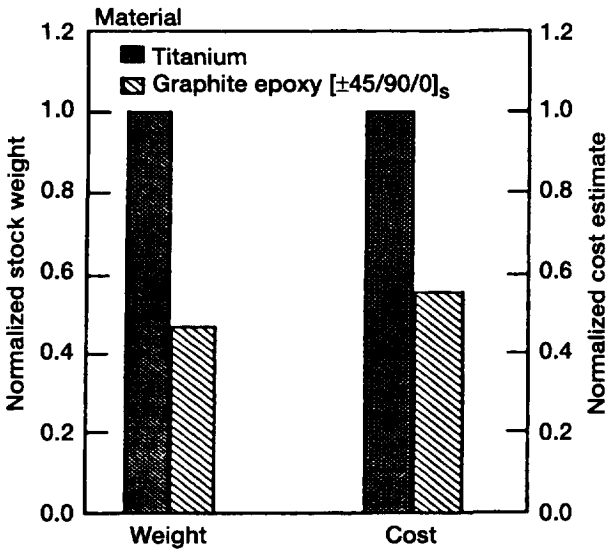

Figure 1.—Maurer stock weight and cost estimation for manufacturing a fan blade.

aerospace technologies and to credibly communicate the benefits of research. Fibrous composites are ideal for structural applications such as high-performance aircraft engine blades where the ratios of high strength to weight and stiffness to weight are required. These factors, along with the flexibility to select the composite system and layup and to favorably orient fiber directions, reduce the displacements and stresses caused by large rotational speeds in aircraft engines.

T/BEST can readily evaluate the benefits of utilizing composites to construct fan and compressor blades and to update the blade geometry to maximize rotor efficiency and the blade manufacturing process. Figure 1 shows the cost benefits of using graphite/epoxy composites instead of titanium in the manufacturing of state-of-the-art blades. The cost required to manufacture composite fan blades is estimated using T/BEST (fig. 2).

Lewis contact: Christos C. Chamis, (216) 433–3252

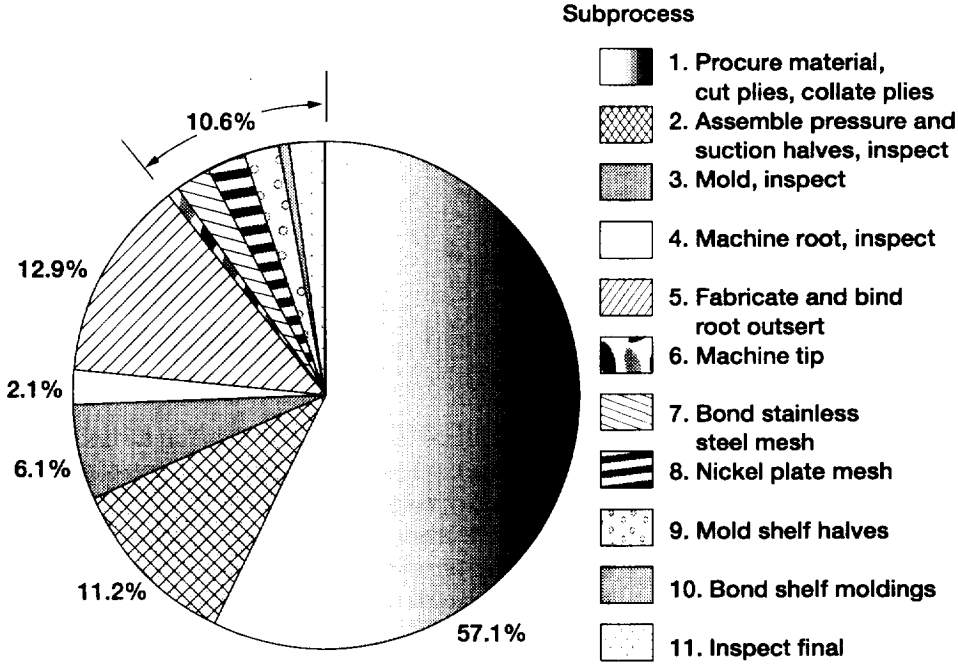

Figure 2.—Cost of manufacturing process of resin matrix composite blades.

Probabilistic Thermomechanical Fatigue of Polymer Matrix Composites

Traditional computational approaches for life and long-term behavior rely on empirical data and are not generic or unique. Also, those approaches are not easy to implement in the design procedure in an effective integrated manner. The focus of ongoing research at the NASA Lewis Research Center has been to develop advanced integrated computational methods and related computer codes to perform a complete reliability-based assessment of composite structures. These methods account for uncertainties in all the constituent properties, fabrication process variables, and loads to predict probabilistic micro, ply, laminate and structural responses. These methods have already been implemented in the Integrated Probabilistic Assessment of Composite Structures (IPACS) computer code. The main objective of the present evaluation was to illustrate the effectiveness of IPACS to predict the long-term behavior of composites under combined mechanical and thermal cyclic loading conditions. A unified time-, stress-, and load-dependent MultiFactor Interaction Equation (MFIE) model developed at the NASA Lewis Research Center was used to simulate the long-term behavior of polymer matrix composites. The MFIE model evaluates the magnitude of the degradation and the properties of constituent materials at every cycle step at that temperature which, in turn, is used for micromechanics and laminate analysis. Possible impending failure modes are checked at every cycle step. The deterministic part of the methodology has been implemented in the in-house computer code ICAN (Integrated Composite Analyzer). A methodology to compute the fatigue life for different ratios of applied stress to the laminate strength based on first ply failure criteria combined with thermal cyclic loads was demonstrated. Degradation effects due to long-term environmental exposure and thermomechanical cyclic loads were considered in the simulation process.

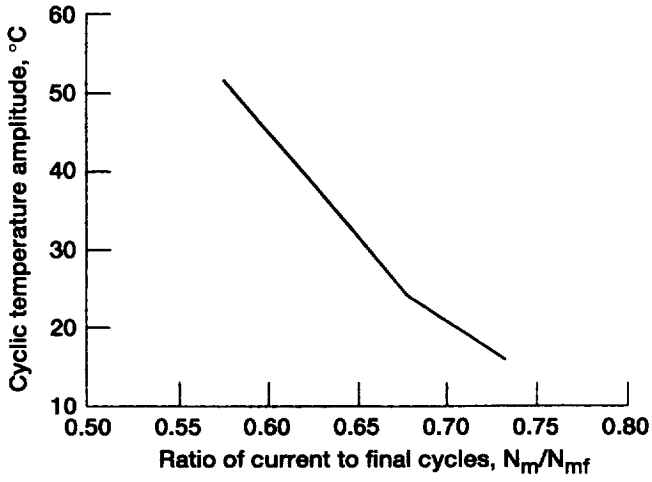

Figure 1.—Fatigue life variation for 0.999-reliability of $[0/\pm45/90]_s$ graphite/epoxy laminate. Ply thickness, 0.127 mm under thermal cyclic load; mean mechanical load = 0.5×static strength.

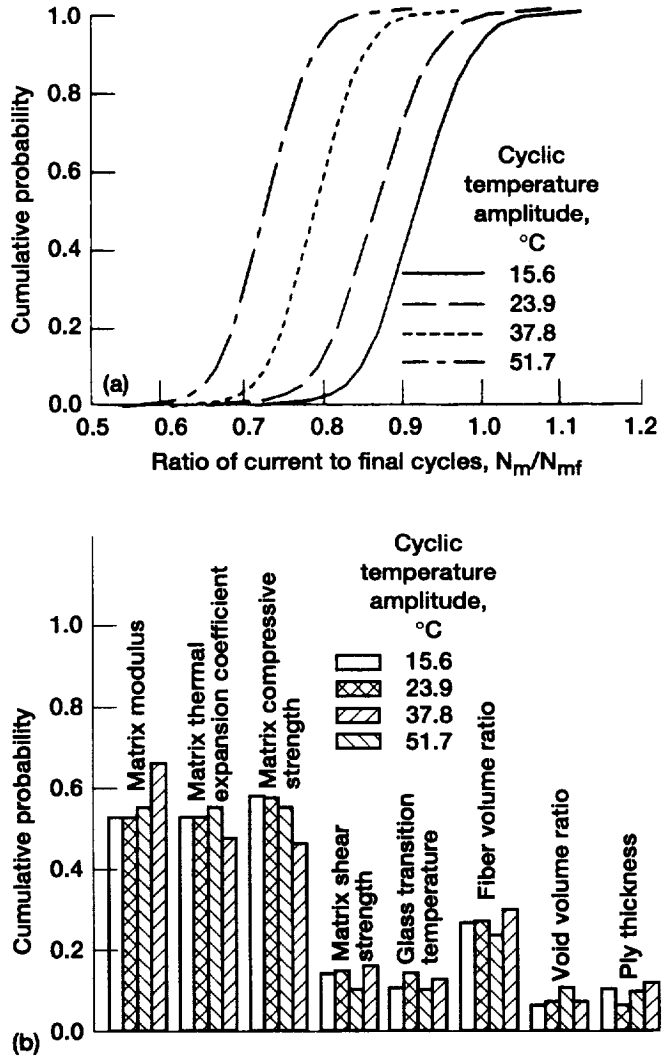

Figure 2.—Cumulative distribution function for and sensitivity of fatigue life for 0.999-reliability of $[0/\pm45/90]_s$ graphite/epoxy laminate. Ply thickness, 0.127 mm under thermal cyclic load; mean mechanical load = 0.5×static strength. (a) Cumulative distribution function. (b) Sensitivity of fatique life for 0.999-reliability.

Application of IPACS was illustrated by considering a $[0/\pm45/90]_s$ graphite fiber/epoxy matrix composite. The fatigue life cycles were computed for different thermal cycles and for different ratios r of the magnitude of applied stress cycles to the laminate strength cycles based on first ply failure criteria. These curves can be used to assess the fatigue life of a component subjected to mechanical cyclic loading for a given reliability (fig. 1). Cumulative probability distribution functions for mechanical fatigue due to different cyclic stress magnitudes and the respective sensitivity factors are shown in figure 2. Note that results similar to those in figures 1 and 2 can also be developed for different stress ratios but with constant temperatures.

Lewis contact: Christos C. Chamis, (216) 433–3252

Prestraining Effects on Fatigue Life

It is generally acknowledged that the fatigue life of metals is influenced by prior prestraining. What is not well understood is the nature and extent of the influence. One school of thought views prior deformation as being beneficial because it imparts cold working that invariably raises the yield and ultimate tensile strengths of metals. These in turn can raise the fatigue strength. This view arises from prior deformation being imposed as a result of rolling, swaging, forging, and other mechanical metal-working operations wherein the applied compressive deformation is not aligned with the direction of subsequent fatigue loading. The opposing view that prior deformation is damaging to ensuing fatigue resistance has its origins in deformations aligned with the direction of fatigue loading. Losses of ductility, flattening of voids into sharp discontinuities with higher stress concentration factors, and actual initiation of microcracks are among the mechanisms for imparting damage. An experimental program was conducted to study the effects of both tensile and compressive axial prestrains on the subsequent fatigue life of the nickel-base alloy Inconel 718. All testing was at room temperature. Completely reversed, axial strain-controlled testing was employed. Baseline tests with zero prestrain were conducted over the range of 103 to 106 cycles to failure. Additional specimens were prestrained 2, 5, and 10 percent in tension and 2 percent in compression prior to conducting fatigue tests at the baseline loading conditions. No beneficial effects were observed, although compressive prestrains were less detrimental than tensile. The general trend of results was for tensile prestrain to cause the greatest life losses at the highest lives (fig. 1). Three fatigue damage lifing models were used to predict the experimental results: the Linear Damage Rule, the Linear Strain/Life Fraction Rule, and the Nonlinear Damage Curve Approach. The

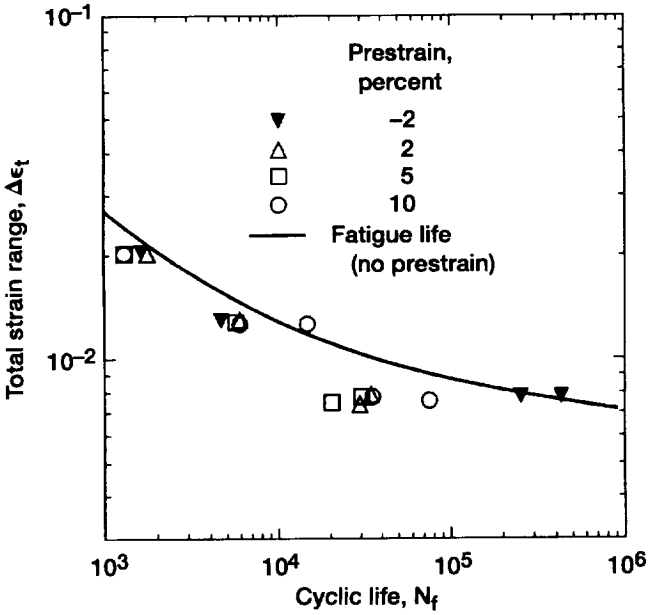

Figure 1.—Fatigue results for prestrained specimens compared with baseline data for Inconel 718 superalloy.

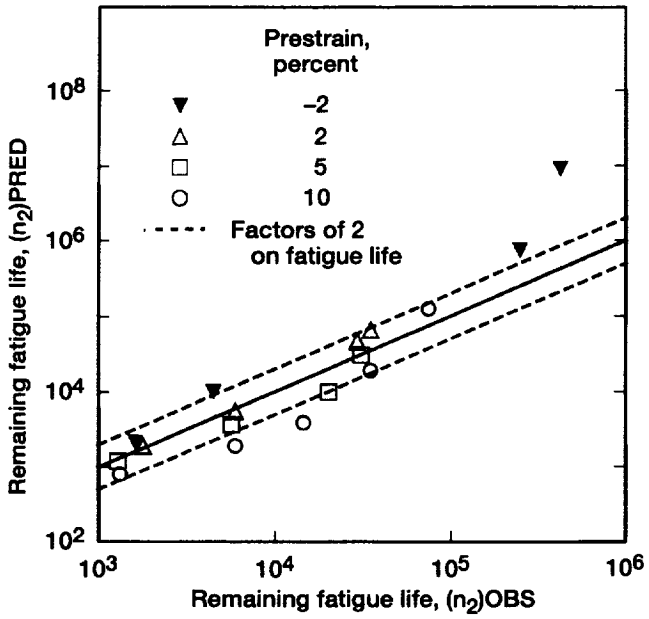

Figure 2.—Remaining fatigue life predicted by nonlinear Damage Curve Approach.

Smith Watson-Topper parameter was used to estimate the effects of any fatigue mean stresses present. The most accurate predictions of fatigue life following prestrain were provided by the Nonlinear Damage Curve Approach (fig. 2).

Lewis contacts: Sreeramesh Kalluri, (216) 433–6727 and Gary R. Halford, (216) 433–3265

Structurally Compliant Rocket Engine Combustion Chamber

A new, structurally compliant design for a rocket engine combustion chamber was validated through a series of analyses and experiments. Subscale, tubular channel, rocket nozzle chambers were cyclically tested and analytically evaluated. Cyclic lives were determined to have a potential for a tenfold increase over those of rectangular channel designs, the current state of the art. Greater structural compliance in the circumferential direction gave rise to lower thermal strains during hot firing, resulting in lower thermal strain ratcheting and longer predicted fatigue lives (fig. 1). Thermal, structural, and durability analyses of the combustion-chamber design, involving cyclic

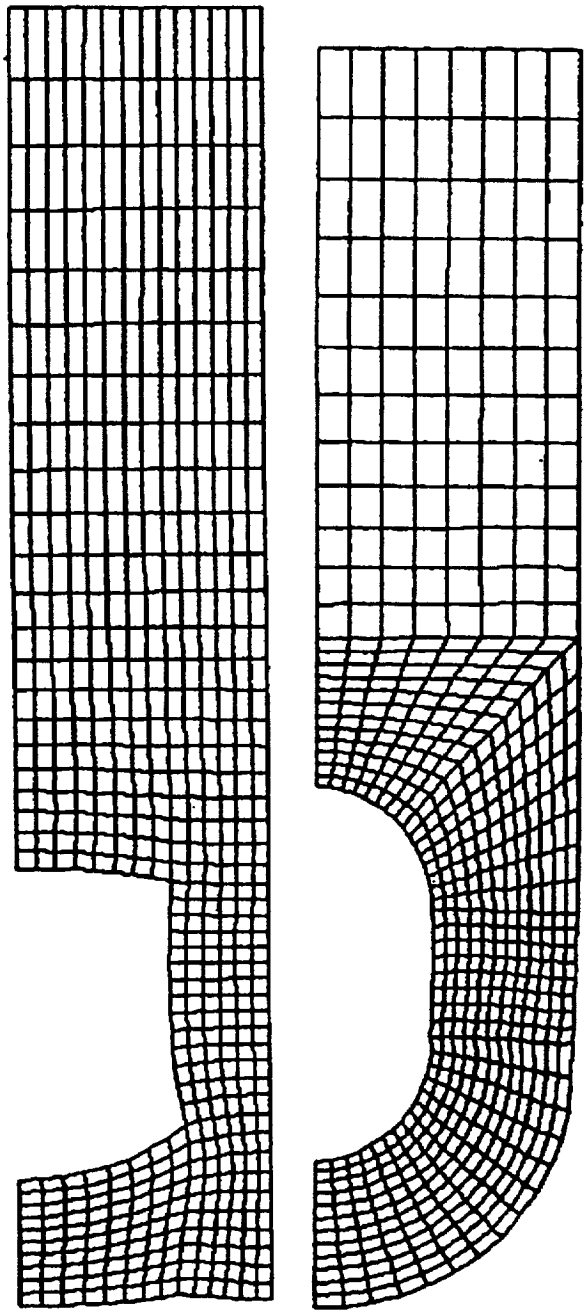

Figure 1.—Computed deformed shapes of conventional rectangular and compliant tubular channels after first five successive cycles of hot firing (1000X).

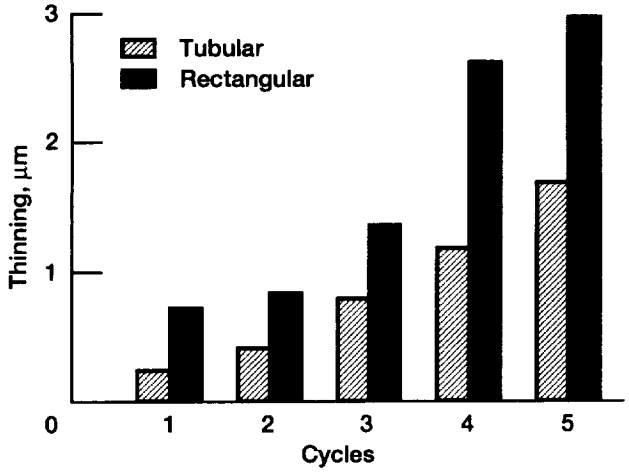

Figure 2.—Calculated thinning of hot-gas wall of conventional rectangular channel and compliant tubular channel configurations.

temperatures, strains, and low-cycle fatigue lives, have corroborated the experimental observations (fig. 2).

Lewis contacts: Robert Jankovsky, (216) 433–7515, Vinod Arya, (216) 433–2816, and Gary R. Halford, (216) 433–3265

Kinetics of Cyclic Oxidation and Cracking and Finite Element Analysis of MA956 and Sapphire/MA956 Composite System

Sapphire fiber-reinforced MA956 composites hold promise for significant weight savings and increased high-temperature structural capability compared with unreinforced MA956. As part of an overall assessment of the high-temperature characteristics of this material system, cyclic oxidation behavior was studied at 1093 and 1204 °C. Initially, both sets of coupons exhibited parabolic oxidation kinetics (fig. 1). Later, monolithic MA956 exhibited spallation and a linear weight loss whereas the composite showed a linear weight gain without spallation. Weight loss of the monolithic MA956 resulted from the linking of a multiplicity of

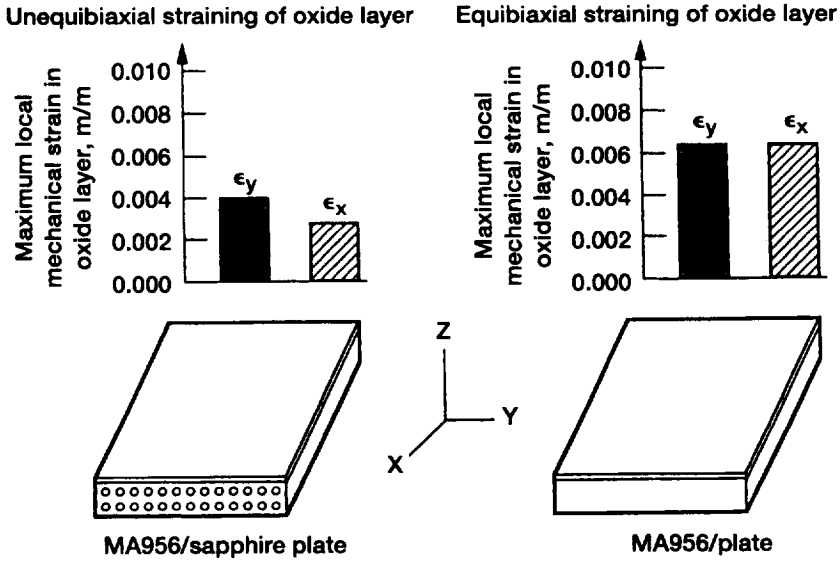

Figure 1.—Maximum mechanical strains in oxide layer of composite (MA956/sapphire) and matrix (MA956) plate (continuum analysis).

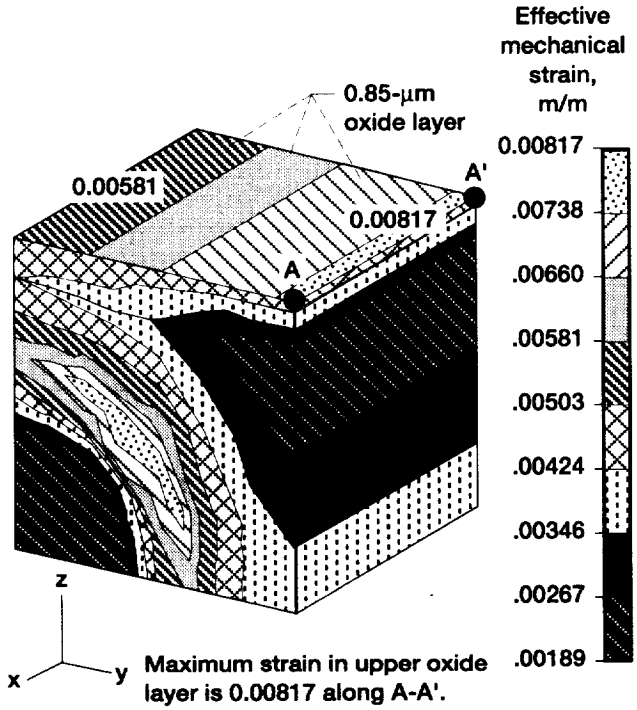

Figure 2.—Effective mechanical strain distribution in MA956/sapphire composite unit cell (micromechanical analysis).

randomly oriented and closely spaced surface cracks that facilitated ready spallation. By contrast, cracking of the composite's oxide layer was nonintersecting and was aligned nominally parallel with the orientation of the subsurface reinforcing fibers. The oxidative lifetime of monolithic MA956 was projected from the observed oxidation kinetics. Linear-elastic, finite element continuum, and micromechanics analyses were performed on coupons of the monolithic and composite materials. Results of the analyses qualitatively agreed well with the observed oxide cracking and spallation behavior of both the MA956 and the sapphire/MA956 composite coupons (fig. 2).

Lewis contacts: Gary R. Halford, (216) 433–3265 and Vinod K. Arya, (216) 433–2816

Large-Displacement Structural Durability Analyses of Simple Bend Specimen Emulating Rocket Nozzle Liners

Large-displacement elastic and elastic-plastic finite element stress-strain analyses using an updated Lagrangian formulation were performed on an OFHC (oxygen-free high-conductivity) copper plate specimen. The plate specimen is intended for low-cost experiments that emulate the most important thermomechanical loading and failure modes of a more complex rocket nozzle. The plate, which is loaded in bending at 593 °C, contains a centrally located and internally pressurized channel (fig. 1). The cyclic crack initiation lives were estimated using the results from the analyses and isothermal strain-controlled low-cycle fatigue data for OFHC copper. The table presents a comparison of the predicted and experimental cyclic lives and shows that an elastic analysis predicts by a factor greater than 4 a longer cyclic life than that observed in experiments. The results from elastic-plastic analysis for the plate bend specimen, however, predicted a cyclic life in close agreement with that of experiment, thus justifying the need for the more rigorous stress-strain analysis.

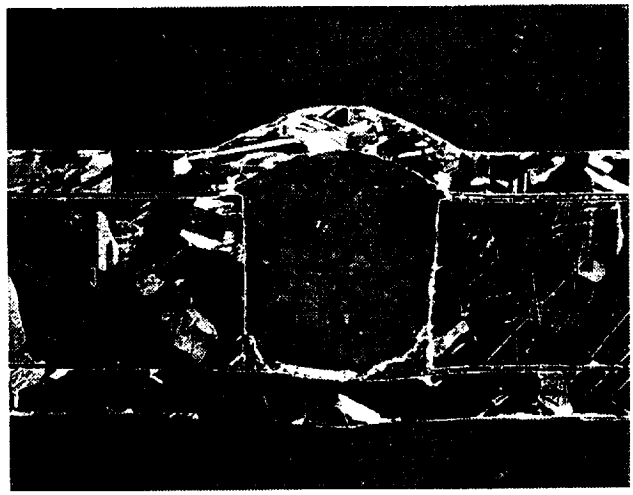

Figure 1.—Deformed channel of plate specimen emulating the "bulging" effect.

EXPERIMENTAL AND PREDICTED CYCLIC LIVES OF PLATE BEND SPECIMEN

Analysis	Maximum total effective strain range, percent	Life, cycles
Large elastic	1.1	500
Large elastic-plastic	1.7	190
Experiment	- - -	109

Lewis contacts: Gary R. Halford, (216) 433–3265 and Vinod K. Arya, (216) 433–2816

Effect of Hoop Stress on Ball Bearing Life

To prevent motion of the inner race of a ball or roller bearing around a shaft, designers have been specifying extremely tight interference fits between the inner race and the shaft when it is not practical to provide a keyway of locknut arrangement. The interference fit is usually based on the anticipated growth of the shaft and the bearing under the most severe operating conditions. These conditions sometimes exist only for short periods in the machine's operating cycle. Nevertheless, it is an extremely important design consideration for both safety of operation and maintainability. In recent years, some engineers have noticed that bearings with tighter than usual press (or interference) fits may have shorter field lives than anticipated or calculated. The failure mechanism is usually classical rolling-element (subsurface) fatigue.

A finite element analysis (FEA) of a generic, dimensionally normalized inner race of an angular-contact ball bearing was performed under varying conditions of speed and press (or interference) fit of the inner-race bore on a journal. The FEA results at the ball-race contact were used to derive an equation from which was obtained the radius of an equivalent cylindrical bearing race with the same or similar hoop stress. The radius of the equivalent cylinder was used to obtain a generalized closed-form approximation of the hoop stresses at the ball-inner-race contact in an angular-contact ball bearing. A life analysis was performed on both a 45- and a 120-mm-bore, angular-contact ball bearing. The predicted lives with and without hoop stress were compared with experimental endurance results obtained at 12 000 and 25 000 rpm with the 120-mm-bore ball bearing (fig. 1). A life factor equation based on hoop stress is presented. A threshold hoop stress below which, for a given bearing steel, hoop stress would be ineffective in decreasing life is suggested.

Lewis contact: Erwin V. Zaretsky, (216) 433–3241

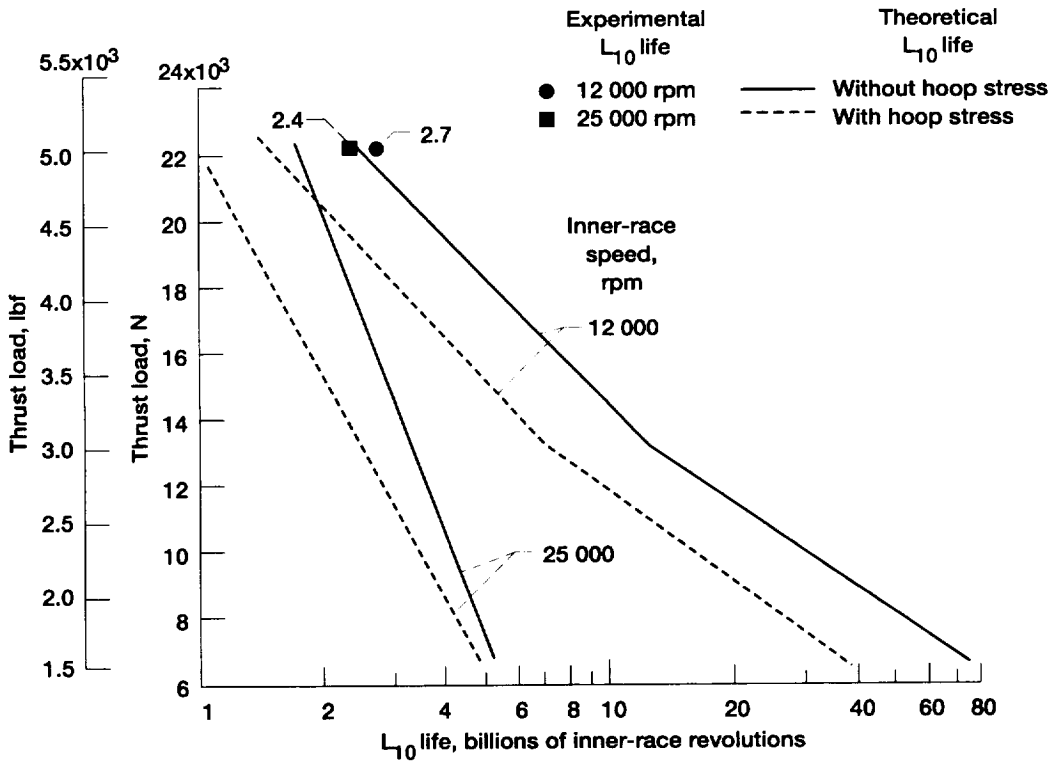

Figure 1.—Comparison of theoretical L_{10} life with and without hoop stress and experimental L_{10} life at a thrust load of 22 241 N (5000 lbf) for 120-mm-bore, angular-contact ball bearings. Contact angle, 24°; race temperature, 218 °C (425 °F); bulk oil temperature, 191 °C (375 °F); material, VIM–VAR AISI M–50 steel; inner race, forged; material hardness, Rc 63; difference between hardness of rolling elements and inner race, 0; lubricant, tetraester MIL–L–23699; life factors, a_2 (material and processing), a_3 (operating conditions).

Predicting Rolling-Element Bearing Life

Nearly five decades have passed since G. Lundberg and A. Palmgren published their life theory in 1947 and 1952 and it was adopted as an ANSI/ABMA and ISO standard in 1950 and 1953. Subsequently, many variations and deviations from their life theory have been proposed, the most recent being that of E. Ioannides and T.A. Harris in 1985. A critical analysis was performed comparing the results of different life theories and discussing their implications in the design and analysis of rolling-element bearings. Variations in the stress-life relation and in the critical stress related to bearing life are discussed using stress fields obtained from a three-dimensional, finite element analysis (FEA) of a ball in a nonconforming race under varying load (fig. 1). The results showed that for a ninth power stress-life exponent, the Lundberg-Palmgren theory best predicts life as exhibited by most air-melted bearing steels. For a 12th power relation reflected by modern vacuum-processed bearing steels, a Zaretsky-modified Weibull equation is superior. The assumption of a fatigue-limiting stress as advocated by Ioannides and Harris distorts the stress-life exponent and overpredicts life.

Lewis contact: Erwin V. Zaretsky, (216) 433–3241

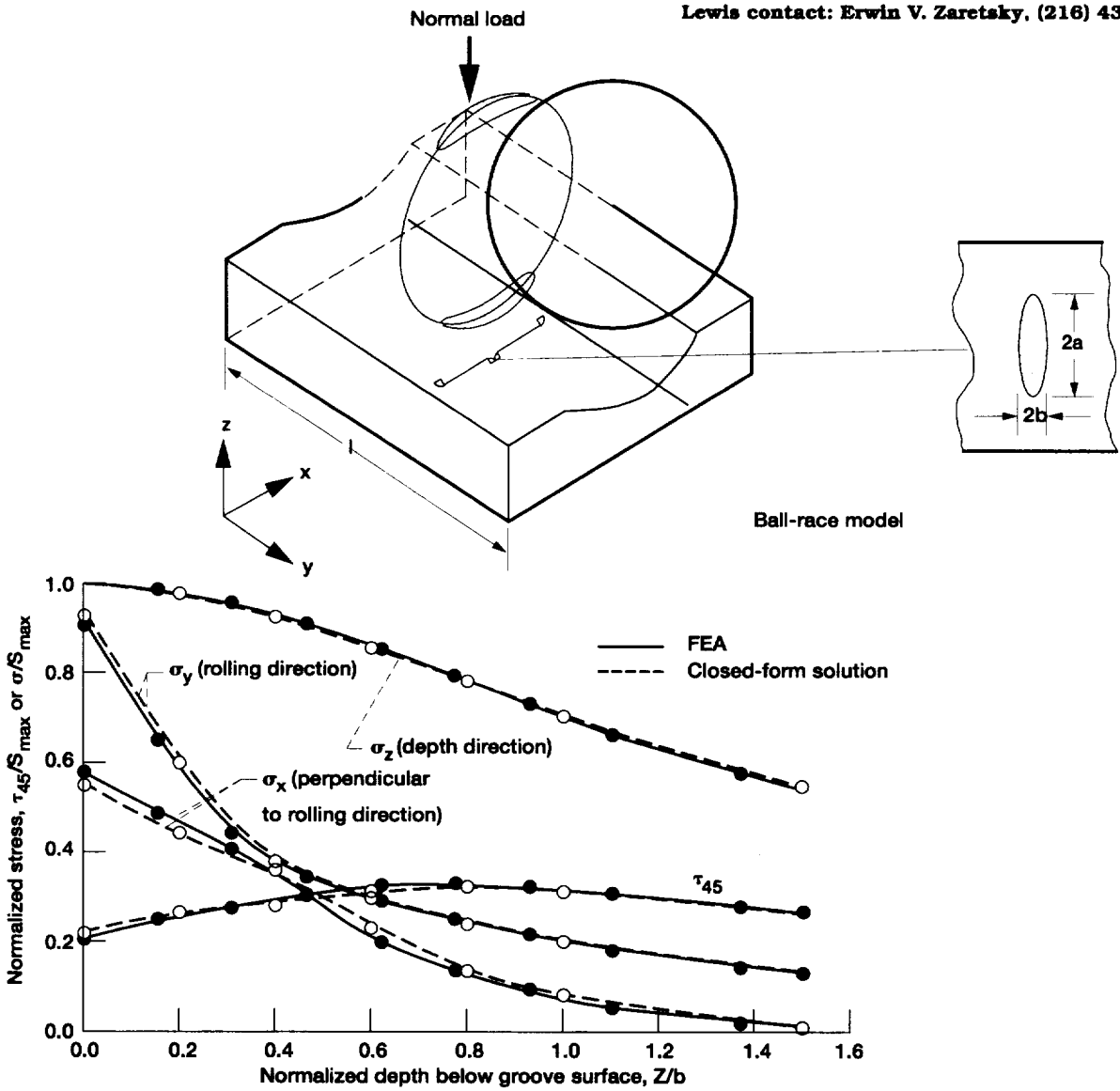

Figure 1.—Comparison of finite-element stress analysis (FEA) with closed-form solution for principal stresses and τ_{45} shear stress as a function of depth below groove surface. Ball diameter, 12.7 mm (0.5 in.); groove conformity, 52 percent; normal load, 623 N (140 lbf); maximum Hertz stress, 1.4 GPa (200 ksi); semimajor contact axis, a, 1.3 mm (0.05 in.); semiminor contact axis, b, 0.16 mm (0.006 in.).

Structural Mechanics

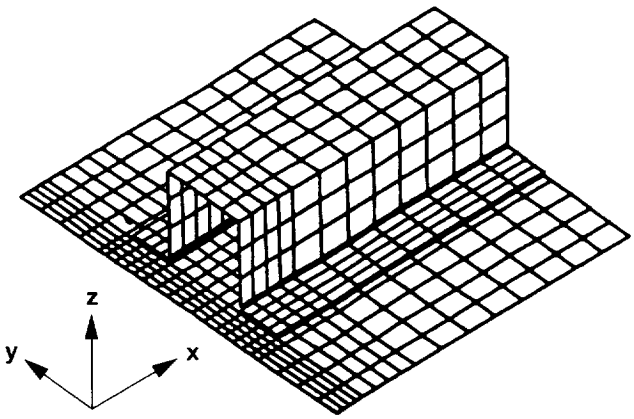

Figure 1.—Stiffness composite panel finite element model.

Effect of Combined Loads on the Durability of a Stiffened Adhesively Bonded Composite Structure

The progressive fracture and damage tolerance characteristics of a stiffened graphite/epoxy panel (fig. 1) were investigated via computational simulation. An integrated computer code, CODSTRAN, was utilized for the simulation of composite structural degradation under loading. Damage initiation, growth accumulation, and propagation to structural fracture are included in the simulation. The results indicated that damage initiation and progression significantly effect structural behavior under loading. The damage versus the applied bending load is plotted in figure 2. For an applied load equal to 88 percent of the failure load (1.1354 kN-m or 10.05 kips-in.), the fracture propagates very quickly and the panel collapses at a load equal to 1.1354 kN-m (10.05 kips-in.).

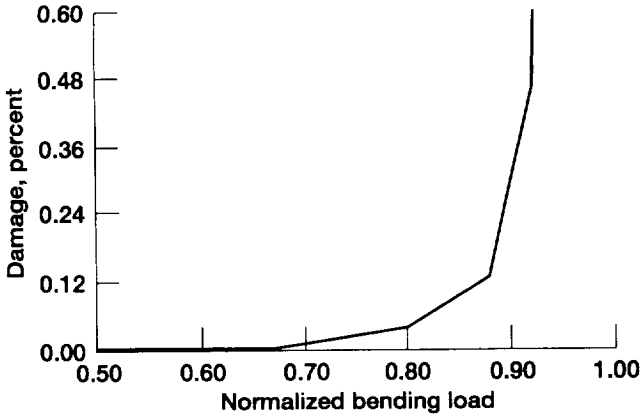

Figure 2.—Damage initiation and growth under bending load.

Lewis contact: Pascal K. Gotsis, (216) 433–3331

Damage Progression in Bolted Composite Structures

Structural durability, damage tolerance, and progressive fracture characteristics of bolted graphite/epoxy composite laminates (fig. 1) are evaluated via computational simulation. An integrated computer code, CODSTRAN, was used for the simulation of structural degradation under loading. Damage initiation, growth, accumulation, and propagation to fracture were included in the simulation. The results showed the damage progression sequence and structural fracture resistance during different degradation stages. The damage versus the applied load is plotted in figure 2. Because of matrix fracture, damage initiation began at a load of 17.792 kN (4 kips). The damage growth accelerated very fast at 51.152 kN (11.5 kips), involving more damage in the matrix and fracture in the fibers. Finally, fracture in the bolted laminate occurred at 191.26 kN (43 kips). The results indicate that damage progression characteristics are not very sensitive to the laminate width or to the bolt space in the investigated range.

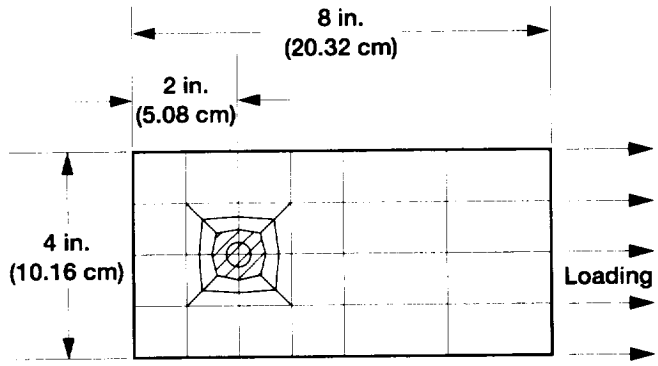

Figure 1.—Bolted laminate finite element model.

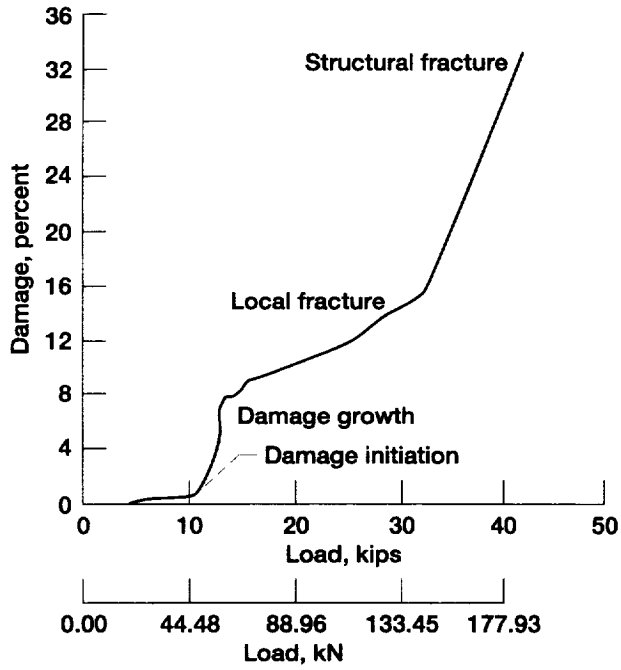

Figure 2.—Damage progression for bolted laminate.

An optimal value of the bolt spacing-to-diameter ratio of 2 gives the best ultimate fracture load of approximately 2.3 MN/m.

Lewis contact: Pascal K. Gotsis, (216) 433–3331

Computational Simulation of Fiber Composite Thin Shell Structures in a Hygrothermal Environment

A computational simulation of fiber composite thin shell structures subjected to static loads in a hygrothermal environment was performed using CSTEM, a three-dimensional finite element computer code. The graphite/epoxy fiber composite cylindrical shell structure is composed of a $[\pm\theta]_2$ angle-ply laminate (fig. 1). The simulation of the processing was taken into account. The results showed that (1) the ply angle θ significantly influenced the global and local behavior of the fiber composite thin shell (fig. 2); (2) the angle of twist

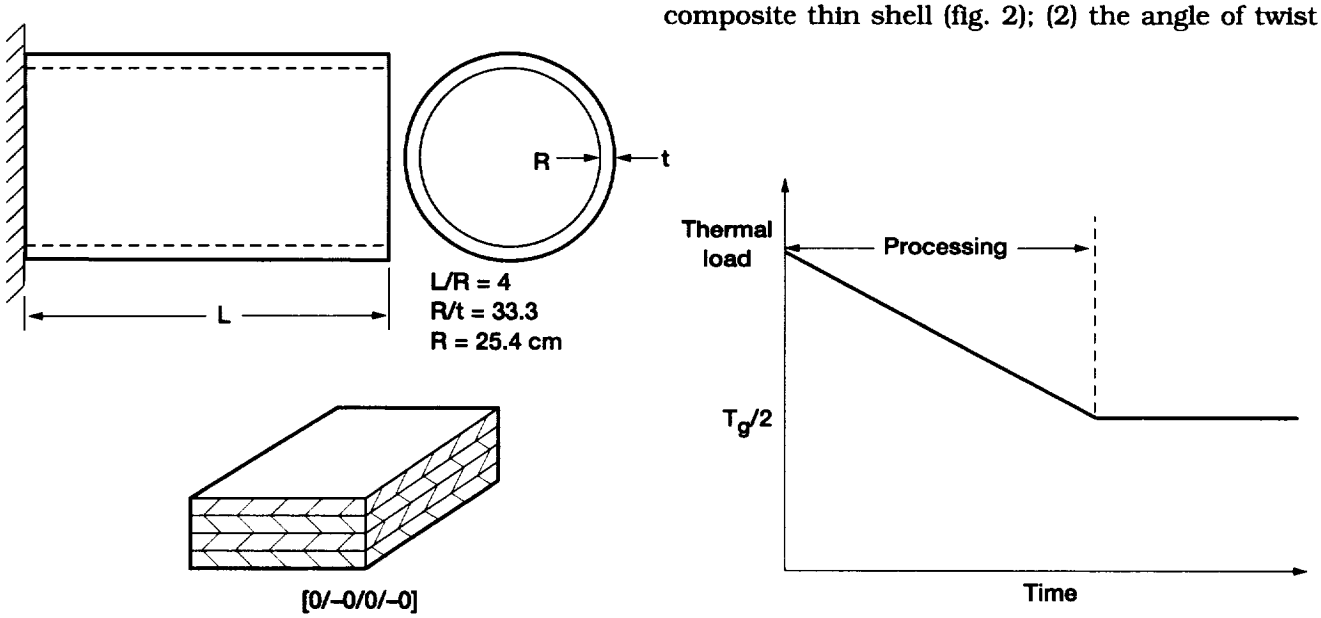

Figure 1.—Geometry, materials, and processing of laminated cylinder. Fiber volume ratio, 55 percent; moisture, 2 percent; fibers, T300; matrix, epoxy with high strength; angle-ply laminate $[\pm 0]_2$; curing temperature T_g of the matrix equal to 215.5 °C.

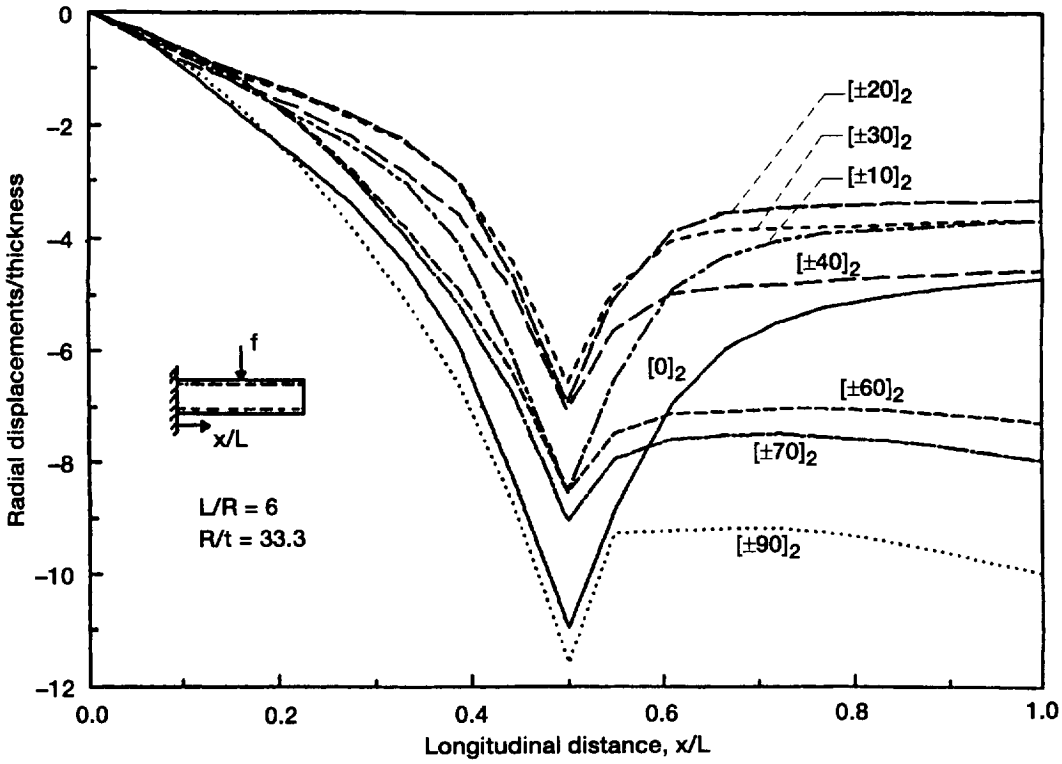

Figure 2.—Radial displacements along axial line that passes through point of contact with concentrated load as function of normalized longitudinal distance x/L. Fiber volume ratio, 55 percent; fibers, moisture, 2 percent; T300; matrix, epoxy with high strength.

was influenced significantly for $0 \le \theta \le 10$ and $80 \le \theta \le 90$, whereas it was influenced moderately for $10 \le \theta \le 80$; (3) the global results obtained using the three-dimensional finite element method were in reasonably good agreement with those obtained using an elementary beam theory.

Lewis contact: Pascal K. Gotsis, (216) 433–3331

Optimization Improves Air-Breathing Propulsion Engine Concept

The optimization of air-breathing propulsion engines with constraints specified on the discharge temperature, pressure ratios, mixer Mach number, compressor and fan maximum speeds and surge margins has been cast as a nonlinear optimization problem. Engine thrust is the merit function, and bypass ratios, R-values of the fans, and fuel flow are typical active design variables. Because of the large number of mission points, diverse constraint types, and overall ill-conditioning of the design space, the most reliable optimizer available in CometBoards (which has 1 dozen, state-of-the-art optimizers) would provide feasible optimum results only for a portion of the flight envelope. Therefore, a solution strategy that soft couples the engine performance analyzer NEPP with the CometBoards design tool was developed. Some of the unique features of CometBoards (cascade strategy, variable and constraint formulations, and scaling devised for difficult multidisciplinary applications) could successfully optimize the performance of both

subsonic and supersonic engines over their flight envelopes. The combined CometBoards and NEPP strategy converged to the same global optimum solution even when it was initiated from different design points. Typically, when NEPP was used alone, many cycles of manual interventions were necessary to extract an acceptable solution because the optimization scheme was unreliable. The reliable and robust combined tool eliminated manual interventions and it was much easier to use, adding value to the engine cycle analysis.

Solutions for two numerical examples, a wave-rotor-topped subsonic engine and a mixed-flow turbofan engine design, illustrate the capability of the combined design tool. A wave-rotor-topped engine with four ports was optimized for a 47-mission flight envelope. So that the benefit of wave-rotor topping could be assessed, most baseline variables and constraints were declared passive, whereas the rotational speed, heat added, and fuel flow were declared active variables. The important active constraints included limits on the temperature and on the maximum speeds and surge margins of all the compressors. Engine thrust was the merit function. The cascade strategy successfully solved the design (with 47 subproblems, one for each mission point). For the mission at Mach 0.1 and a 5000-ft altitude, figure 1 shows the convergence of the two-optimizer cascade strategy (sequential quadratic programming (SQP) followed by the method of feasible directions (FD)). The SQP optimizer produced an infeasible design at a 67 060.87-lb thrust. At a thrust of 66 901.28 lb, the second FD optimizer produced a feasible optimum design that was verified graphically. Engine thrust was the merit function for the optimization of a mixed-flow supersonic engine with constraints specified on the maximum compressor speed, acceptable surge margins, discharge temperatures, pressure ratios, and mixer Mach number. The bypass ratio, mixer pressure balance, fuel flow, and R-values for fan and compressor were active design variables. The 122-mission flight envelope required the solution of 122 optimization subproblems. The combined tool successfully solved the engine problem producing the same global solution even when it was initiated from different points. Figure 2 depicts the engine solutions, which were normalized with respect to NEPP answers. The combined tool was superior for most of the 122 missions, successfully solving the 122 mission mixed-flow turbofan engine design optimization problem.

Lewis contacts: Dale A. Hopkins, (216) 433–3260 and Surya N. Patnaik, (216) 962–3135

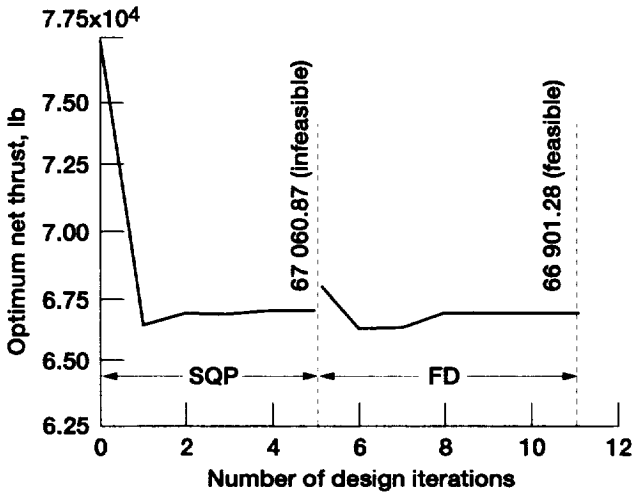

Figure 1.—Convergence of cascade solution for a wave-rotor-topped engine.

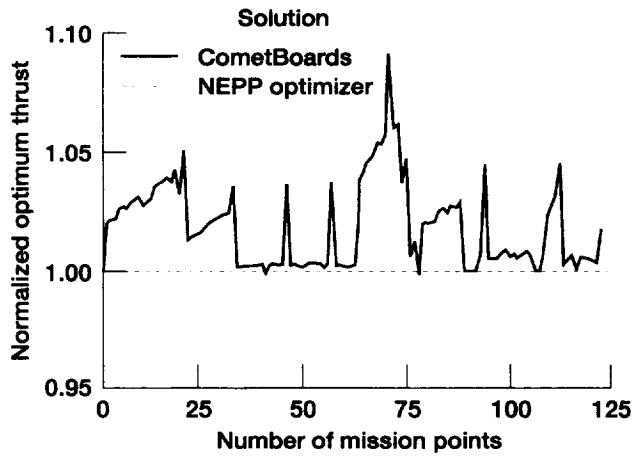

Figure 2.—Value-added benefit in design of mixed-flow turbofan engine.

A Novel Boundary Condition Completed the Beltrami-Michell Formulation in Elasticity

In elasticity, the method of forces, wherein stresses are considered the primary unknowns, is known as the Beltrami-Michell Formulation. This method can solve only stress boundary value problems; it cannot handle the more prevalent displacement or mixed-boundary-value problems of elasticity. Therefore, the classical method, which has restricted application, could not become a true alternative to the Navier's displacement method, which can solve all three types of boundary value problems. The restriction was alleviated by augmenting the classical formulation with a novel set of conditions identified as the boundary compatibility conditions. This new method, which completes the classical force formulation, has been termed the Completed Beltrami-Michell Formulation. The completed formulation can solve general elasticity problems with stress, displacement, and mixed-boundary conditions in terms of stresses as the primary unknowns. The completed formulation is derived from the stationary condition of the variational functional of the Integrated Force Method. In the completed Beltrami-Michell formulation, stresses for kinematically stable structures can be obtained without any reference to displacements either in the field or on the boundary. Displacements, if required, can be back calculated from stresses.

The solution obtained through the completed Beltrami-Michell formulation for a composite shell with mixed-boundary conditions is shown in figure 1. The composite shell, made of two different materials, is subjected to thermomechanical loads. Notice the peak response and the discontinuity at the shell interface.

Lewis contacts: Dale A. Hopkins, (216) 433–3260 and Surya N. Patnaik, (216) 962–3135

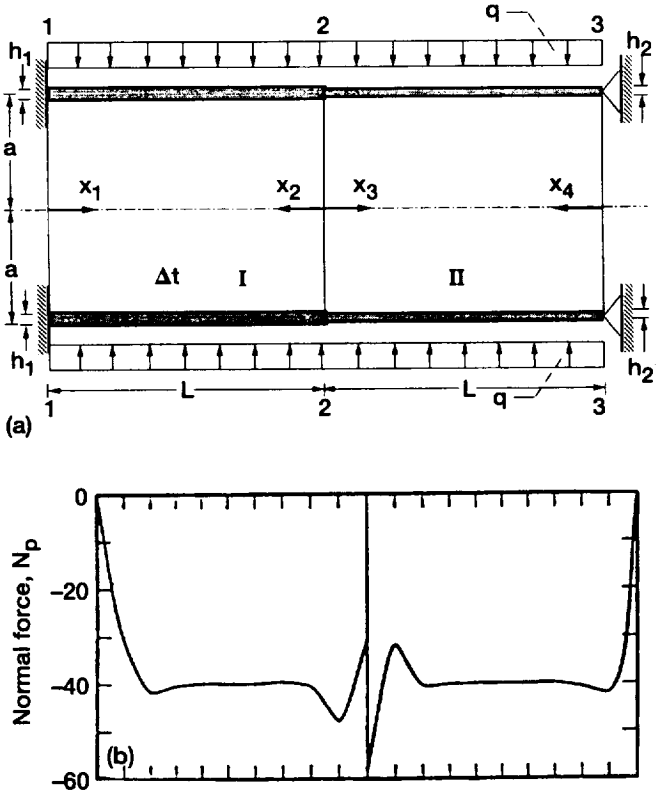

Figure 1.—Analysis of composite cylindrical shell. (a) Composite cylindrical shell. (b) Normal force distribution along x-axis.

Active Thermal Distortion Management With Smart Piezoelectric Structures

The development of smart piezoelectric structures offers great potential for their use in advanced aerospace applications. By combining the traditional performance advantages of composite materials with the inherent capability of piezoelectric materials to sense and adapt to their environment, piezoelectric composite materials can provide dramatic advantages in the development of smart structures with the capability to actively manage adverse thermomechanical conditions. To investigate potential applications for active thermal distortion management, a thermal analysis capability was incorporated in a refined laminate theory and a finite element formulation developed for both beam and plate elements. A numerical study was performed on a cantilevered $[45_3/-45_3]$ graphite/epoxy plate with attached piezoceramic patches. The application of a thermal gradient, with the piezoceramic patches grounded, resulted in the combined bending and twisting deformation shown in figure 1 (also shown is the original undeformed geometry). Through the application of active voltages with varying polarities, the bending and twisting deformation of the plate can be controlled either individually or simultaneously. The resulting deformation from inhibiting both the bending and twisting behavior simultaneously is shown in figure 2. These results demonstrate the potential

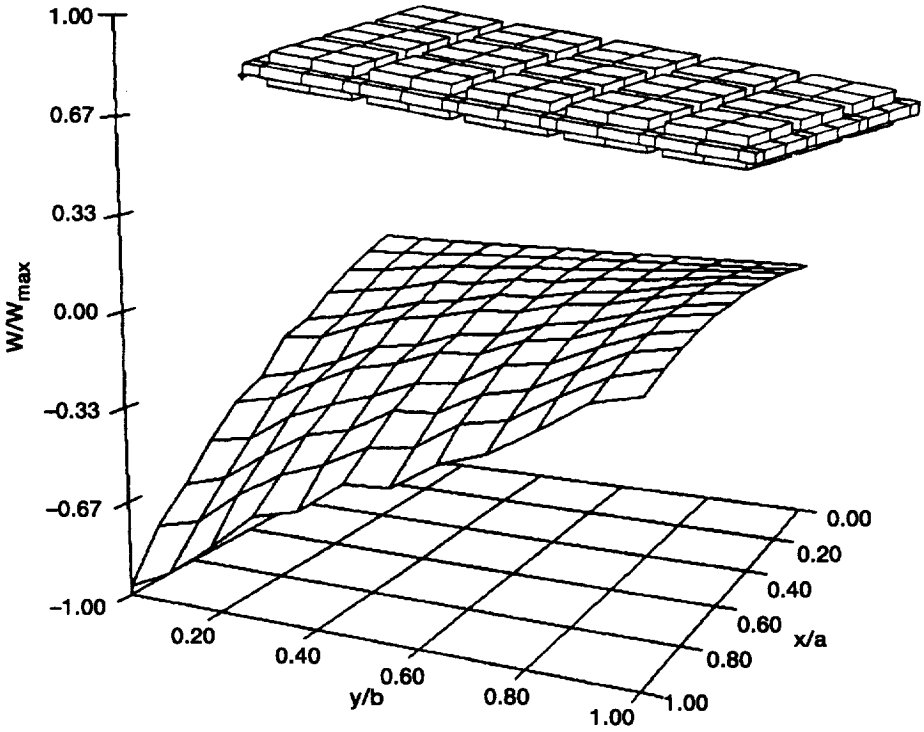

Figure 1.—Initial thermal bending and twisting deformation of [45$_3$/–45$_3$] plate under a thermal gradient.

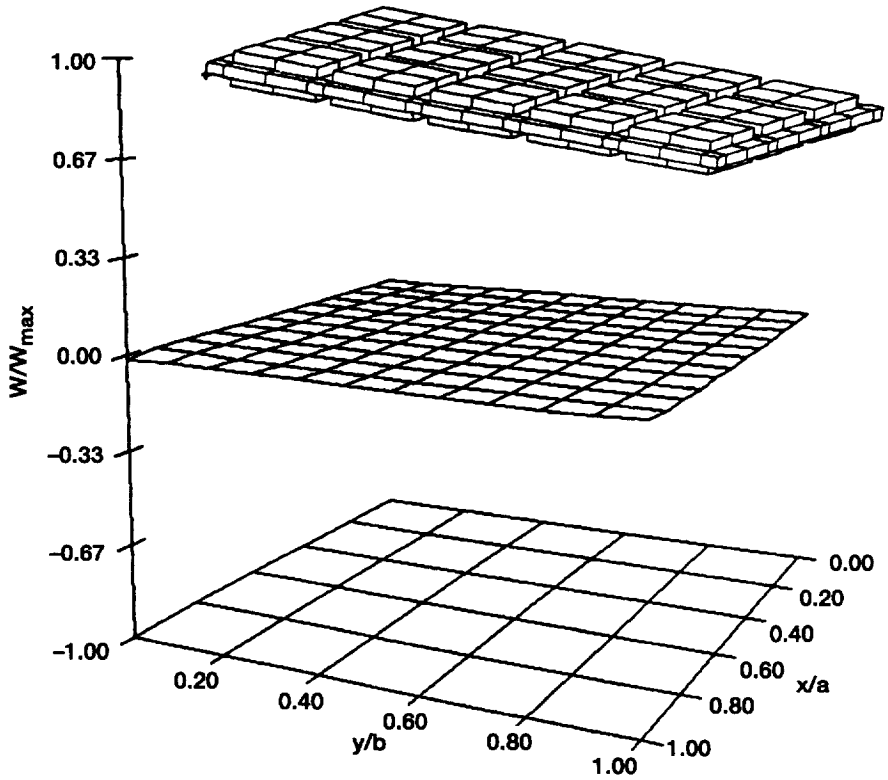

Figure 2.—Active compensation of thermal bending and twisting deformation of [45$_3$/–45$_3$] plate under a thermal gradient.

application of smart piezoelectric structures for active thermal distortion management of propulsion components and space structures.

Lewis contacts: Ho-Jun Lee, (216) 433–3316 and Dimitris A. Saravanos, (216) 962–3211

Micromechanics for Woven Composites

There is a growing interest in the use of woven composites for structural applications. Reinforcement of these composites is accomplished by various processes such as weaving, braiding, or knitting. Woven composites, in particular, are constructed by weaving two fiber tows into each other to form a layer. The interlacing of fiber bundles has several advantages such as increasing the intra- and interlaminar strength, providing greater damage tolerance, and making it possible to produce near net shapes for thick structural components. The design methodologies for such composites must account for geometrical as well as processing parameters. A micromechanics-based technique that is used in combination with micromechanics-based analysis codes was developed to analyze such composites. The intention of the present work was to develop a methodology that could make use of the capabilities that already exist for the analysis of laminated continuous fiber-reinforced composite mechanics codes developed in-house at the NASA Lewis Research Center and yet account for fiber waviness and fiber-end distributions through the thickness. Because this technique is based on simplified micromechanics equations, it is inherently more efficient than numerical analysis techniques and provides a very detailed response. The properties for a generic graphite/epoxy plain-weave textile composite and a SiC/SiC plain-weave composite were generated using the above technique, ICAN (Integrated Composite Analyzer), and CEMCAN (Ceramic Matrix Composite Analyzer) computer codes. Limited verification with a set of detailed three-dimensional finite element analyses as well as with available experimental data shows good agreement (table I). Fabrication-related issues and environmental degradation effects can be easily taken into account using this micromechanics-based technique (fig. 1). Work is underway to incorporate this model into the existing composite mechanics codes and to develop capabilities that will allow prediction of the composite properties and/or response of three dimensionally reinforced fabric composites.

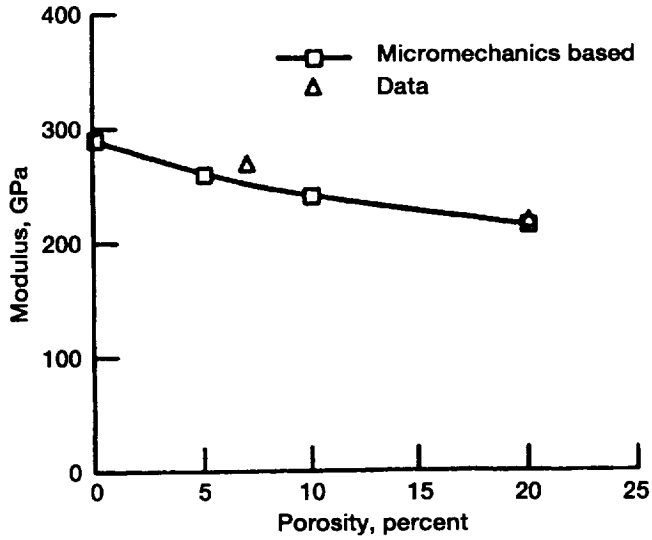

Figure 1.—In-plane modulus versus porosity of SiC/SiC composite. Fiber volume ratio, 0.4.

TABLE I.—SiC/SiC COMPOSITE PROPERTIES
[Fiber volume ratio, 0.4; void, 0.2.]

Property	Micromechanics prediction	Measured
Density, g/cm³	2.45	2.5
E_{xx}, GPa	214.4	214
E_{zz}, GPa	193	—
G_{xy}, GPa	80	—
G_{yz}, GPa	79.3	0.17
ν_{xy}	.18	—
ν_{yz}	.2	—

Lewis contacts: Subodh Mital, (216) 433-3261 and Pappu Murthy, (216) 433-3332

Ballistic Impact Research in Support of HSCT Engine Fan Containment

Ballistic impact tests and analyses are being conducted at the NASA Lewis Research Center to support the development of a lightweight, high-temperature, engine fan containment system for the High Speed Civil Transport initiative. During 1995, materials and concepts were evaluated by conducting impact tests on flat 2- by 2-ft panels and structures in the Structures Division's Ballistic Impact Facility. Disk-shaped projectiles (4.5 in. (11.43 cm) in diam by 0.75 in. (1.90 cm) thick) weighing 2 lb (0.09 kg) were accelerated to speeds in excess of 1200 ft/sec and were impacted on the test articles. A number of different concepts and materials were found to be viable candidates for reducing the weight of a baseline fan containment system.

Computer analyses were conducted to support these tests and the large subcomponent tests at the

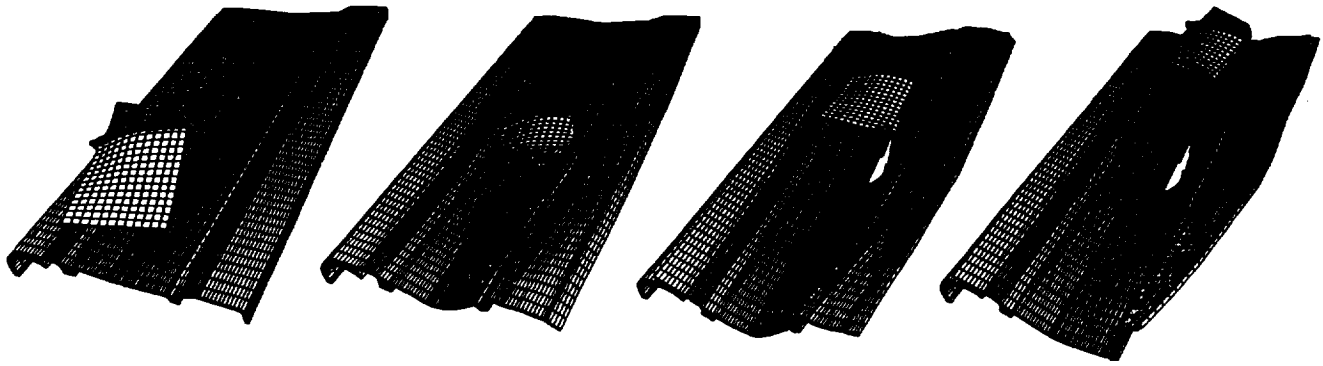

Figure 1.—Typical progression of fan blade impact on subcomponent panel.

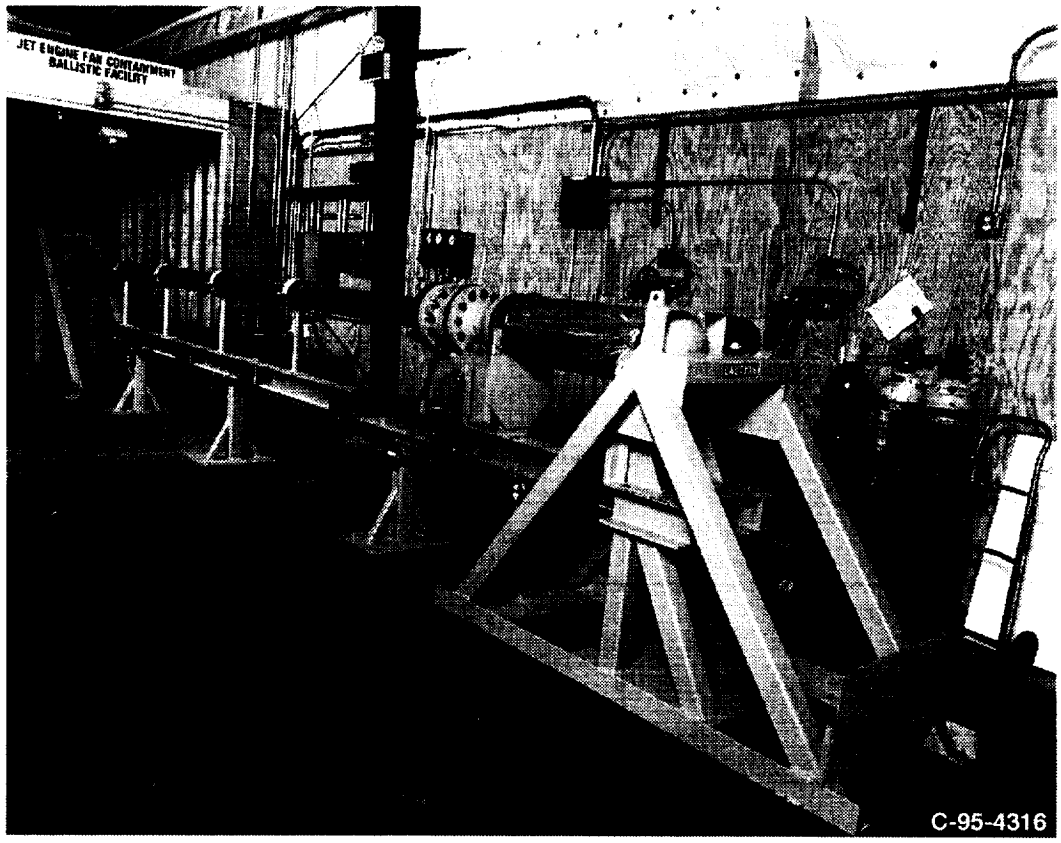

Figure 2.—Ballistic impact facility showing 6-in. (15.24-cm) gun.

University of Dayton Research Institute. The LSTC DYNA three-dimensional explicit finite element code was used to design the experiments and to predict their outcomes. Test conditions and test article configurations were determined based in part on the finite element predictions. Figure 1 depicts the progression of a fan blade impacting a subcomponent panel.

The Ballistic Impact Facility (fig. 2) has several guns with barrels ranging from 0.0625 to 8 in. (0.1588 to 20.32 cm) in diameter and is capable of shooting projectiles at velocities in excess of the speed of sound. The facility is supported by high-speed data acquisition, video and film photography, and modeling with DYNA.

Lewis contacts: J. Michael Pereira, (216) 433-6738 and Matt Melis, (216) 433-3322

Monitoring Damage Progression in Ceramic Matrix Composites

Ceramic matrix composites (CMC's) are being evaluated for use in the engine for the High Speed Civil Transport. There is a need to understand how these materials respond to extreme mechanical and thermal conditions. Traditional nondestructive techniques have had limited success in evaluating these materials. A unique vibration technique was used on a model CMC material to obtain a specimen's natural frequency and damping value.

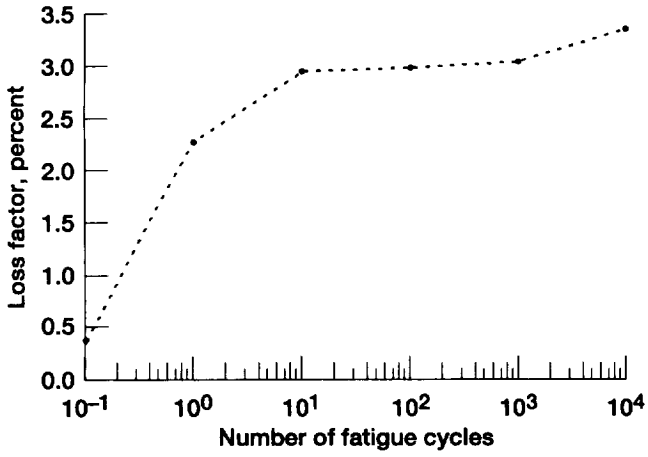

Figure 1.—Vibrational NDE loss factor versus mechanical cycles for SiC/SiC [45/–45] composite.

After various mechanical loading cycles at room temperature, measurements were conducted on an enhanced SiC/SiC CVI (chemical vapor infiltration) material with three layup configurations and two stress levels. The frequency decreased dramatically after the first mechanical loading cycle and then leveled off after successive cycles. The loss factor, twice the damping value, increased dramatically after the first mechanical cycle and then slowly increased, as shown in figure 1. Gripping of the sample had negligible effect on either frequency or loss factor. The greater the stress, the greater the decrease in frequency. The modulus calculated from the frequency response compared well with the direct measurement. The changes in frequency and loss were associated with damage in the material. The conclusion was that the most significant damage occurred in the first loading cycle. This vibration technique tracked modulus changes and damage progression in CMC's.

Lewis contacts: Christopher Rabzak, (216) 977-1238 and J. Michael Pereira, (216) 433-6738

High-Temperature Strain Gage and Adhesive System Development and Testing

Polymer-matrix-based composites continue to be evaluated for high-temperature applications in engine components. A unique strain gage and adhesive system was developed for the mechanical property measurement of polymers and polymer composites at elevated temperatures. This system overcomes some of the problems encountered in using commercial strain gages and adhesives. An important limitation with typical commercial strain gage adhesives is that they require a postcure at temperatures substantially higher than the maximum test temperature. The exposure of the specimen to this temperature may affect subsequent results; in some cases, the postcure temperature may be higher than the glass transition temperature of the polymer. In addition, although typical commercial strain gages can be used for short times at temperatures up to 370 °C (700 °F), their long-term use is limited to 230 °C (450 °F). This precludes their use in testing some high-temperature polyimides near their maximum temperature capability. The system that was developed consists of a nonencapsulated, unbacked gage grid that is bonded directly to the polymer

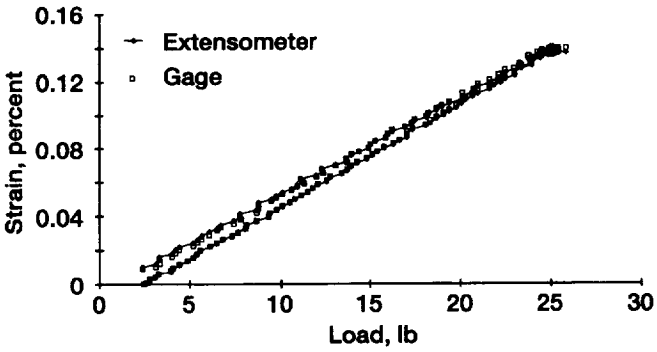

Figure 1.—Comparison of elevated-temperature strain gage and extensometer on PMR-15 specimen at 315 °C (600 °F).

using a specially formulated adhesive. The gage is applied after the specimen has been cured but prior to the normal postcure cycle. The adhesive was formulated to cure under the specimen postcure conditions. Special handling, mounting, and electrical connection procedures were developed; a fixture was designed to calibrate each strain gage after its application on the specimen. At elevated temperatures, a variety of tests was conducted to determine the performance characteristics of the gages on PMR-15 neat resin specimens. These tests included static tension and compression, thermal exposure, and creep. Figure 1 compares the gage and an extensometer on PMR-15 at 315 °C (600 °F). The gage and adhesive system performed within normal strain gage specifications at temperatures up to 315 °C (600 °F).

Lewis contact: Christopher Rabzak, (216) 977-1238 and J. Michael Pereira, (216) 433-6738

Micromechanics Predict Uniaxial Response and Local Stresses of Composites With Shape Memory Alloy Fibers

Shape memory alloys (SMA's) have found increasing applications as candidate smart materials and components of adaptive structures. One potential application of shape memory alloys is their use as fibrous sensors or actuators within a composite material system. The development of fibrous shape memory (SM) composites will provide weight savings, directionality in actuation and sensing, and some control over the resultant SM effect. However, to analyze the complicated thermomechanical response of unidirectional composite systems with continuous shape memory alloy fibers, the development of new micromechanical models is required. Such a micromechanical method based on a combination of the three-concentric-cylinder model (fibers, matrix, and equivalent shape memory composite) with the multicell micromechanical method was developed. The micromechanics can predict the uniaxial response and the local stresses in the composite when the fibers undergo martensitic or reverse-phase transformations as a result of applied mechanical or thermal loads.

Applications on candidate shape memory composite systems with Nitinol fibers (~30 percent) in an epoxy matrix illustrated that these composites may exhibit a unique longitudinal response under isothermal loading and unloading conditions (fig. 1). The capability of shape memory composites to induce very high longitudinal strains upon the application of mechanical stress (fig. 1) or with a variation of temperature was also demonstrated. The ranges of stress, strain, and temperature where such actuation may occur may be also predicted. The evolution of microstresses in the composite during stress- or temperature-

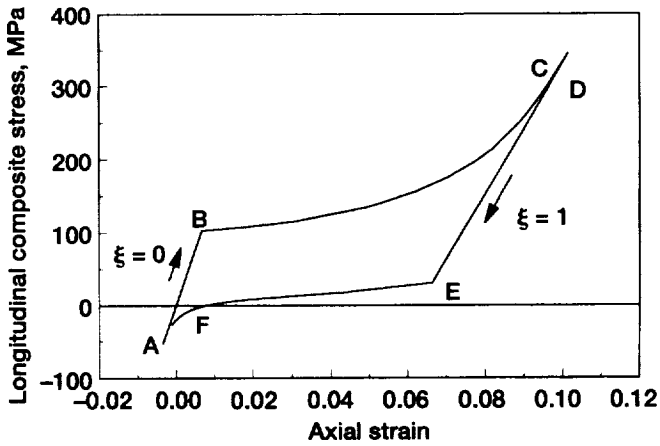

Figure 1.—Predicted isothermal loading-unloading stress-strain cycle of 30-percent-fiber-volume-ratio nitinol/epoxy composite (40 °C). Segment AB, loading with fibers in parent (austenite) phase (ξ = 0); segment BC, loading with fibers undergoing transformation to martensitic phase (0<ξ<1); segment DE, unloading with fully transformed fibers (ξ = 1); segment EF, unloading with fibers undergoing reverse phase transformation.

induced phase transformations can be also simulated. In summary, the research has enabled the modeling of the complex, yet promising, active response of SM composites and has outlined some of their unique advantages as active materials in the management of thermal distortions in advanced propulsion components.

Lewis contacts: Dimitris A. Saravanos, (216) 962-3211 and Dale Hopkins, (216) 433-3260

Generalized Finite Element Enables Prediction of Global and Local Response of Multilayered Composite Plates With Embedded Piezoelectric Actuators and Sensors

The development of a new class of smart composite materials and adaptive structures with sensory and active capabilities is expected to further improve the performance and reliability of aeronautical structural systems. However, such an effort requires the development of admissible mechanics entailing capabilities to model the unified electromechanical response of sensory/active structures as well as the evolution of the complicated stress-strain fields in smart composites and the interfacial phenomena between the embedded microdevices and the passive composite plies.

Recent developments in generalized mechanics for smart composite laminates with embedded piezoelectric actuators and sensors have culminated in the development of a specialty four-node finite element for adaptive piezoelectric plates. The finite element provides unique features not found elsewhere, including the capabilities to model (1) the global response of structures with embedded actuators and/or sensors; (2) the local through-the-thickness response (intralaminar and interlaminar stresses, interfacial phenomena between structure and piezoelectric devices, etc.); (3) a wide spectrum of thicknesses, ranging from very thin to very thick structures; and (4) continuous or discrete piezoelectric actuators and sensors.

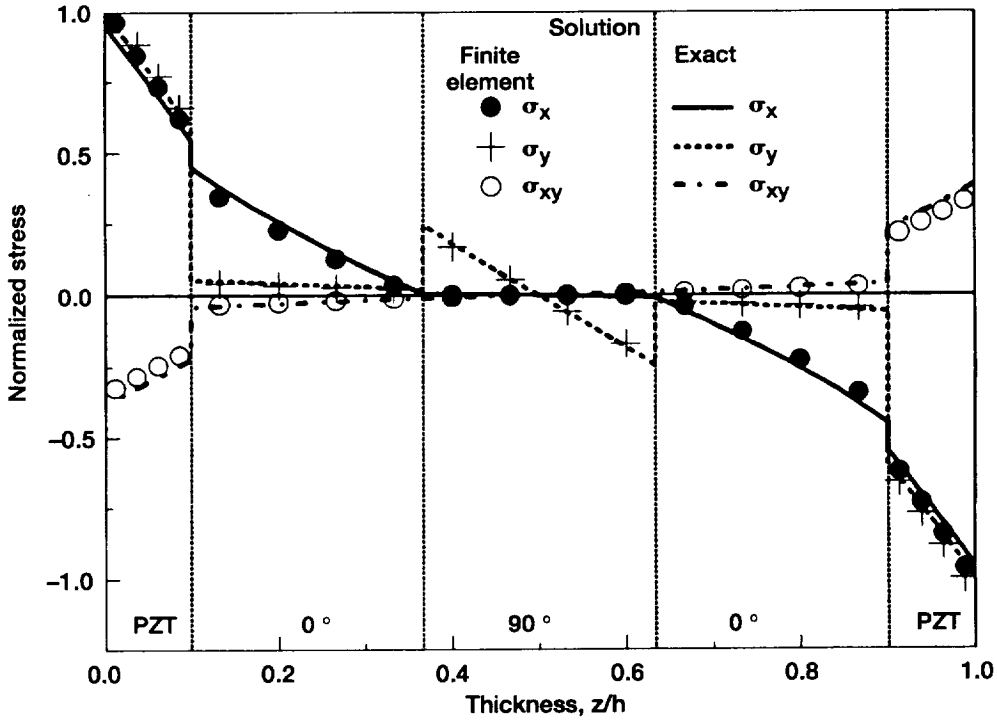

Figure 1.—In-plane modal stresses for fundamental mode in thick [0/90/0] square plate with surface-bonded piezoceramic sensors and comparisons with exact solution. Span/thickness ratio, 4.

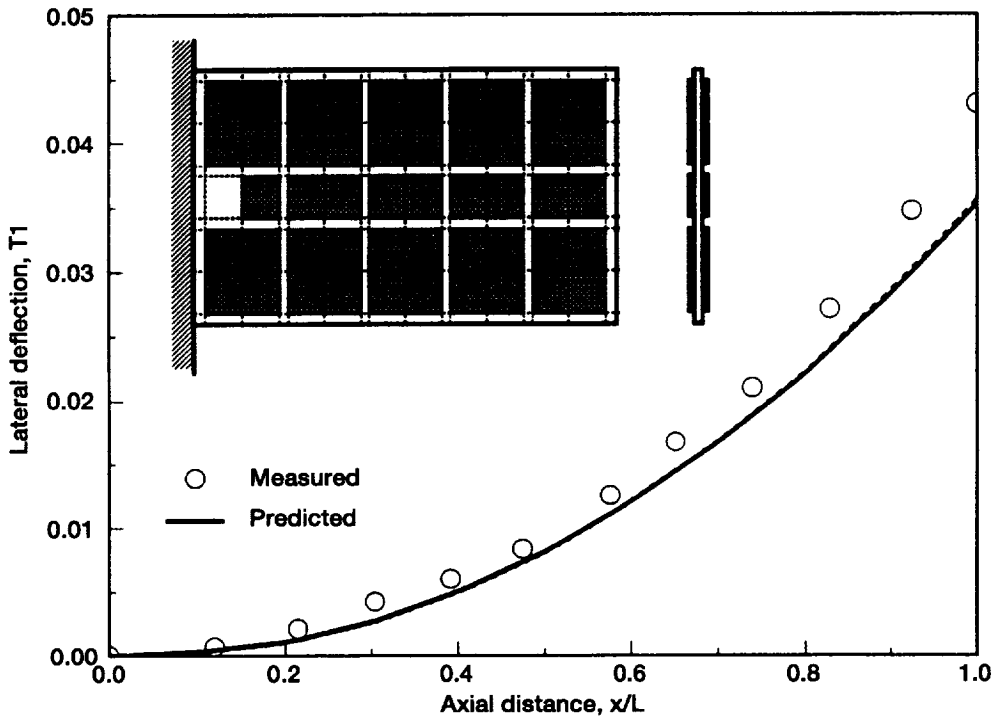

Figure 2.—Predicted bending deformations of $[0/\pm45]_s$ cantilever plate beam induced by opposite-polarity electric field applied on shown surface-bonded actuators. Measurements reported by Crawley and Lazarus (1989).

Numerous case studies have provided analytical and experimental verification of the finite element and the prototype software. Figure 1 illustrates one of the extreme capabilities of the mechanics: the excellent prediction of local axial stresses in a thick composite plate with surface-bonded piezoceramic (PZT–4) sensory layers. A typical simulation of the global deformation of a laminated cantilever plate with discrete piezoelectric actuators is shown in figure 2. In summary, the evaluations have demonstrated the versatility of the finite element to analyze and thus to facilitate the formal development of adaptive piezoelectric components for advanced propulsion systems.

Lewis contacts: Dimitris A. Saravanos, (216) 962–3211 and Dale Hopkins, (216) 433–3260

Fatigue and Fracture

A Study to Optimize a Ring-On-Ring Test Fixture for Testing CMC's Under In-Plane Biaxial Loading Conditions

A study was conducted to optimize a ring-on-ring test fixture to investigate the applicability of composite materials to key engine components used in high-speed aircraft. These components operate under severe and highly complex loading conditions and are continuously exposed to high temperatures and aggressive environments that lead to cracking and other structural deficiencies. The ability to reliably design and life-test these components depends on the generation of a comprehensive data base for composite materials under complex loading conditions. Equibiaxial bending, a condition that occurs in many components, is a through-thickness thermal gradient. Because no experimental results are available in the open literature for equibiaxial bending failure of fiber-reinforced ceramic composites, a test method was proposed. Analytical verification of the testing setup is the first step to develop a standard test procedure.

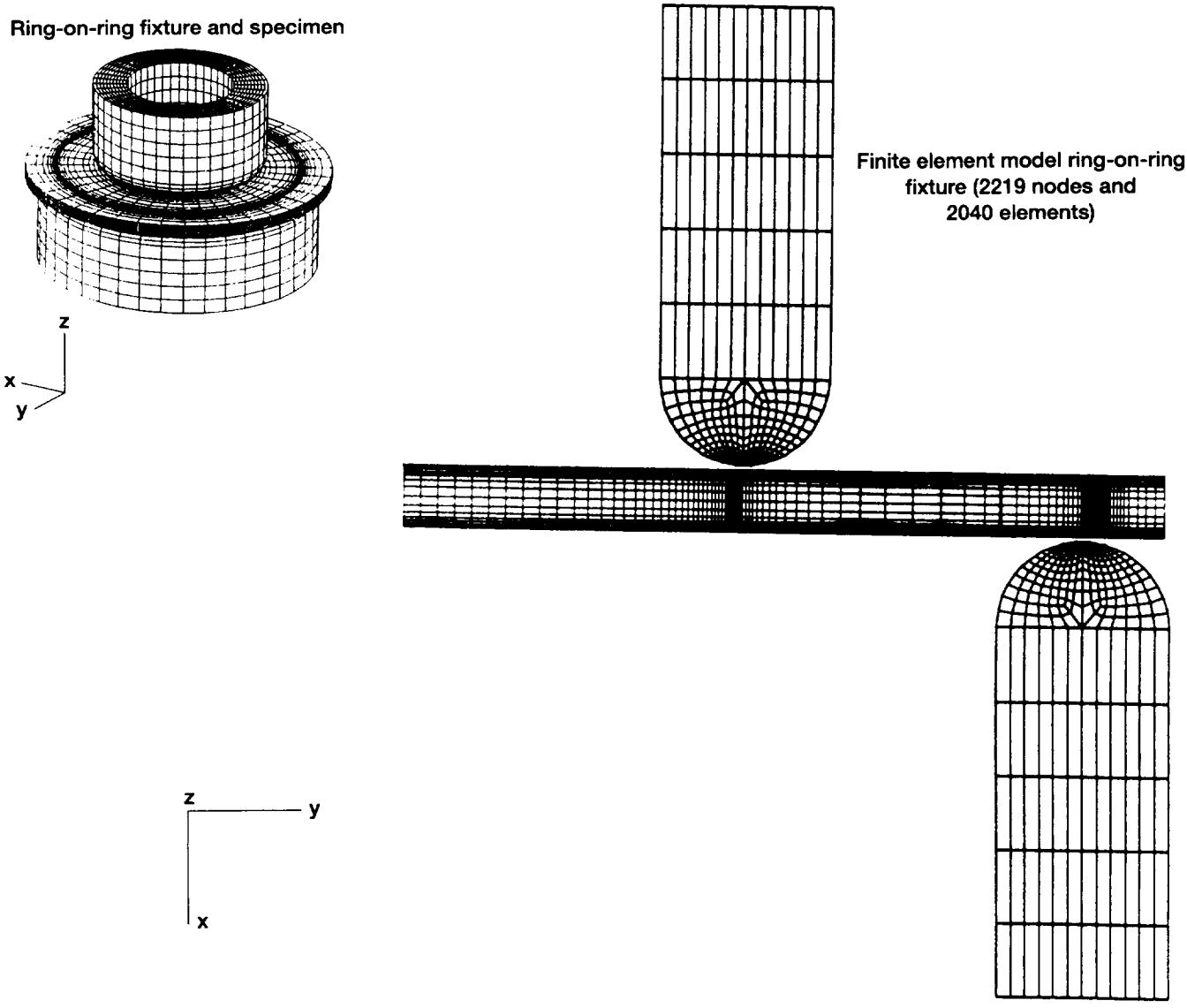

Figure 1.—Finite element model of ring-on-ring biaxial flexure specimen.

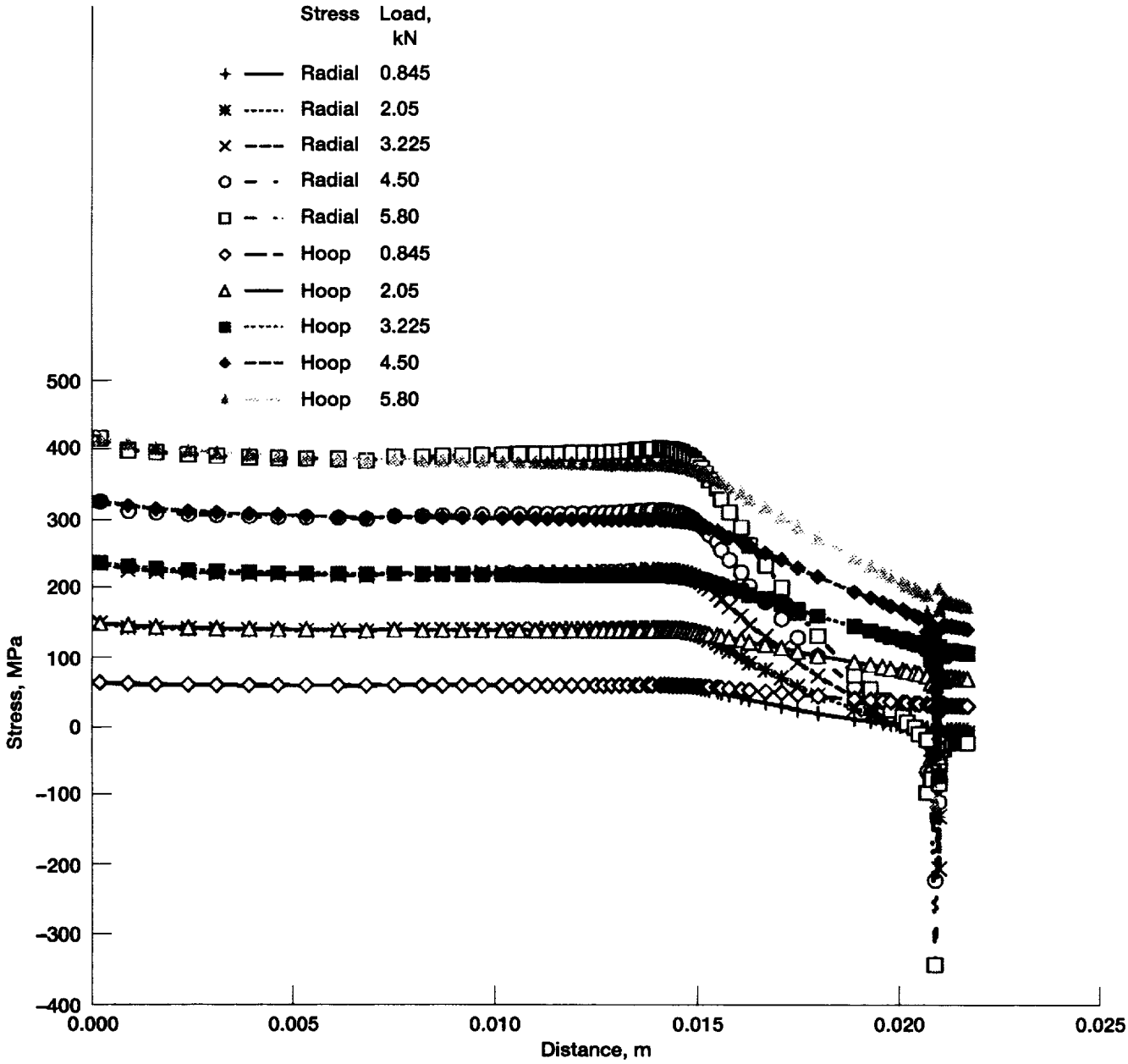

Figure 2.—Contact stresses at ring-specimen interface.

A finite element analysis was conducted on a biaxial-flexure specimen ring-on-ring setup (fig. 1) to evaluate the stress-strain field for monolithic and ceramic matrix composite materials. The evaluation included a comparison of the finite element results with a closed-form solution and experimental data. Effects of the disk geometry and the material characteristics on the resulting stress-strain field and the contact stresses were explored (fig. 2), modeled, and discussed. The analysis considered two-dimensional axisymetric calculations as well as a three-dimensional anisotropic solution. Another objective of this work was to further promote the adoption of the disk and related test procedures as a standard biaxial flexure specimen.

Lewis contacts: Ali Abdul-Aziz, (216) 433–6729 and Dave Brewer, (216) 433–3304

Yield Surface Study of Cast Gamma Titanium Aluminide (TiAl)

Cast gamma TiAl has been identified for advanced aeropropulsion components where high stiffness and low weight at high temperatures are required. These components are geometrically complex and are composed of relatively thin (1.0- to 2.0-mm) structural elements. The typical TiAl microstructure has grain sizes ranging from 0.5 to 1.0 mm. The combination of thin structural members and large grains can provide a potential for nonhomogeneous material behavior (e.g., anisotropy). In an attempt to investigate this potential, a series of yield surface tests were conducted at room temperature on two cast TiAl materials (Ti–48Al–2Cr–2Nb and proprietary XD).

The tests were conducted under in-plane biaxial loading conditions at room temperature. The cruciform specimen used in these tests has a test section 95 by 95 mm in area and 2 mm in thickness (fig. 1). For both materials, an equivalent inelastic strain limit of 150 microstrain was used to define the yield surface. This small strain limit was measured using several strain gages mounted in the test section. A final equiaxed tensile test was performed for each specimen after establishing the yield surface.

As illustrated in figure 2, the XD material exhibited a typical polycrystalline material yield surface. In contrast, the Ti48Al–2Cr–2Nb (48–2–2) TiAl yield surface indicated a preferential yield in the Y-loading axis. This yielding behavior is typical of a material that has a texture. A macroetching technique revealed flow patterns in the grain structure of the 48–2–2 material. A study is currently investigating the relationship of this flow pattern to the observed texturing effect.

Customers: General Electric Aircraft Engines and Pratt & Whitney

Lewis contacts: Paul A. Bartolotta, (216) 433–3338, Peter Kantzos, (216) 433–5202, and David L. Krause, (216) 433–5465

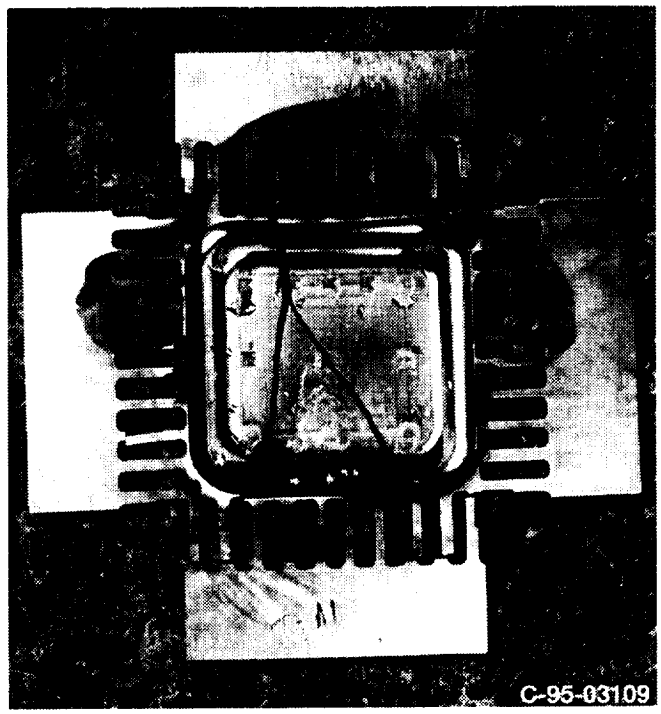

Figure 1.—Failed in-plane biaxial specimen of cast TiAl.

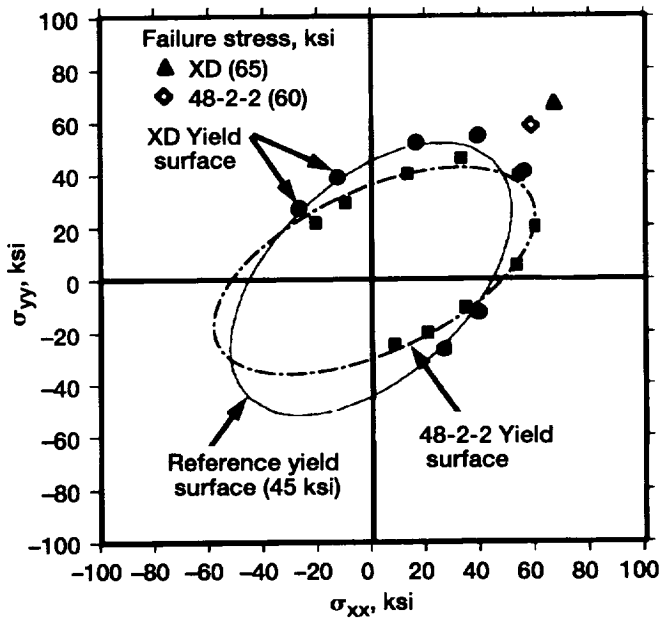

Figure 2.—150-microstrain yield surfaces for 48-2-2 and XD TiAl at room temperature.

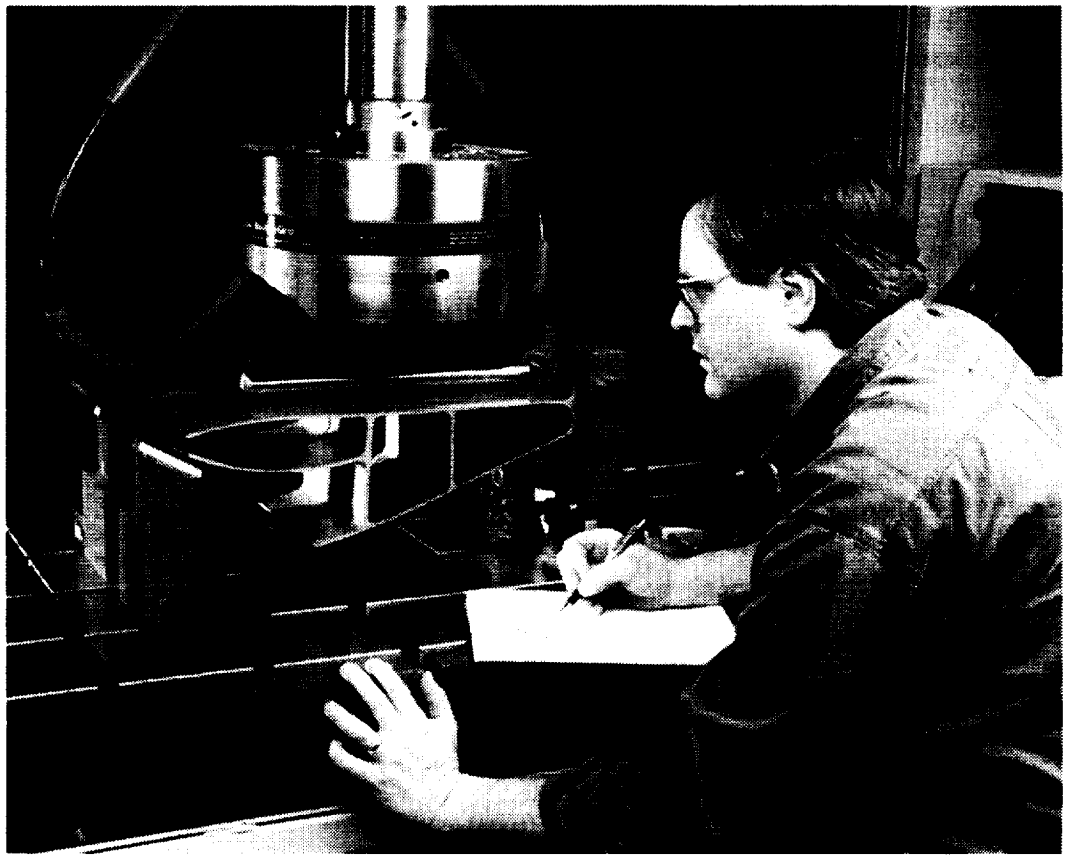

Figure 1.—Mechanical loading fixture with demonstration component, loading ram, universal support pivots, and sliding rockers.

EPM Structural Component Successfully Tested Under Pseudo-Operating Conditions

A fabrication feasibility demonstration component for the Enabling Propulsion Materials (EPM) program was evaluated under prototypical engine loading conditions at the Structural Benchmark Test Facility at the NASA Lewis Research Center. The purpose of this test was to verify EPM casting, joining, coating, and life-prediction methods. The component was fabricated by joining two large superalloy cast sections of an exhaust nozzle flap. These two sections were then joined together using electron beam welding techniques developed in the EPM program. After the joints were inspected, the component was coated with an oxidation-resistant barrier coating and was sent to Lewis for testing.

A special test fixture (fig. 1) was designed and built at Lewis to produce a biaxial bending condition similar to the loading condition this part would encounter in engine operation. Several finite element analyses were conducted to validate the mechanical test method. A floating furnace was then designed to provide prototypical thermal profiles in the component. An isothermal low-cycle fatigue (LCF) test was used to evaluate the component. A cyclic load of 13 kN (max) to 1 kN (min.) at a frequency of 1 Hz was employed. Component failure was defined as a 30-percent increase in compliance. Based on this definition, the LCF life of this component was 35 000 cycles.

As predicted, a fatigue crack was initiated in the welded joint associated with the high-stress location. The local temperature at the failure site was 425 °C. The predicted life of the component was 18 000 cycles. This prediction was based on several lifing methods developed for conventional superalloys. As shown in figure 2, using average material properties (solid circle symbol) would predict lives that were not very conservative (54 000 cycles) and were more representative of those of an unwelded component. To account for the welded

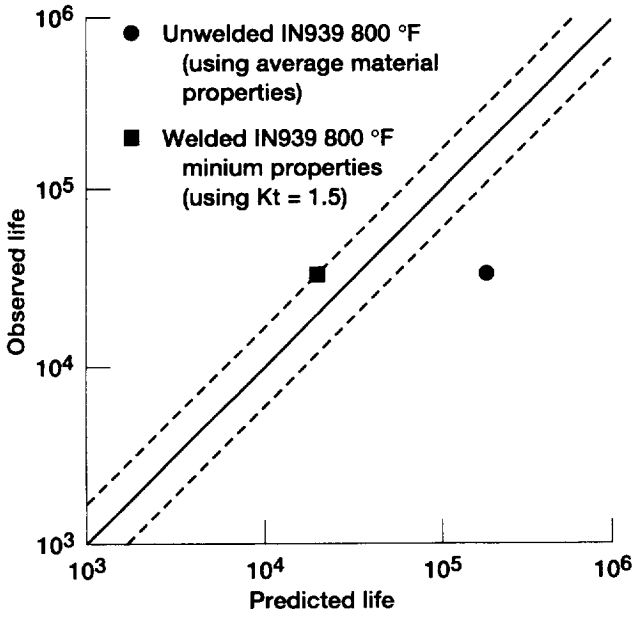

Figure 2.—Life prediction of demonstration component showing predicted life for welded and unwelded component. Component life, 35 000 cycles.

joint and its unknown properties, minimum parent material properties and a stress concentration factor *Kt* of 1.5 were used as knockdown factors. Thus, the predicted life of the welded component was 18 000 cycles (solid square symbol). The Lewis life-prediction method was within a factor of 2 in life from the actual demonstration component life.

Note that specifics on test conditions, material details, and engine operation conditions have been omitted because of Limited Exclusive Rights restrictions.

Customers: General Electric Aircraft Engines and Pratt & Whitney

Lewis contacts: Paul A. Bartolotta, (216) 433–3338, Gary R. Halford, (216) 433–3265, and David L. Krause, (216) 433–5465

Fatigue Behavior of Haynes 188 Under Thermomechanical, Axial-Torsional Loading

It has been shown that multiaxial loading and thermomechanical loading can cause changes, relative to uniaxial isothermal loading, in the deformation and damage accumulation displayed by a material. Seldom have both multiaxial and thermomechanical loading been combined in a single experiment. The results of axial-torsional, thermomechanical fatigue experiments on thin-walled tubular specimens fabricated from the wrought cobalt-base superalloy Haynes 188 are shown in figure 1. The fatigue test matrix consists of uniaxial, thermally in-phase (TIP, maximum temperature coincides with the maximum mechanical strain) and thermally out-of-phase (TOP, maximum temperature coincides with the minimum mechanical strain) experiments; a torsional thermomechanical experiment; a mechanically in-phase (maximum axial mechanical strain occurs at the same point in time as the maximum torsional strain), thermally in-phase experiment (MIPTIP); a mechanically in-phase, thermally out-of-phase experiment (MIPTOP); a mechanically out-of-phase (maximum axial mechanical strain occurs when the torsional strain passes through zero), thermally in-phase experiment (MOPTIP); and a mechanically out-of-phase, thermally out-of-phase experiment (MOPTOP). In all the experiments, the imposed maximum and minimum temperatures and axial and torsional strain ranges were the same. Four multiaxial life models were used to predict the fatigue lives of these experiments. Using fatigue life parameters derived from previous axial and torsional experiments at the peak temperature, it was found that the Von Mises equivalent strain range and modified multiaxiality factor approaches predicted the thermomechanical fatigue lives somewhat better than both the Smith-Watson-Topper and the Fatemi-Socie-Kurath parameters. In general, the largest deviations from the experimentally observed lives were exhibited by the Fatemi-Socie-Kurath model.

Lewis contacts: Peter J. Bonacuse, (216) 433–3309 and Sreeramesh Kalluri, (216) 433–6727

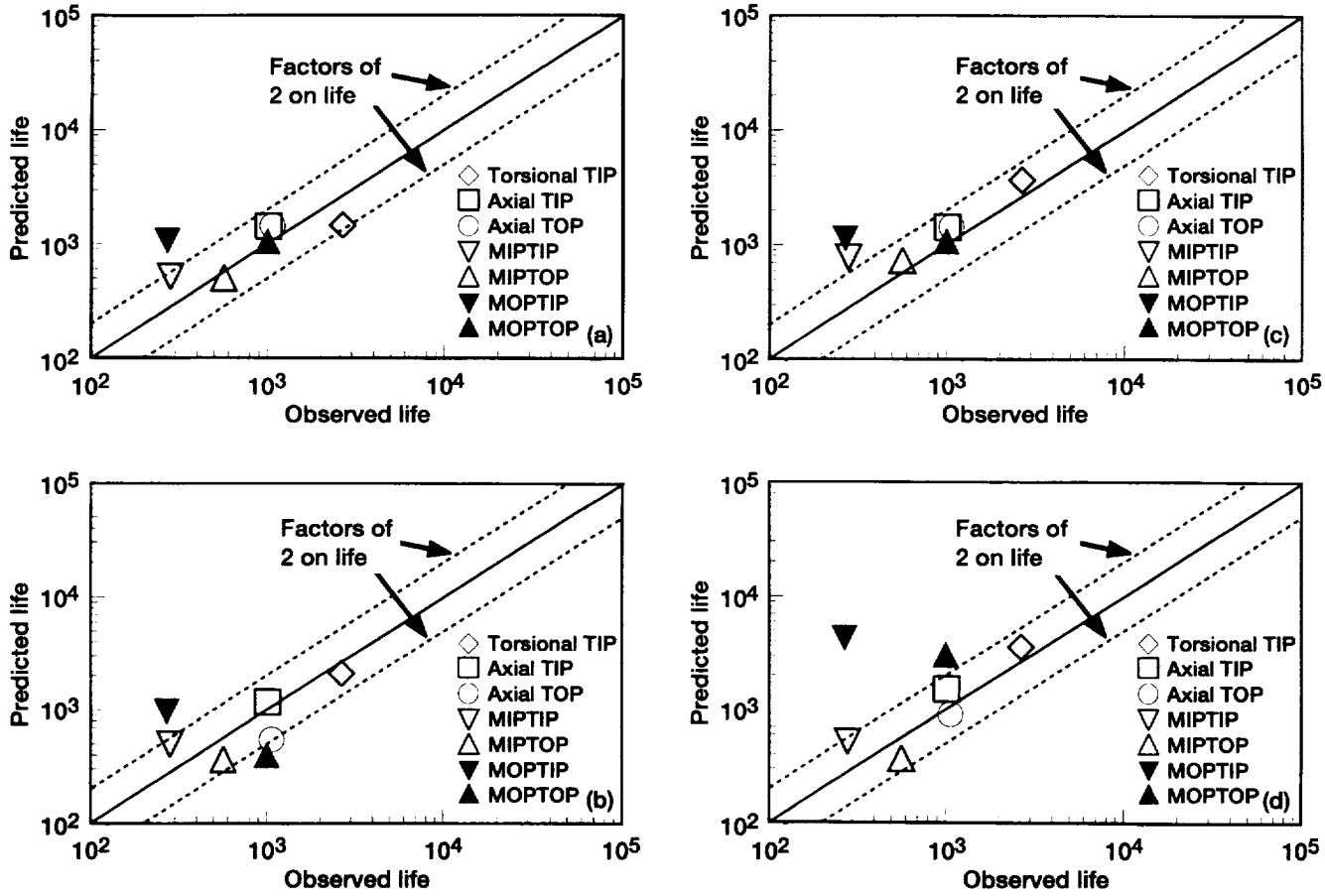

Figure 1.—Observed versus predicted fatigue lives for various fatigue life models. Thermomechanical, axial-torsional fatigue of Haynes 188. (a) Von Mises equivalent strain range model. (b) Smith-Watson-Topper model. (c) Modified multiaxiality factor approach. (d) Fatemi-Socie-Kurath model.

Retirement for Cause as an Alternate Means of Managing Component Lives

In the current budgetary environment, fielded equipment will often be used beyond its design life. To avoid the large cost of replacing critical rotating parts as they reach their safe-life limits, a retirement for cause (RFC) program may prove to be a cost-effective and safe alternative. Studies indicate that a full 80 percent of parts replaced at low-cycle fatigue (LCF) calculated safe-life limits have at least a full order of magnitude remaining fatigue life. The Air Force has embraced RFC and currently successfully uses it to manage parts life for several of their gas turbine engines. RFC involves periodic nondestructive evaluation (NDE) to access the damage state (whether or not detectable cracks exist) of components (fig. 1). Those components that do not have detectable cracks are returned to service. This approach allows low-life parts to be detected and discarded before they can cause an incident, and high-life parts to be used to their full potential. Although there are initial and ongoing costs associated with the procurement of the inspection equipment and the performance of the inspections, these costs have been more than offset by the savings in replacement parts. Basic to an RFC program is the calculation of crack growth rates under the expected service loads (mechanical and thermal). The results are used to define safe-use intervals between required (NDE) inspections. The starting crack size for the fracture mechanics analysis is a flaw that is just below the detection limit of the NDE technique employed. Crack growth in ductile materials is sensitive to loading sequence in that large-amplitude load excursions in the early

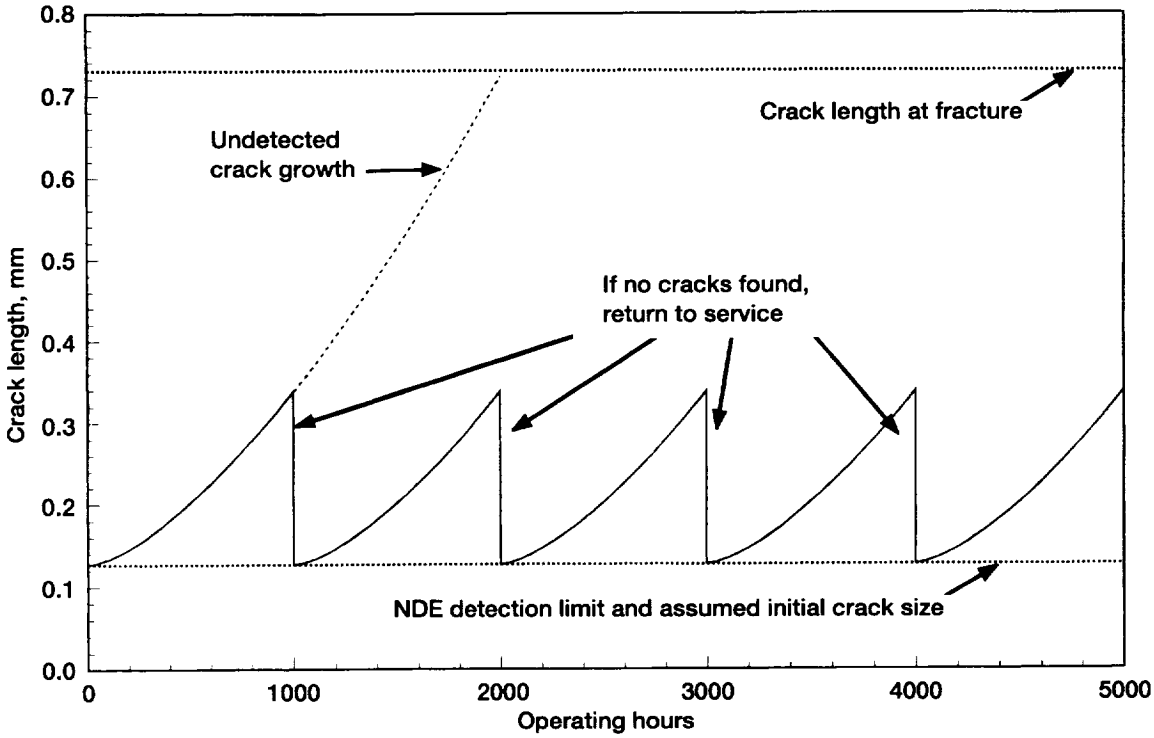

Figure 1.—Fatigue crack growth under retirement for cause (RFC) inspection regimen. Inspection interval, 1000 hr.

stages of crack formation can retard the crack growth rate whereas in the later stages of crack growth, these same overloads can lead to catastrophic failure. A population of components subjected to variable-amplitude loading will exhibit a distribution in crack growth lives (in excess of that observed in constant-amplitude loading). To accurately assess the component reliability, this variability must be characterized. A NASA/Army Research Laboratory (ARL) team is in the process of providing analytical support to Aviation and Troop Command (ATCOM) in the development of an RFC program for the T700–700 engine used in the Blackhawk helicopter. The FASTRAN-II fracture mechanics analysis code developed at NASA is being employed to estimate crack growth lives.

Lewis contacts: Pete Bonacuse, (216) 433–3309, Anthony Calomino, (216) 433–3311, Louis Ghosn, (216) 433–3249, Pete Kantzos, (216) 433–5202, Jane Mandersheid, (216) 433–3314, John Shannon, (216) 433–3321, and Jack Telesman, (216) 433–3310

Thermomechanical Deformation and Strain Rate Sensitivity of the Dynamic Strain Aging Alloy Haynes 188

Over the past several years, the Structural Fatigue Branch at the NASA Lewis Research Center has had an ongoing effort to develop a comprehensive high-temperature fatigue data base on the cobalt-base superalloy Haynes 188 as it has been consistently down-selected for use in many high-temperature structural aeronautics and space applications. These data are being used for both characterizing the alloy and for guiding the development and verification of deformation and damage models for this class of materials. Initial research of this alloy revealed that the high-temperature deformation behavior is extremely complex and strongly influenced by a number of interacting time- and temperature-dependent phenomena, such as inelastic flow, dynamic strain aging (DSA), and dynamic precipitation. Thus, to gain a thorough mechanistic understanding, examination of the material deformation behavior was pursued at the macroscopic (phenomenological) and microscopic (substructural) levels. To this end,

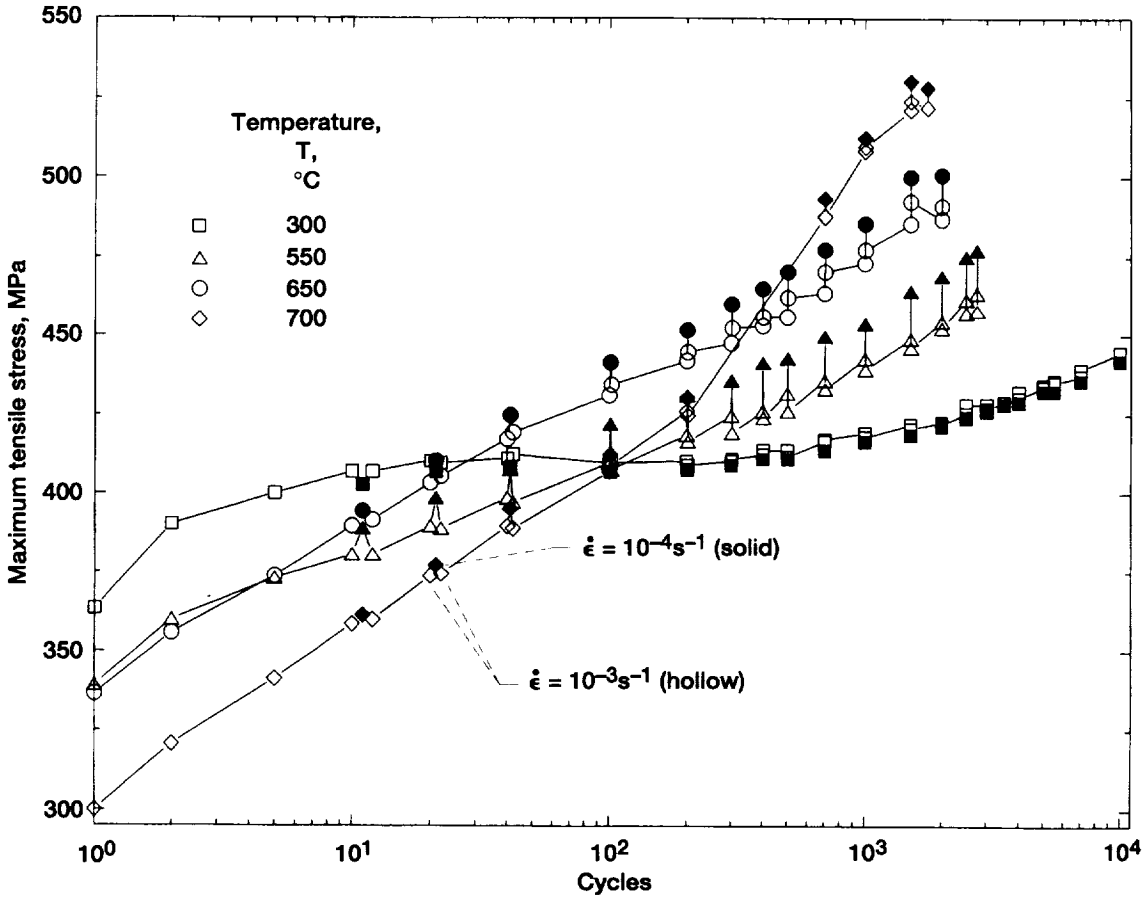

Figure 1.—Cyclic stress response during instantaneous strain-rate sensitivity tests with $\Delta\epsilon = \pm 0.4$ percent and $\dot{\epsilon} = 10^{-3}s^{-1}$ to $10^{-4}s^{-1}$.

a comprehensive effort was undertaken to evaluate the isothermal low-cycle fatigue (LCF) and thermomechanical fatigue (TMF) behavior of Haynes 188 over the temperature range 25 to 1000 °C at multiple strain rates.

To obtain insight into the macroscopic aspects of DSA during LCF loadings, the instantaneous strain rate sensitivity (ISRS) of the cyclic stress was examined by conducting instantaneous strain-rate-change tests at several temperatures. A negative ISRS is a well-documented phenomenon that is generally indicative of DSA. These tests were accomplished by periodically changing the strain rate $\dot{\epsilon}$ to $10^{-4}s^{-1}$ for one cycle and then returning it to the higher $\dot{\epsilon}$ of $10^{-3}s^{-1}$. Representative results from these tests (fig. 1) indicated that the ISRS was positive below 300 °C, was strongly negative between 400 and 650 °C, was slightly negative at 700 and 750 °C, and was positive again above 800 °C. The ISRS became substantially negative only in the temperature range where serrated yielding was also observed at both $\dot{\epsilon}$ values (i.e., 400 to 650 °C), thus possibly indicating that this is the true range over which DSA mechanisms are operative.

The evolution of tensile and compressive stresses under in-phase (IP) TMF conditions with various temperature intervals is given in figure 2 with each TMF test shown by two curves representing the two stress amplitudes that occurred at the maximum and minimum temperatures. In all the TMF tests, the maximum stresses achieved just prior to the onset of failure at the maximum temperatures of the cycles were comparable to those attained in corresponding isothermal LCF tests; however, the number of cycles needed to attain the maximum in each of the TMF tests was less. In contrast, the

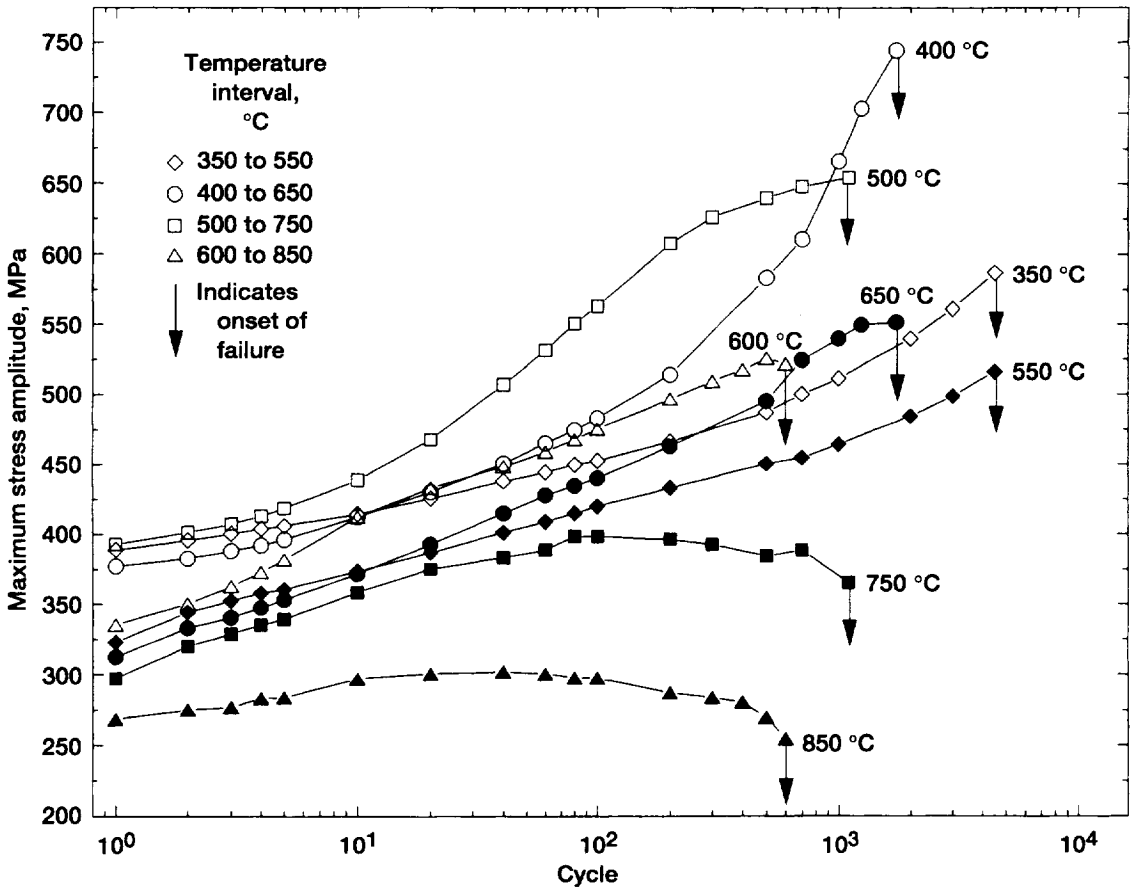

Figure 2.—Cyclic maximum (solid symbols) and minimum (absolute value) stress amplitude for in-phase thermomechanical fatigue (TMF) tests with $\Delta\epsilon = \pm 0.4$ percent and $\dot{\epsilon} = 10^{-4}s^{-1}$.

maximum stresses attained at the minimum temperatures in the TMF tests were not well represented by the corresponding isothermal LCF tests. In particular, the tests with ΔT = 400 to 650 °C, which is contained entirely within the DSA domain, experienced stress hardening at the 400 °C amplitudes, which was 65 percent greater than that experienced in the 400 °C LCF test. Even more noteworthy, this extreme TMF hardening exceeded the greatest hardening level achieved in the entire isothermal LCF data base (at 650 °C) by 35 percent. Thus, Haynes 188 clearly exhibits thermomechanical path-dependent behavior, indicating the need for such data during the process of developing and characterizing deformation theories intended to predict material behavior for this class of materials.

Lewis contacts: Michael G. Castelli, (216) 433–8464 and Rod Ellis, (216) 433–3340

A Study of Elevated-Temperature Testing Techniques for the Fatigue Behavior of PMC's

The development of polyimides and other advanced thermoset polymers has expanded the role of polymer matrix composites (PMC's) to elevated temperatures, such as airframe and propulsion system components, where severe operating environments are encountered. The use of PMC's in these harsh conditions has raised concerns relating to the degradation of the physical properties under simultaneous mechanical and environmental loads. Few studies have been published dealing with the high-temperature quasi-static and uniaxial fatigue behavior of polymer composites, and fewer still when thermochemical fatigue (TMF) testing is involved. Because of the limited number of studies and the wide array of objectives, a focused effort is required to develop experimental procedures for elevated-temperature (ET) uniaxial testing of PMC's.

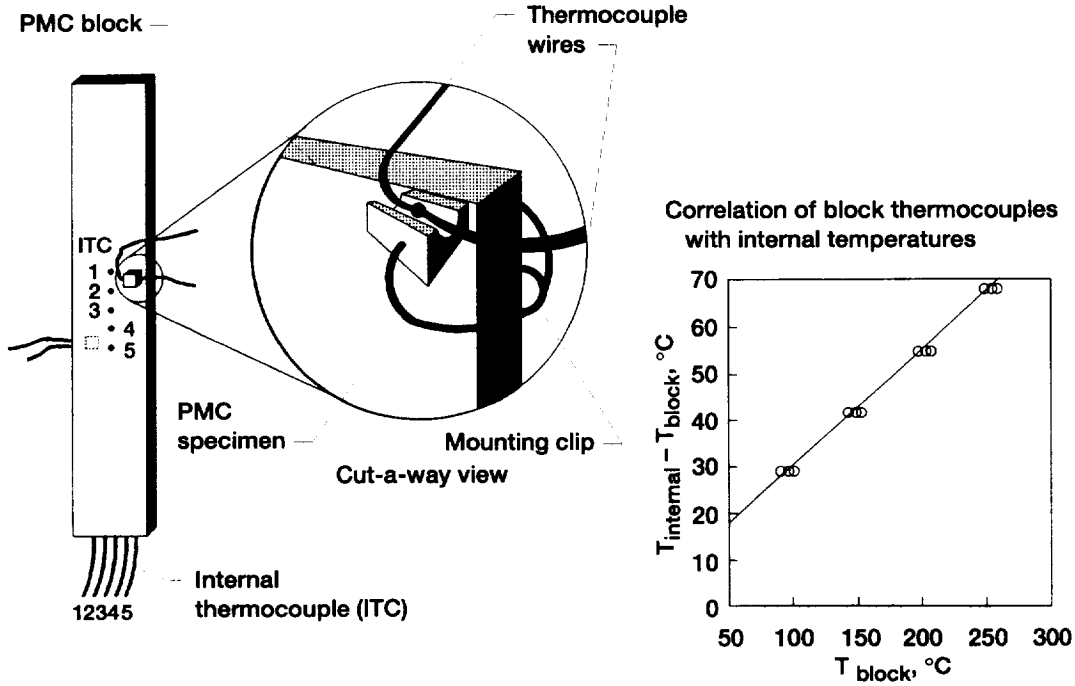

Figure 1.—Thermocouple block (used as controller) and correlation curve. The graph relates block to calibration specimen that contains internal thermocouples.

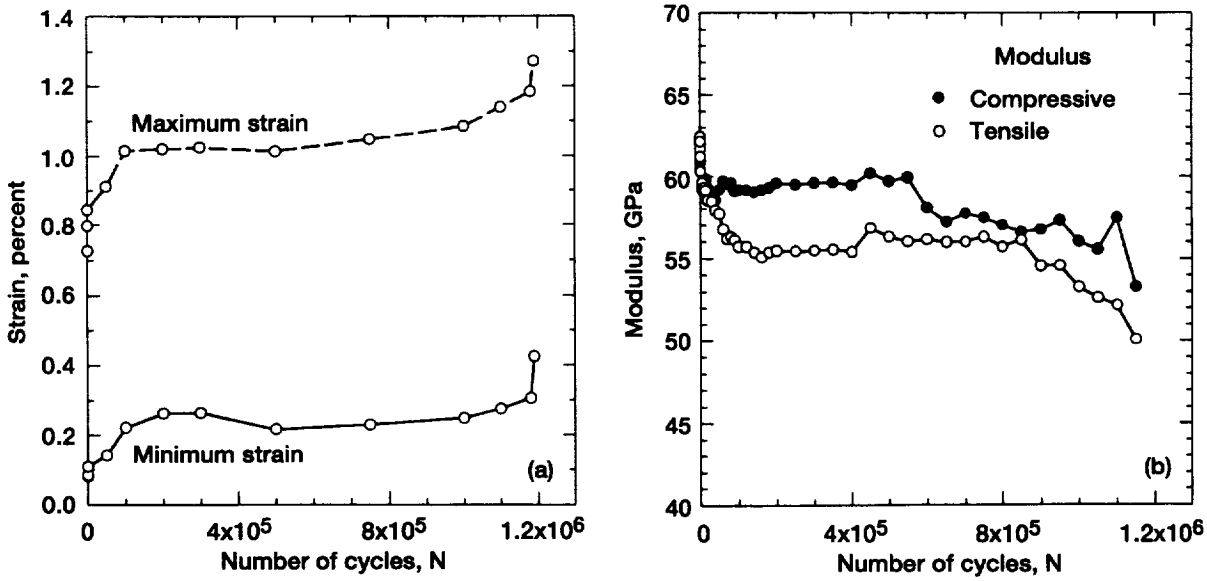

Figure 2.—Typical behavior of 255 °C fatigue specimen A10; $\sigma_{max} = 0.7\sigma_{ult}$; $R_\sigma = 0.1$; $N_f = 1189090$. (a) Strain ratcheting. (b) Static moduli degradation.

This technology is critical to the structural and long-term durability evaluations of PMC's and is currently undergoing transition to the Advanced Subsonic Technology Program (AST) in support of the PMC's static engine structures element. This investigation was conducted to evaluate experimental techniques for ET uniaxial mechanical testing of PMC's. To this end, the tensile and cyclic fatigue behavior of a carbon/polyimide eight-harness satin-weave system, T650–835/AMB21, was investigated. Isothermal fatigue tests ($R_\sigma = 0.1$) were conducted at 22 and 255 °C below T_G, glass transition temperature in an effort to resolve issues such as optimal specimen design, strain measurement techniques, and temperature control and measurement methods for quartz lamp heating

(employed for TMF capability). Finally, the subject of a measurable fatigue damage metric was addressed. Test procedures were implemented to measure the stiffness degradation and strain ratcheting that occurred during the fatigue tests. Such data are considered fundamental input for future life-prediction modeling efforts. Given the primary focus on ET experimental techniques for PMC's, only general trends in mechanical behaviors were examined. The results are summarized as follows: (1) an untabbed dog-bone specimen design was achieved with consistent gage failures; (2) an accurate temperature control and measurement technique was developed (figs. 1); and (3) post-processing of stress-strain data allowed for monitoring of fatigue damage through various moduli degradation curves and strain accumulation data (fig. 2). The static tensile and fatigue behavior of the material showed that the polyimide composite maintained its properties at 255 °C. The static ultimate tensile strength σ_{ult} displayed a reduction of only 4 percent at the elevated temperature (800 versus 772 MPa). Also, the fatigue behavior for these relatively short-term tests showed no significant differences between the two temperatures in cycles to failure for the load levels of 0.7, 0.8, and 0.9 σ_{ult}.

Contacts: Andrew L. Gyekenyesi, (216) 433–8155 and Michael M. Castelli, (216) 433–8464

Model Determined for Predicting Fatigue Lives of Metal Matrix Composites Under Mean Stresses

Aircraft engine components invariably are subjected to mean stresses over and above the cyclic loads. In monolithic materials, it has been observed that tensile mean stresses are detrimental and compressive mean stresses are beneficial to fatigue life as compared with a base of zero mean stress. Several mean stress models exist for monolithic metals, each differing quantitatively in the extent

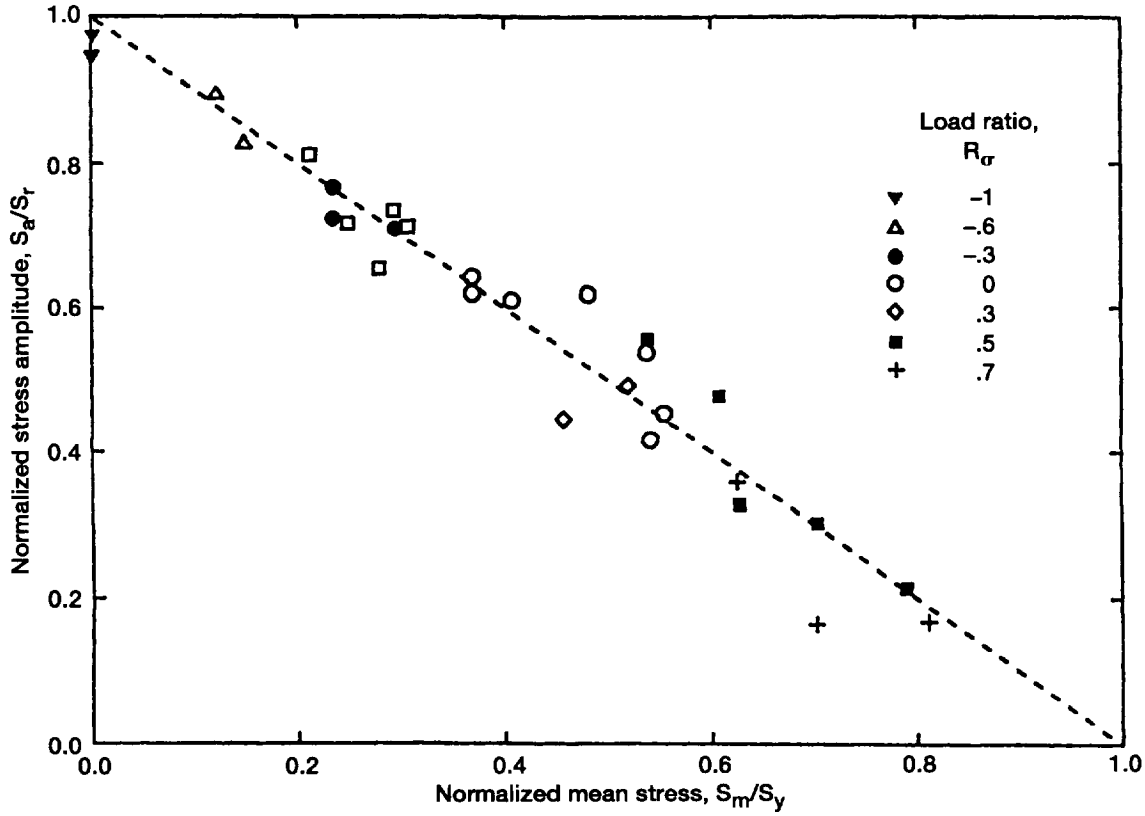

Figure 1.—Prediction of mean stress effects on fatigue lives of SiC/Ti-15-3 using Soderberg approach.

to which detrimental or beneficial effects are ascribed. There have been limited attempts to apply these models to metal matrix composites (MMC's). However, because most of the fatigue data has been limited to tension-tension loading, there has been a limited range of mean stresses over which models could be assessed. In this work, a unidirectional SiC/Ti–15–3 composite was tested with both tension and compressive stresses, thus extending the range of imposed mean stresses. The results showed that tensile mean stresses were detrimental and compressive mean stresses were beneficial to the fatigue lives.

Several mean stress models were examined for applicability to this class of composite materials. The models were Smith-Watson-Topper, Walker, Normalized Goodman, and Soderberg. The Soderberg approach, which normalizes the mean stress to the 0.02-percent yield strength, represented the effect of mean stresses best over the range covered (fig. 1). The other models had significant variation in their predictability and often failed to predict the composite behavior at very high tensile mean stresses. This work is the first to systematically demonstrate the influence of mean stresses on MMC's and to model their effects.

Attention was also given to fatigue-cracking mechanisms in the Ti–15–3 matrix and to micromechanics analyses of mean stress effects.

Lewis contacts: Brad Lerch, (216) 433–5522 and Gary Halford, (216) 433–3265

Oxidation Embrittlement Observed in SiC/SiC Composites

As part of a comprehensive materials characterization program, tensile creep-rupture tests were performed on a SiC fiber-reinforced SiC matrix composite. The results of these tests and subsequent analysis revealed an oxidation embrittlement phenomenon that occurs readily at a discreet temperature range below the maximum use temperature. Figure 1 shows rupture lives for a creep stress of 83 MPa as a function of temperature. Note that the rupture time is constant at an intermediate temperature range of 700 to 982 °C. Also shown in the figure is the failure location, as measured from the center of the specimen. Whereas failure occurred in the specimen gage section for temperatures of 500 to 700 °C, at

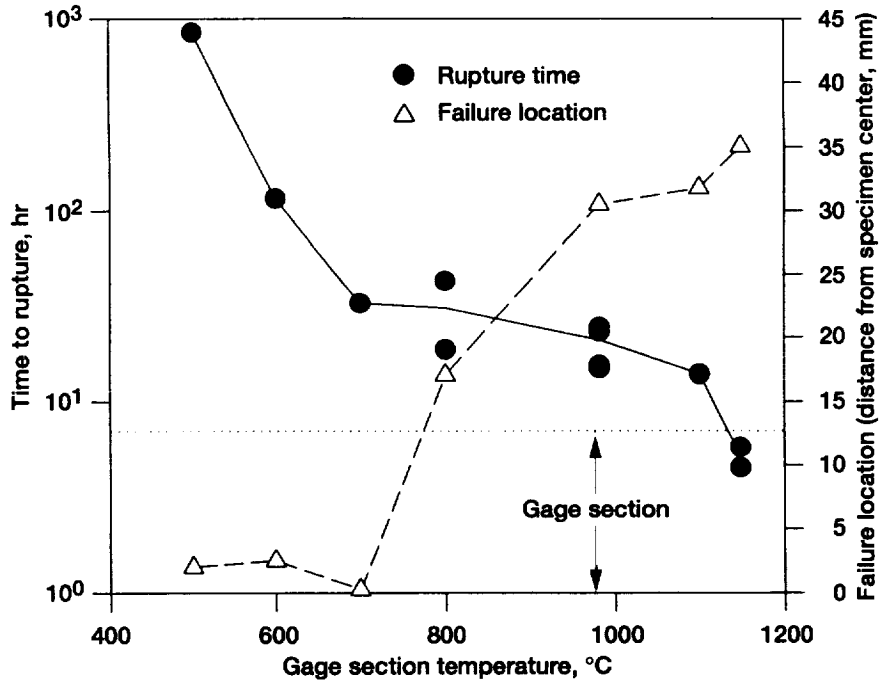

Figure 1.—Stress rupture data for [0/90] Dupont enhanced CVI SiC/Nicalon SiC composite as function of gage section temperature at creep stress of 83 MPa. Also shown is failure location as function of gage section temperature.

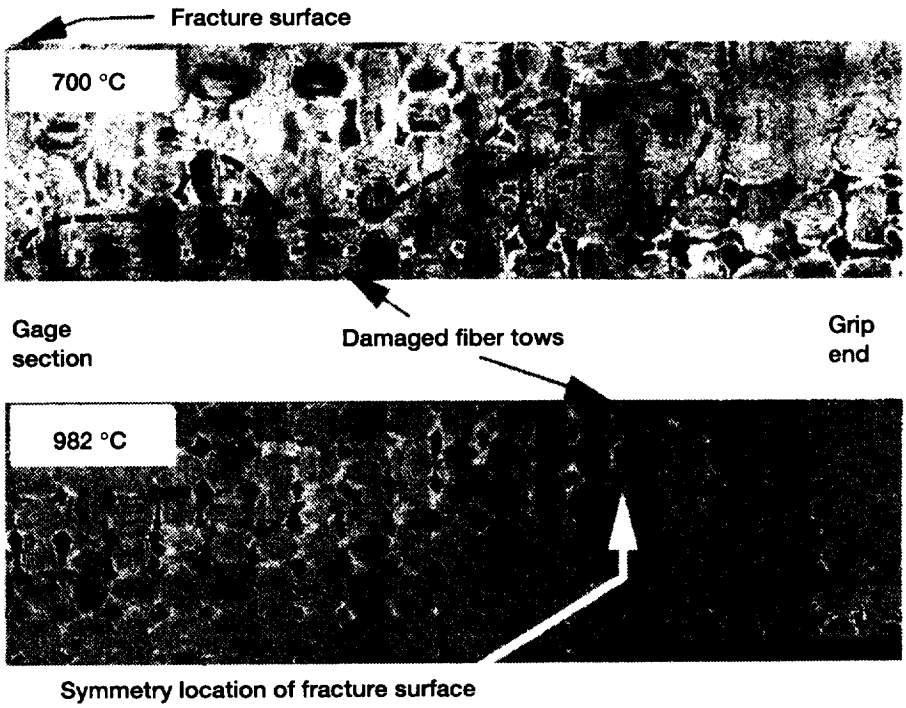

Figure 2.—Creep damage distribution of two [0/90] Dupont enhanced CVI SiC/Nicalon SiC specimens tested at stress of 83 MPa. Damaged fiber tows were found throughout gage section of 700 °C specimen. However, for the 982 °C specimen, damage was concentrated at point outside of gage section where temperature was 700 to 800 °C.

higher temperatures, the failure location migrated toward the cooled grip ends. Although the results initially suggested that the test procedure was influencing the measured creep-rupture lives and was also driving the failure location out of the gage section, subsequent additional experiments and a thermal stress analysis verified the robustness of the test method employed.

Metallurgical examination of failed specimens revealed an environmentally assisted material degradation operating in the temperature range of 700 to 800 °C. Figure 2 shows the damage distribution of two specimens tested at the same stress but at different gage section temperatures. The views shown in figure 2 are sections polished in the thickness direction, showing the broad specimen face. The loading direction is horizontal. In the 700 °C specimen, creep damage is distributed throughout the uniformly heated test section; however, in the 982 °C specimen, damage is concentrated only at the point outside the gage section where the temperature was 700 to 800 °C and less damage occurred within the hotter gage section. Both specimens failed because of an aggressive environmental attachment of the SiC fibers at a location where the temperature was in the 700 to 800 °C range.

SiC/SiC composites are candidates for a combustor liner application in the engine of the High Speed Civil Transport (HSCT). During its service cycle, the combustor liner will experience a thermal gradient, being cooled near attachment regions and exposed to combustor gases on the inner wall. The existence of a minimum in creep-rupture behavior over a discreet temperature range indicates that the kinetics of this process are unconventional. Thus, material properties must be well characterized over the temperature range of expected operation. Also, the design and lifing of components must account for this behavior.

Lewis contacts: Michael J. Verrili, (216) 433–3337, Anthony M. Calomino, (216) 433–3311, and David N. Brewer, (216) 433–3304

Structural Dynamics

Rotordynamics on the PC: Transient Analysis With ARDS

Personal computers can now do many jobs that formerly required a large mainframe computer. For example, the program ARDS (Analysis of RotorDynamic Systems) uses the component mode synthesis method to analyze the dynamic motion of up to five rotating shafts. As originally written in the early 1980's, this program was considered large for the mainframe computers of the time.

Written in Fortran 77, ARDS has been successfully ported to a 486 personal computer. Plots appear on the computer monitor via calls programmed for the original CALCOMP plotter; plots can also be output on a standard laser printer. The executable code uses the full array sizes of the mainframe version and easily fits on a high-density floppy disk. The program runs under DOS with an extended memory manager.

In addition to transient analysis of blade loss, step turns, and base acceleration, with simulation of squeeze film dampers and rubs, ARDS calculates natural frequencies and response to imbalance.

Some examples of ARDS-PC capability are seen in its use to analyze a magnetic-bearing-supported rotor as it experiences a sudden increase in imbalance or drops onto backup bearings. ARDS drew an outline of the configuration (fig. 1) of the small rotordynamics demonstrator rotor that was modeled with 9 elements, resulting in 10 rotor stations. Concentrated masses were attached to the shaft at five of the stations. An electromagnetic bearing was at station 3 and a bronze bushing supported the shaft at station 8. Magnetic bearings are customarily used with backup bearings that can support the rotor in the event of magnetic bearing failure. For the present example, a backup bearing in the form of a loose bushing was modeled in addition to the magnetic bearing at station 3. No contact occurs in the backup bearing during normal (magnetically suspended) operation; the backup bearing is therefore nonlinear in that the stiffness is zero until the radial clearance is taken up. It was then assumed to have a constant stiffness in the radial direction; the tangential force was calculated as the radial force times a friction coefficient. This bearing model was built into ARDS. Each computer run used 100 time steps per revolution; on the 50-MHZ 486 computer, 4000 time steps took slightly less than 2 min of calculation time.

A blade loss in a turbine engine introduces a sudden imbalance that can be many times the normal operating imbalance. Under this condition, the magnetic bearing supporting the rotor can become overloaded such that the backup bearing comes into

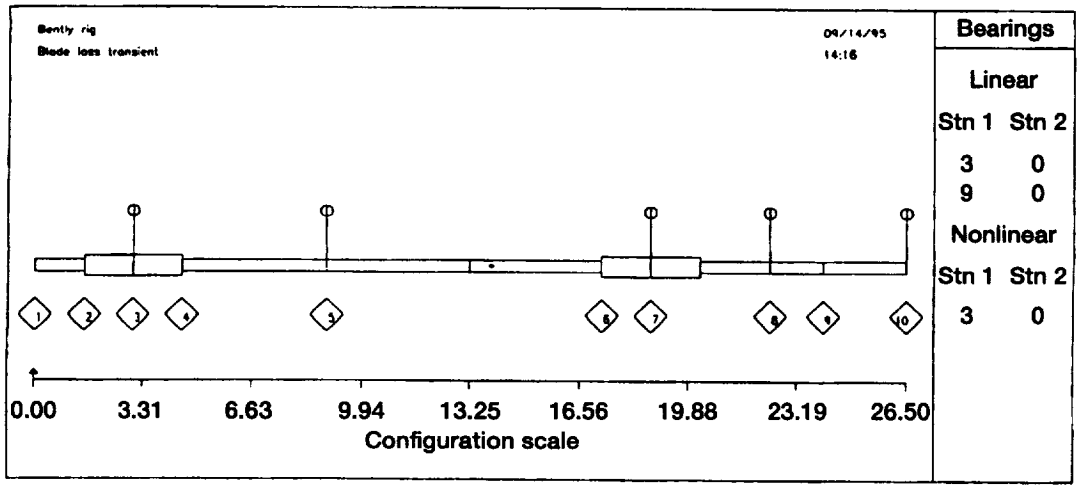

Figure 1.—ARDS drawing of example rotor.

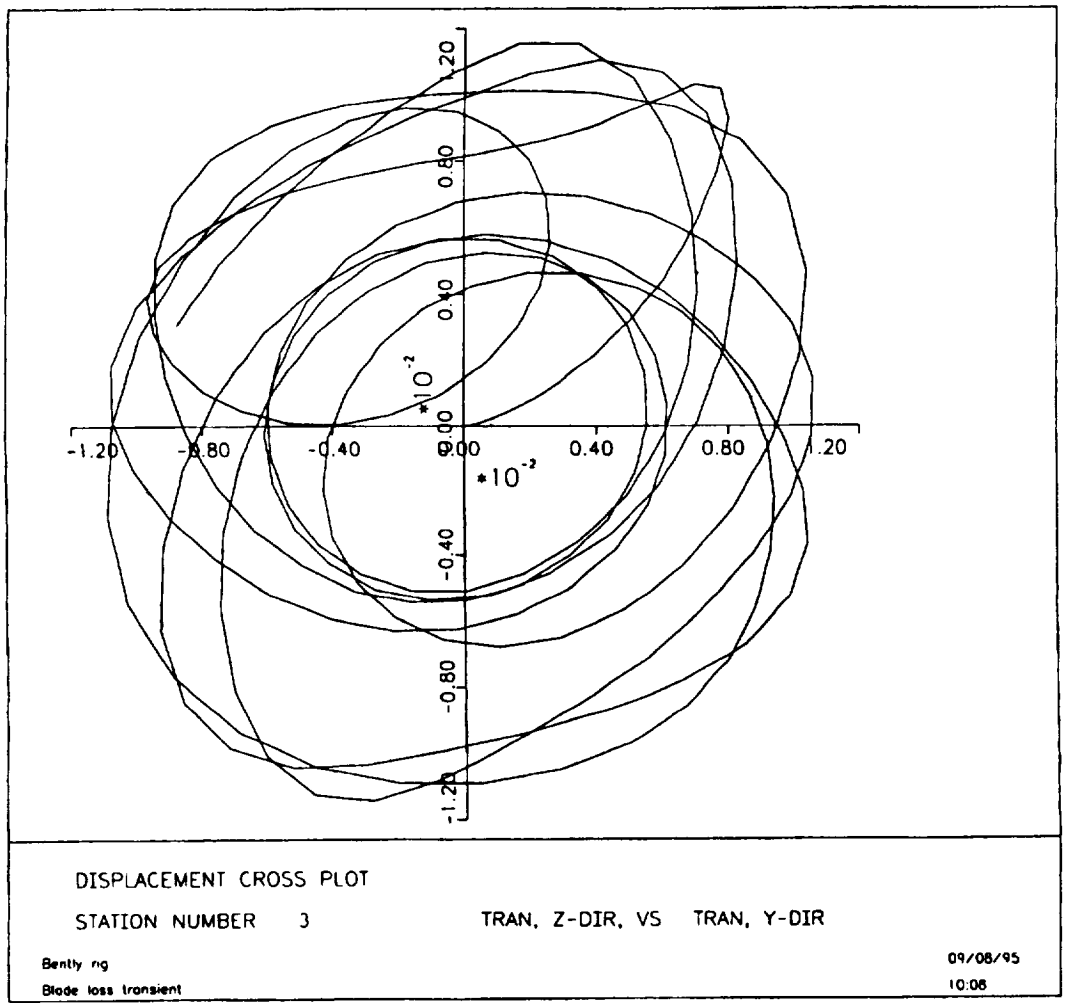

Figure 2.—Orbital motion of magnetic and backup bearing for sudden imbalance.

operation. The situation as the bearing makes contact is similar to that of a turbine wheel contacting its outer shroud. Figure 2 shows 10 revolutions of a blade-loss transient. The imbalance is applied to the rotor at station 5. A friction coefficient of 0.4 was assumed for the backup bearing; the linear magnetic bearing is also active. Figure 2 is an orbital plot of the rotor at station 3, the magnetic bearing location, and shows that the rotor flies out, hits the backup bearing, bounces off, and repeats this behavior for the entire time period plotted.

Figure 3 plots the dynamic behavior of the rotor when the magnetic support fails and the rotor drops onto the backup bearing. The rotor walks up the side of the bearing, although the more sensitive scale for the horizontal axis in figure 3 exaggerates the motion. The vibratory motion eventually dies down.

In the analysis, excitation forces can be combined; for example, a turn in combination with blade loss and base acceleration.

Lewis contact: David P. Fleming, (216) 433–6013

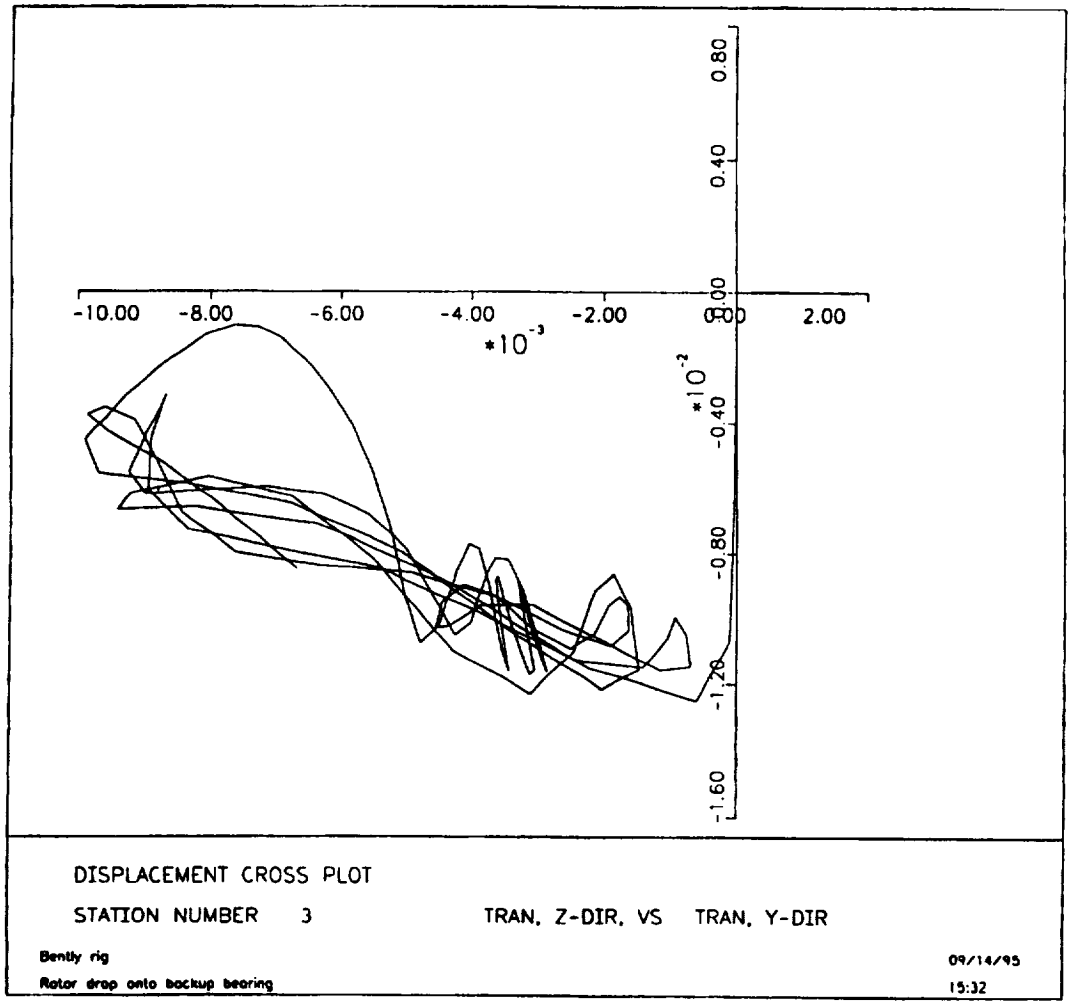

Figure 3.—Rotor drop onto backup bearing.

A Magnetically Sealed Bearings System

The goal of this project is to develop a retainerless, noncontacting magnetically sealed bearing that can be directly substituted for current satellite bearings. Bearings are becoming life-limiting components in long-duration satellite missions. Typically bearings are poorly sealed, resulting in premature failure by lubricant loss and contamination of instrument sensors by lubricant vapor. Current bearings also can cause mechanical noise when the ball retainer rubs or jams against the raceways. This project focuses on the development of a bearing for use in satellite scanning mechanisms.

The magnetically sealed bearing will use permanent magnets and a magnetic fluid to form a complete seal on both external faces of the bearing. The ball retainer will be eliminated and the ball pocket will be flooded with liquid lubricant. Ceramic balls will be utilized with metal raceways. Both the magnetic fluid and the liquid lubricant will have low vapor pressure characteristics.

Three major milestones for the first year were the development of a magnetic fluid, the design of first-generation bearing prototypes, and the tribological testing of the magnetic fluid. The development of the magnetic fluid was conducted in conjunction with the largest U.S. magnetic fluid production company. A special hydrocarbon-based fluid was designed and synthesized. The hydrocarbon base was NYE–2001, a newly developed, extremely low-vapor-pressure space lubricant. Two magnetic strength levels of fluid were developed: 100- and 400-G-saturation magnetization, designated N100

and N400. No existing magnetic fluids met the requirements for this system. The successful completion of this milestone provided the enabling technology for this project.

The design of first-generation bearing prototypes resulted in four different concepts. A 40-mm-bore bearing size was chosen for the first designs. This bearing is larger than the scanner bearing, enabling easier testing at this stage. Second-generation prototypes will be based on the MPB 17-mm-bore scanner bearing. Three of the four bearing designs utilize the fully flooded concept whereas the final bearing is only lubricated on the wear track. Bearings using magnets with both axial and radial magnetization were designed. One prototype was designed to reuse the magnetic rings after the bearing failed. All the bearings have been fabricated and the assembling and preliminary testing have begun on two of the designs.

A pin-on-disk tribometer was used for the tribological testing that was conducted to determine the effect of magnetic fluid migration into the wear region. Eight fluids were tested: four existing magnetic fluids, the two fluids developed for this program, the NYE-2001 base oil used in the magnetic fluid, and the current liquid lubricant used in space. The results showed that the base oil performed best; however, the N100 magnetic fluid outperformed all other fluids, including the current space lubricant.

We have successfully met all the first-year milestones. Three goals for the second year are (1) two test rigs must be constructed, one for seal pressure testing and one for bearing tests; (2) the existing bearing prototypes must be tested, and the second-generation prototypes need to be designed and fabricated; (3) a technology transfer agreement with ITT Aerospace needs to be formulated.

Lewis contact: Ralph Jansen, (216) 433-6038

An Active Magnetic Bearing With High-Temperature Superconductor Coils and Ferromagnetic Cores

A proof-of-feasibility demonstration showed that high-temperature superconductor (HTS) coils can be used in a high-load active magnetic bearing in liquid nitrogen (figs. 1 and 2). A homopolar radial bearing with commercially wound HTS (Bi 2223) bias and control coils produced a radial load capacity of over 890 N (200 lb) (measured non-rotating) and supported a shaft to 14 000 rpm. The

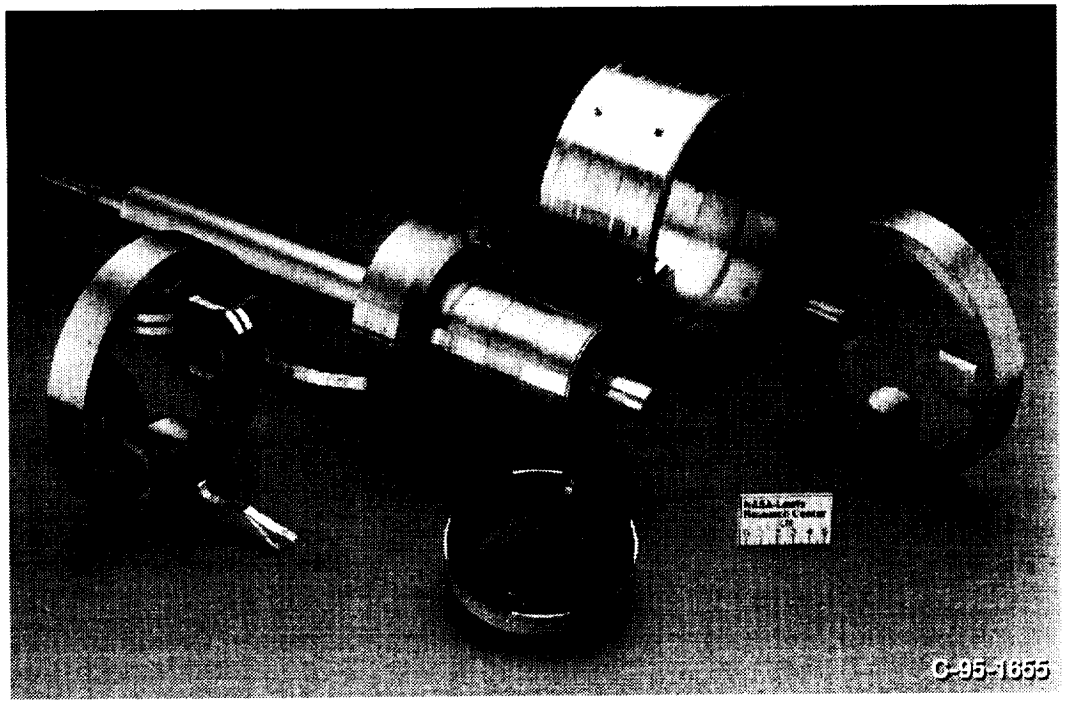

Figure 1.—Components of high-temperature superconducting magnetic bearing.

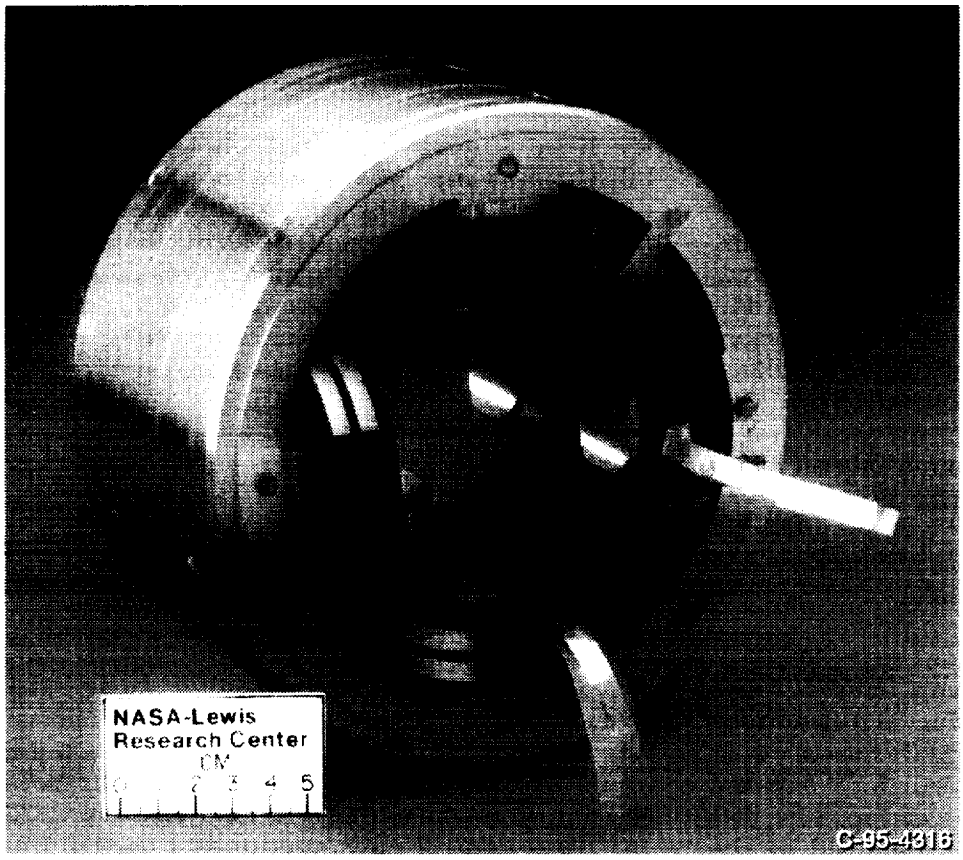

Figure 2.—Stator assembly of high-temperature superconducting magnetic bearing.

goal was to show that HTS coils can give stable operation with ferromagnetic cores in a feedback-controlled system at a current density similar to that for copper in liquid nitrogen.

The bias coil, wound with a nontwisted multifilament HTS conductor, dissipated negligible power for its direct current. The control coils, wound with a monofilament HTS sheathed in silver, dissipated negligible power for direct current. Alternating-current losses increased rapidly with frequency and quadratically with ac amplitude. Above about 2 Hz, the effective resistance of the control coils exceeds that of the silver which is in electrical parallel with the oxide superconductor. These results show that a twisted multifilament conductor is not needed for stable levitation but may be desired to reduce control power for sizable dynamic loads.

This type of bearing could have application in cryogenic rocket turbopumps and possibly in future cryogenically fueled (e.g., liquified natural gas or slush hydrogen) aircraft turbine engines. Large HTS electric motors being developed for industrial applications could have HTS magnetic bearings because the cryogenic cooling would already be present.

High-temperature superconductor technology has already improved since the coils for this bearing were purchased and much higher current density is already possible; hence, still more compact coils are now possible, allowing cryogenic magnetic bearings to be either more compact or stronger.

Lewis contacts: Gerald Brown, (216) 433–6047, Eliseo DiRusso and Andy Provenza, (216) 433–6025

Application of Magnetic Bearing to Dynamic Spin Rig

The Lewis Research Center's Dynamic Spin Rig, located in building 5, test cell CW–18, is used to test turbomachinery blades and components by rotating them in a vacuum chamber. The rotor is supported by two mechanical bearings, and during rotation it is vibrated by voice-coil-type linear electromagnetic shakers to obtain natural frequencies of blades. As an alternative exciter, a magnetic bearing was incorporated in the rig. The operation of the magnetic bearing as an exciter was successful and compared favorably with the electromagnetic shakers.

The rig was modified to allow the magnetic bearing to operate not only as an exciter but as a fully functioning magnetic bearing. The magnetic bearing provided support for the rotor at one end that had previously been supported by a mechanical bearing. Additionally, the magnetic bearing provided active control of stiffness and damping at the point of action. Testing yielded successful magnetic bearing operation for rotational speeds up to 9000 rpm in a vacuum, with control gains producing stiffness up to 60 000 lb/in. (67 818 N/mm). Plans are to replace the second mechanical bearing with a magnetic bearing.

Lewis contacts: Dexter Johnson, (216) 433–6046, Oral Mehmed, (216) 433–6036, and Gerald Brown, (216) 433–6047

Measurement of Gust Response on a Turbine Cascade

Benchmark experimental data on the gust response of an annular turbine cascade are presented. The experiment was particularly designed to provide data for comparison with the results of a typical linearized gust response analysis. Reduced frequency, Mach number, and incidence were varied independently. Except for the lowest reduced frequency, the gust velocity distribution was nearly sinusoidal. For the high-inlet-velocity series of tests, the cascade was near choking. The mean flow was documented by measuring blade surface pressures and the cascade exit flow. High-response pressure transducers were used to measure the unsteady pressure distribution. Inlet-velocity components and turbulence parameters were measured using a hot wire. In addition to the synchronous time-average pressure spectra, typical power spectra are included for several representative conditions.

The gusts were generated by a rotor consisting of pins having either a 3.17- or a 4.7-mm diameter. The number of pins on the rotor was either 6, 12, or 24, which resulted in gust reduced frequencies of 2.5, 5, and 10. The annular turbine cascade had 24 blades and was positioned 3.9 axial chord lengths behind the rotor. Figure 1 illustrates the instrumentation port locations, and the representative root-mean-square (rms) spectra are illustrated in figure 2. The synchronous peaks in this figure could also have been obtained using linear phase-lock averaging; however, the rms-averaged spectra also include the nonsynchronous origin and the random pressure fluctuations. The frequency units are engine orders; thus, the synchronous peaks appear at the frequency equal to the number of rotor pins used to generate wakes. The position-axis units correspond to blade port numbers in figure 1; thus, position 0 corresponds to the port nearest to the leading edge on the suction

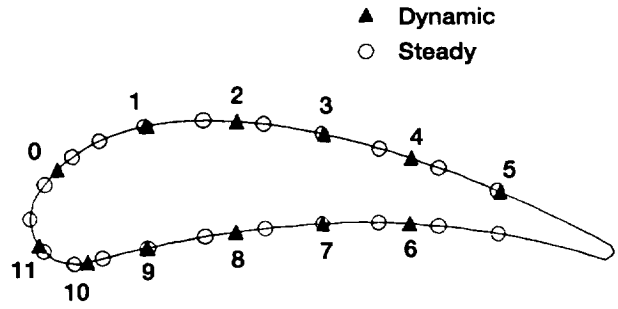

Figure 1.—Instrumentation ports.

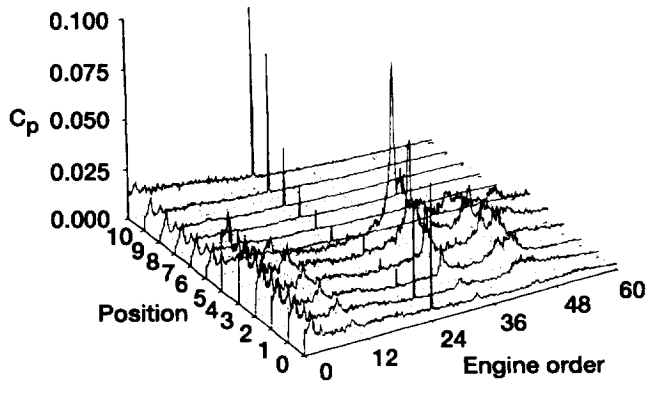

Figure 2.—Root-mean-square pressure spectra. (a) Reduced frequency, ω, 10; inlet Mach number, M_1, 0.27; positive incidence, $\beta_2 > 0$.

surface side, and 11 corresponds to the port nearest to the leading edge on the pressure side.

The gust amplitude varied somewhat with the reduced frequency; however, it did not appear to have a dominant effect. Unsteady, synchronous-response blade pressures are strongly dependent on reduced frequency and incidence. Mach number dependence is weak for negative incidence and significant for positive incidence at lower reduced frequencies. The mean blade pressure distribution is to some extent dependent on the reduced frequency, particularly for the negative incidence and the higher inlet Mach number. At a reduced frequency of $\omega = 10$, an inlet Mach number of $M_1 = 0.27$, and a positive incidence $\beta_2 > 0$, a magnification of the turbulent pressure fluctuations on the suction side of the aft portion of the blade resulted in a significant excitation concentrated at an integral engine order much higher than the synchronous excitation frequency.

Lewis contacts: Anatole Kurkov, (216) 433–5695 and Barbara Lucci, (216) 433–5902

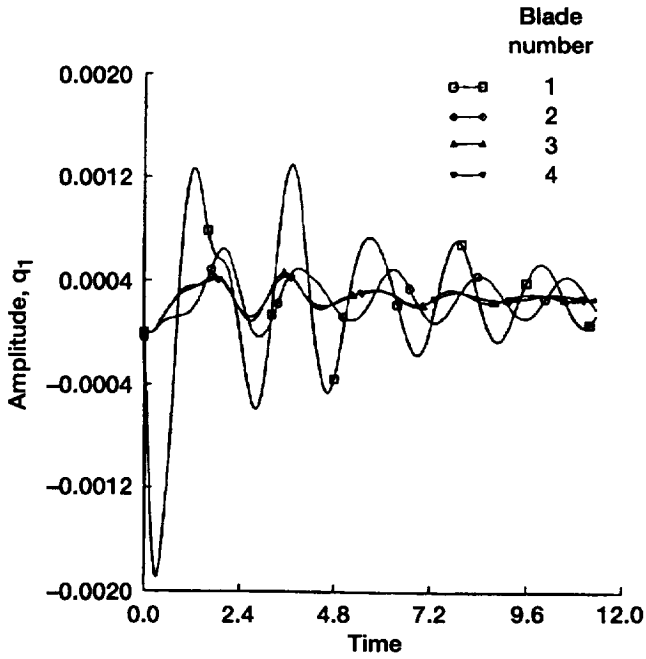

Figure 1.—Response of rotor blades for tip gap = ∞ (unducted rotor). Free-stream Mach number, M_∞, 0.5; advance ratio, J, 3.55; setting angle, β, 61.2°.

Flutter Analysis of Ducted Rotors

An aeroelastic analysis procedure (DuctE3D) was developed to investigate the flutter of turbomachine configurations. In the analysis, the unsteady air loads on vibrating blades are obtained by solving three-dimensional unsteady Euler equations, and the blade structural properties are obtained from a three-dimensional finite element model. The duct is assumed to be infinitely long and structurally rigid. Any number of structural modes of blade vibration can be included in the analysis. The aeroelastic equations are formulated in normal mode and are solved for flutter in the time domain, allowing the analysis of all possible interblade phase angles. For verification, the analysis is applied to a ducted fan configuration.

The three-dimensional Euler equations are solved using an implicit-explicit hybrid scheme. The scheme results in a large saving of CPU time as well as of memory requirements because only two matrix inversions are required as opposed to three for fully implicit schemes. The structural analysis is carried out using the normal mode approach, assuming the hub and duct to be rigid. The flutter analysis is carried out by perturbing the blades from steady state and solving the combined aeroelastic equation, aerodynamic and structural, in a sequential fashion while marching in time. The response of the blades to initial perturbation is calculated. Increasing the amplitude of the response implies instability. Any number of normal modes can be included in the analysis. Further, no knowledge of interblade phase angle or flutter frequency is required a priori. A single run is sufficient to provide information on the blade aeroelastic characteristics for the particular flight condition. The response of the blades may be Fourier analyzed to provide flutter frequency and interblade phase angle.

The analysis was applied to an eight-bladed ducted fan obtained by enclosing the SR3C–X2 propfan in a rigid cylindrical duct. The SR3C–X2 propfan, in the unducted configuration, showed flutter in the the NASA Lewis Research Center wind tunnel tests at a free-stream Mach number M_∞ of 0.6 for the eight-bladed configuration operating at an advance ratio J of 3.55 and a setting angle β of 61.2°. The analysis was conducted at $M_\infty = 0.5$ using the first three normal modes for two different tip gaps (1 and 0.4 percent of the rotor radius) and the unducted configuration. The analysis showed the

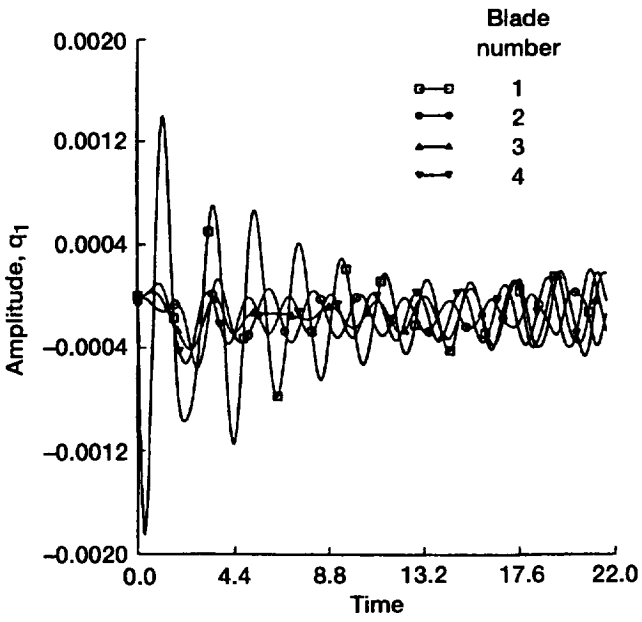

Figure 2.—Response of rotor blades for tip gap of 1 percent. Free-stream Mach number, M_∞, 0.5; advance ratio, J, 3.55; setting angle, β, 61.2°.

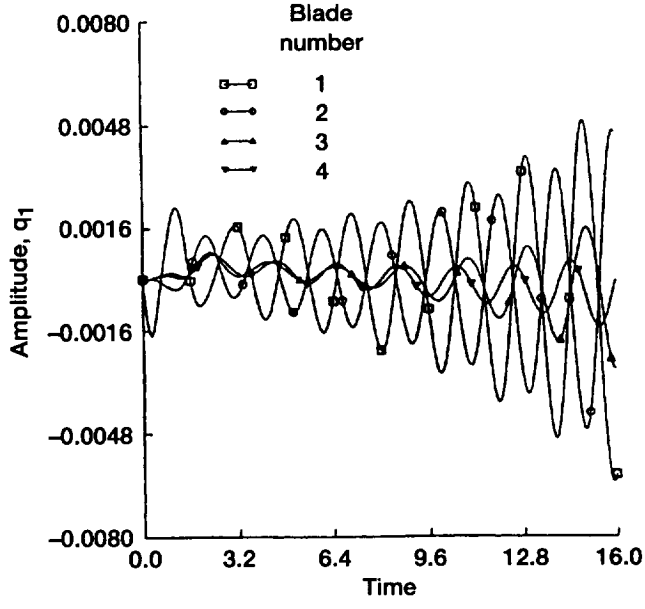

Figure 3.—Response of rotor blades for tip gap of 4 percent. Free-stream Mach number, M_∞, 0.5; advance ratio, J, 3.55; setting angle, β, 61.2°.

rotor in the unducted configuration to be stable at M_∞ = 0.5, correlating with the experimental observation. The initial perturbations died out rapidly with the decaying response of all the blades. The response is shown in figure 1 for only the first normal mode response of the four blades. A similar response was observed for other modes and the other four blades. The analysis for the tip gap of 1 percent indicated the rotor to be marginally unstable. The first mode response of four of the blades is shown in figure 2. For the configuration with a 0.4-percent tip gap, the initial perturbation of one blade results in a rapidly increasing response in all the blades, indicating a flutter instability. The response for this case in shown in figure 3. These calculations show that the presence of the duct changed the aeroelastic characteristics of the rotor.

Lewis contacts: R. Srivastava, (216) 433–6045 and T.S.R. Reddy, (216) 433–6083

Fan Blade Deflection Measurement and Analyses Correlation

Steady deflection measurements were taken of a NASA/Pratt & Whitney fan blade design while it was rotating in a vacuum in the Lewis Dynamic Spin Facility. The 1/5-scale fan blades had a tip diameter of 22 in. (55.88 cm), a pin-root retention, and a spar-shell construction. The purpose of the test was to measure the radial deflection of the blade tip and the blade angle change at selected radial stations along the blade span. The fan blades were unducted for the test. The procedure for radial deflection measurement had no precedent and was newly developed for this test.

The data were compared with analytical predictions made at NASA Lewis. Radial deflection measurements were used to assure that adequate tip clearance existed between the fan blades and the duct for a follow-on wind tunnel test. Also, blade angle deflection measurements were desired before pitch-setting parts for the wind tunnel test were finish machined.

Laser beams were aimed across the blade path at photodiodes, the signals of which were used to determine blade angle change or tip radial deflection. These laser beams were set parallel to the spin axis at selected radial stations.

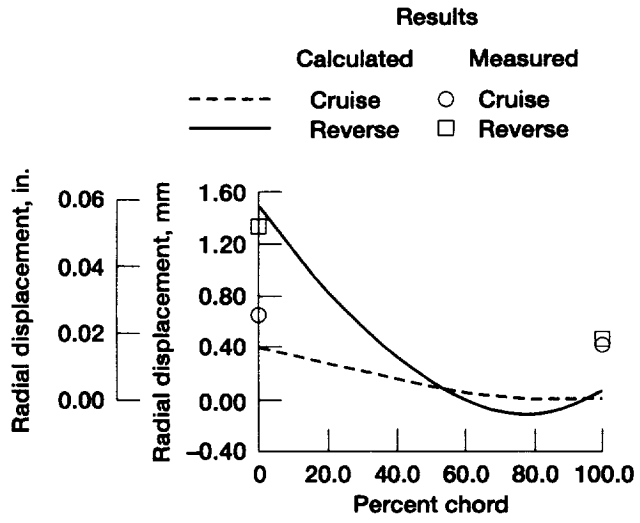

Figure 1.—Measured and calculated blade tip radial displacements at 10 000 rpm.

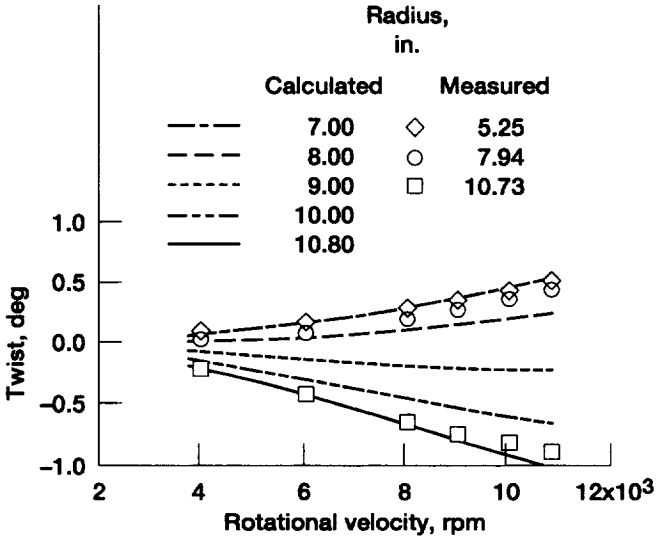

Figure 2.—Measured and calculated blade twist at cruise.

Some results from the test are shown in figure 1, which compares measured and calculated values for tip radial deflection at 10 000 rpm for the cruise and reverse staggers, and in figure 2, which shows the measured and calculated change in blade angle versus the rotational speed for the cruise stagger measured at three radial stations.

Lewis contacts: Oral Mehmed, (216) 433–6036, Dave Janetzke, (216) 433–6041, and Anatole Kurkov, (216) 433–5695

Space Mechanisms Lessons Learned Study

A Space Mechanisms Lessons Learned Study was conducted (1) to determine which mechanisms have worked in the past and which have failed and (2) to insure against a U.S. corporate memory loss with regard to building space mechanisms (mechanical moving components) for long life and reliability. A large number of satellite failures and anomalies have occurred recently (e.g., Galileo and Hubble). In addition, because of more demanding operating requirements, failures or anomalies have occurred during the qualification testing of future satellite and space platform mechanisms, even before they were launched (GOES-NEXT, CERES, Space Station Beta Joint Gimbal, etc.). For these reasons, it was imperative to determine what worked and what failed so that the best selection of mechanical components could be made and to make timely decisions on initiating research to develop any needed technology. Thus, the purpose of this study was to capture and retrieve information relating to the performance of mechanical moving equipment operating in space to determine which components have operated successfully and which have produced anomalies such as those listed in table I.

Data were obtained from various sources: (l) an extensive literature review that included government contractor reports and technical journals; (2) communication with and visits to (when necessary) the various NASA and DOD centers and their designated contractors, including contact with project managers of current and prior NASA satellite programs as well as with their industry counterparts. Unpublished information was then requested from NASA and industry. (4) A mail survey was designed to establish specific mechanism experience and also to solicit opinions of material to be included in a future Space Mechanisms Design Guidelines Handbook.

The majority of the work was done at Mechanical Technologies Inc. (MTI) under contract NAS3–27086.

Lewis contact: Robert L. Fusaro, (216) 433–6080

TABLE I.—MECHANICAL ANOMALIES IN SPACECRAFT

System	Conditions	Problem	Impact
Momentum wheel spin bearing	Grease-packed bearings; 3600 rpm, room temperature to 100 °F	Torque/temperature anomalies	Single-point mission failure; possible indication of failure
Sensor support bearing	Preloaded ball bearings; oscillatory motion	Failure in test	>$500K for additional testing
Sensor launch clamp	Located inside craft; thermal blanketed	Seizure on launch pad	Single-point failure; launch prohibited or mission failed
Harmonic drive ATP control	Fluorocarbon lubricant; very low speed; temperature <1 to 50 °F; boundary condition	Excessive wear; lubricant failure in test	Degraded mission or possible mission failure; changed lubricant
Sliprings, brush contacts	MoS_2/Ag/C brushes on Ag rings; numerous recurrences	Excessive electrical noise due to moisture and corrosion	Inability to point communications antennas; reduced mission objective
Potentiometer for ATP control	Low-temperature, light-load fluid lubricant	Electrical noise and open circuit due to lubricant thickening	Mission reduced due to loss of pointing; ~$500K for additional testing
Control moment gyroscope	Oil injection on bearing land	Bearing failure; lubrication design wrong	Premature mission failure
	Very high torque for slewing	Bearing failure	Loss of mission; >$1M for additional testing and annealing
Momentum wheel	Grease-lubricated	Torque and temperature anomalies	Possible mission failure
Propellent pump gearbox	High speed	Contractor switching lubricants	Possible launch failure with new lubricant
Sliprings, brush contacts	MoS_2/Ag/C brushes on Ag rings	Excessive noise due to oxidation of MoS_2	Reworking of brushes and rings; delivery delay
Gear mechanism	Fluorocarbon grease; high loads; boundary conditions	Lubricant degradation	System failure
Synchronous motor assembly	Mineral-oil-grease-packed bearings	Motor failure due to increased bearing drag	Degraded mission due to failure
Momentum wheel spin bearings	Mineral oil grease; high speed	Possible lubricant degradation in testing	Single-point mission failure
Inertial guidance synchronous motor bearing	Mineral oil grease; high speed	Possible chemical reaction between grease and iron surface during storage	Guidance failure
Harmonic drive	Fluorocarbon grease; low-temperature operation	Excessive torque caused by low-temperature viscosity of grease	Degraded mission due to failure
Momentum wheel active lubrication system	High-speed, long-life requirement	Inability to deliver adequate lubricant quantity	Lifetime requirement not met by system
Solar Array Deployment Mechanism (SADM)	Large launch loads on MoS_2-lubricated bearings	Testing of static loads	Possible single-point failure; passed test
Gimbal bearings on telescope	Dry MoS_2 lubricant; low temperature	Friction increase due to testing in air	Modified specification to do inert gas test; passed
Spin bearing	Large-diameter, thin-cross-section bearing	Humidity-induced dimensional instability of cotton-phenolic retainer	Possible target acquisition failure; changed to metal ball separator
Gas bearing, gyroscope	Alumina surfaces, stearate lubricant	Erratic friction on startup; uneven lubrication during testing	Reliability problem for flight units; major rework if failure
Foil bearings for turbomachinery	High-strength alloy; CF_x-polyamide lubricant; temperature extremes	High-friction startup after standing	Potential system failure; inability to start turbine

Alternative Operating Modes for Magnetic Bearing Control

Most magnetic bearing control schemes use a bias current with a superimposed control current to linearize the relationship between the control current and the force it delivers. For most operating conditions, the existence of the bias current requires more power than alternative methods that do not use conventional bias. With the existence of the bias current, even in no-load conditions, there is always some power consumption. In earthbound applications of magnetic bearings, this constant power loss may not be of critical importance but in aerospace applications, it becomes an important concern. This research examines alternative methods that diminish or eliminate bias current.

The alternative methods presented here consequently reduce electrical power loss but do not necessarily provide equal or better performance. Comparisons of the performance of these methods are made with the industry standard bias method. Some of the characteristics that are examined are slew rate, force output, response to saturation effects, control amplitude and frequency dependency, and steady state operation. When several methods are evaluated, an optimization strategy is used to choose control parameters that result in the best tradeoff between power consumption and control performance. Subsequently, all methods are compared and ranked according to their power loss and performance tradeoff results.

This analysis is performed using computer simulation, after which the proposed methods are used in a physical laboratory experiment. The computer simulation uses Matlab/Simulink^{tm} simulation software on a microcomputer. The experiment involves a magnetic bearing apparatus and supporting electronics. The magnetic bearing apparatus includes a flexible shaft, two magnetic bearings, various disks that are used for rotational inertias, and a motor. Only one magnetic bearing is used for control.

Lewis contact: Dexter Johnson, (216) 433–6046

A New Antiwear Additive for Bearings Used in Spacecraft

Bearings currently used in spacecraft for rotating systems are not completely sealed. If they were used on satellites, the lubricants used for ground-based applications would vaporize, form a "cloud" around the spacecraft, and then condense on the sensors and solar cells, impairing their sensitivity and ability to operate. For this reason, low-vapor pressure lubricants called PFPE's are used on spacecraft. Unfortunately, the PFPE lubricants used are so stable that commonly used antiwear additives are not soluble in them. In addition, they tend to degrade under boundary lubricating conditions, limiting the life of bearings. The purpose of this study was to determine if a silane added to a PFPE as an emulsion or applied as a coating to the counterfaces could reduce the wear of bearings and/or the degradation of a PFPE lubricant. To evaluate the effect, long- and short-sliding-duration tests were performed using a pin-on-disk tribometer.

The results indicated that silane coatings and/or emulsions, when used in conjunction with PFPE oils, reduced the wear of 440C balls and disks as compared with similar tests on an untreated PFPE oil. Figure 1 and table I compare the wear rate of the balls for short and long sliding durations. For the short-term tests, the silane decreased the pin wear rate by an average of about 50 percent, and there did not seem to be any clear advantage in using coatings instead of emulsions or in combining coatings with emulsions. However, it should be emphasized that neither the coatings nor the emulsions were optimized in this study. In general, ball wear rates were an order of magnitude lower for the long-term tests than for the short-term tests, which could be attributed to run-in effects.

Optical and microFourier transform infrared (μFTIR) microscopy observations performed on the sliding specimen surfaces after the tests were completed indicated that the silane disk coatings and/or emulsions could form thin layerlike transfer films on ball wear surfaces. Strong evidence was also found that the silane mitigated the degradation of this particular PFPE oil.

Lewis contact: Robert L. Fusaro, (216) 433–6080

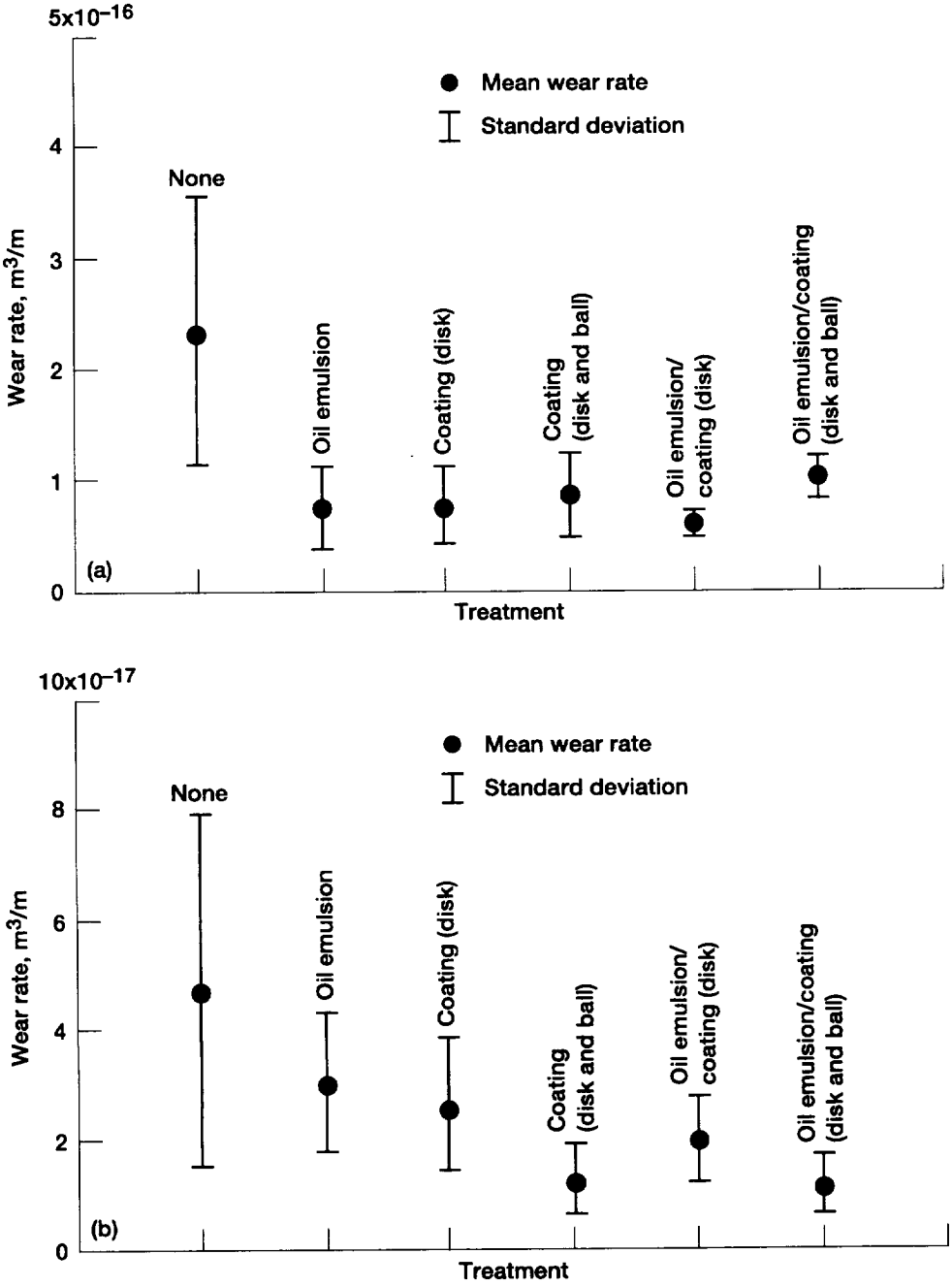

Figure 1.—Comparison of mean ball wear rates and standard deviations for (a) short-term and (b) long-term test intervals.

TABLE I.—COMPARISON OF BALL WEAR RATES FOR SHORT- AND LONG-DURATION TESTS
[Experimental conditions: temperature, 25 °C; atmosphere, dry air (100 ppm moisture content); load, 2 kg; speed, 200 rpm; 440C stainless steel specimens.]

Disk or ball treatment with oil	Short-term tests (0 to 30 kc)					Long-term tests (50 to 4500 kc)				
	Number of tests	Pin wear rate, m^3/m				Number of tests	Pin wear rate, m^3/m			
		Maximum	Minimum	Median	Standard deviation		Maximum	Minimum	Median	Standard deviation
None	6	455×10^{-18}	131×10^{-18}	240×10^{-18}	120×10^{-18}	7	40×10^{-18}	23×10^{-18}	48×10^{-18}	31×10^{-18}
Oil emulsion	6	129×10^{-18}	21×10^{-18}	81×10^{-18}	36×10^{-18}	4	45×10^{-18}	21×10^{-18}	31×10^{-18}	13×10^{-18}
Coating (disk)	8	139×10^{-18}	34×10^{-18}	84×10^{-18}	34×10^{-18}	6	49×10^{-18}	15×10^{-18}	27×10^{-18}	12×10^{-18}
Coating (disk and ball)	3	134×10^{-18}	62×10^{-18}	91×10^{-18}	38×10^{-18}	2	18×10^{-18}	9×10^{-18}	14×10^{-18}	6×10^{-18}
Oil emulsion/ coating (disk)	4	79×10^{-18}	51×10^{-18}	65×10^{-18}	12×10^{-18}	4	29×10^{-18}	10×10^{-18}	21×10^{-18}	8×10^{-18}
Oil emulsion/ coating (disk and ball)	2	120×10^{-18}	93×10^{-18}	107×10^{-18}	19×10^{-18}	2	16×10^{-18}	9×10^{-18}	12×10^{-18}	5×10^{-18}

Users Guide for ECAP2D: An Euler Aeroelastic Stability Analysis Code for Oscillating Cascades

An accurate analysis of the blade row aeroelastic stability is essential for predicting the flutter characteristics of turbomachinery blades. Toward this goal, the aeroelastic program ECAP2D was developed. The program can be used for unsteady aerodynamic and aeroelastic analyses of isolated blade rows.

The unsteady aerodynamic forces are obtained from solving two-dimensional Euler equations using a finite volume method with a combination of flux vector splitting and flux differencing splitting. The Euler solution scheme is third-order accurate in space and second-order accurate in time. The flow equations are solved on one or more passage-centered H-grids. The structural model is a typical section with bending- and torsional-motion degrees of freedom for each blade in the cascade. The solution methods include the harmonic oscillation, the influence coefficient, the pulse response, and time integration using Newmark's method. The program has been calibrated for several examples.

A guide was written to help the user prepare the input data file required by the ECAP2D code. Also provided in the guide are a complete description of the input data; input and output for four examples from published papers; references for detailed explanations of the aerodynamic analysis, the numerical algorithms, the aeroelastic analysis; and a job control file for executing the program on Cray YMP computers.

Lewis contacts: T.S.R. Reddy, (216) 433–6083 and G.L. Stefko, (216) 433–3920

Users Guide for FPCAS3D: A Three Dimensional Full-Potential Aeroelastic Solver

The FPCAS3D computer code was developed for the aeroelastic stability analysis of bladed disks such as those in fans, compressors, turbines, propellers, and propfans. A guide was written to help the user prepare the input data files required by the code.

The users guide contains a complete description of the input data and inputs and outputs for six examples from published papers. Detailed explanations of the aerodynamic analysis, the numerical algorithms, and the aeroelastic analysis are not given. Instead, the reader is directed to specific references that deal with these items.

The FPCAS3D code was developed in the Structural Dynamics Branch. The aerodynamic analysis used in this code is based on the unsteady three-dimensional full-potential equation, which is solved for a complete blade row or for a specified number of blade passages in a blade row. A finite volume approach is adopted and a Newton iteration method is used to solve the nonlinear problem as a series of linear problems at each time step. The structural analysis is based on a finite element model for each blade. Either a frequency-domain or a time-domain flutter analysis is possible with this code.

Lewis contact: Milind A. Bakhle, (216) 433–6037

Accelerated Testing of Spacecraft Mechanisms Study

The goal of building longer life unmanned satellites and space probes has created a demand for meaningful accelerated test methods to simulate long-term service in space. This is particularly true for tribological components such as bearings, seals, and gears that are used in space. There is an urgent need for lightweight, low-torque, durable mechanisms that can operate efficiently in a hard vacuum environment.

In response to this need, a study was conducted to determine for space operation the significant mechanical components that would benefit from accelerated test techniques. Table I identifies those mechanisms that could benefit and table II lists the components used in them. The study also looked at the current types of accelerated testing techniques, their shortfalls, and the need to develop new techniques.

An accelerated testing technology roadmap was developed to assess the life and reliability of spacecraft mechanical systems and consisted of integrating system components testing, analytical modeling, computer codes, computer smart systems, and so forth into a methodology that could be used to predict or verify the life and reliability of a mechanical system.

Based on the results of the accelerated testing technology roadmap study, a space mechanism mechanical system was suggested for testing to demonstrate that the methods developed would adequately predict the life and/or performance of a mechanism. The roadmap developed includes experimental equipment, test procedures, time guidelines, and a cost analysis.

TABLE I.—MECHANISMS IDENTIFIED FOR ACCELERATED TESTING

Momentum/reaction wheels
Gyroscopes
Scanning devices for Earth sensors
Solar array devices
De-spin mechanisms
Motors
Storage life, deployment mechanisms
Speed reducers, harmonic drives, and other gear systems
Slider devices (linear actuators)
Tape recorders
Power/signal transmission devices
Robotic joints
Connectors

TABLE II.—COMPONENTS NEEDED FOR RELIABLE OPERATION OF SPACE MECHANISMS

Bearings (rolling element, journal, slider)
Gears
Rings (slip, roll, O-)
Commutators
Gears
Flex harnesses and cables
Low-cycle devices, (springs, switches, cams, etc.)
Seals
Lubricants

Lewis contact: Robert L. Fusaro, (216) 433–6080

GE Uses NASA Seals to Meet JTAGG Engine Goals

The NASA Lewis Research Center developed and delivered to General Electric (GE) high-temperature (>1500 °F) braided rope seals to provide a combined seal/compliant mount to minimize thermal stresses in high-temperature nickel-aluminide (NiAl) turbine vanes (fig. 1). The new seal/compliant-mount approach has allowed GE to overcome the serious NiAl vane-cracking problem (observed while using the conventional brazing approach) that was threatening the future use of the NiAl alloy system. The NASA-provided seals consist of a ceramic fiber core overbraided with fine superalloy wires, providing a high-temperature (>1500 °F), compliant, flow-resistant structure well suited for GE's application.

GE successfully tested the vane/rope seal system in a full-scale JTAGG (Joint Technology Advanced Gas Generator) engine, meeting phase 1+ temperature goals (4th quarter of 1995 calendar year). The NiAl vane/seal system was tested for hours and no thermal distress or cracking problems were revealed, thus enabling this system to be considered for future IHPTET (Integrated High Performance Turbine Engine Technology) program elements.

Lewis contact: Bruce Steinetz, (216) 433–3302

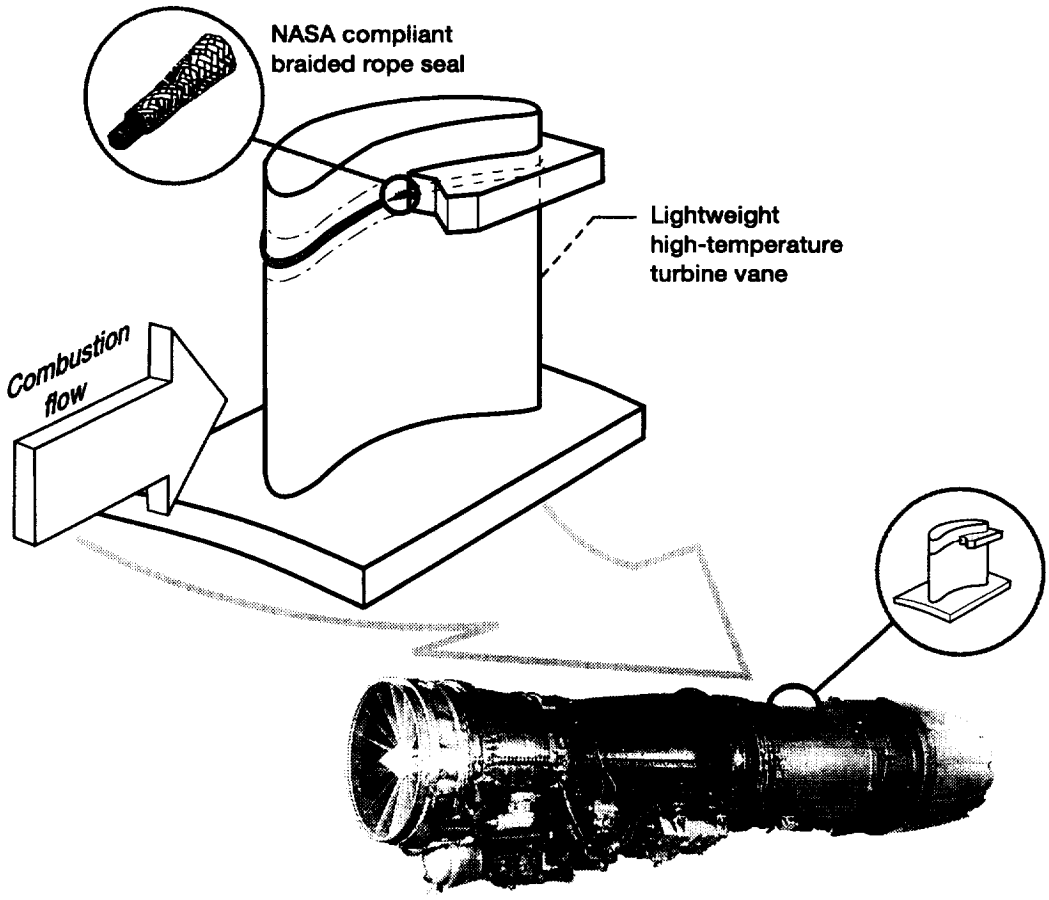

Figure 1.—High-temperature braded rope seal.

Structural Integrity

Acousto-Ultrasonics and Tensile Cycle Degradation in Ceramic Matrix Composites

Advancements in the processing and fabrication of ceramic matrix composites (CMC's) require appropriate mechanical and nondestructive testing methods to characterize properties, assess integrity, and predict the life of engine components. A serious form of degradation in CMC's is fatigue from the formation and propagation of matrix cracks due to mechanical stresses experienced during service.

In the work described here, mechanical stress was introduced by way of tensile cycling on SiC/SiC specimens having four architectures: two-dimensional balanced weave, [0/90], [+45], and $[0,+45,90,-45]_s$. At selected intervals during the cycling, acousto-ultrasonic (AU) measurements were made under specific conditions so as to determine the exponential time rate of the ultrasonic decay (UD) of the signal as it passed from the point of introduction into the specimen to the point of detection. The UD is a measure of the signal attenuation. These measurements were performed at room temperature and employed 2.25-MHZ-center-frequency broadband transducers. The UD rates were taken from the power spectrum of the detected AU signal. The 1.5- to 2.0-MHZ portion of the spectrum was used.

Figure 1 shows typical results for a tensile fatigue cycling experiment on a two-dimensional balanced-weave SiC/SiC specimen. The UD rate monitors the fatigue state up to and at failure. This result was obtained for all specimens for all four architectures tested. It is concluded that this AU technique, once calibrated to a composite system and component geometry, may be used for lifing aerospace components.

This work was done in conjunction with Pratt and Whitney and General Electric by virtue of their participation in the EPM program.

In general, AU has been applied to manufacturing problems for wire rope and wood fiber hardboard and work was done in cooperation with the MacWhyte Company and the Masonite Corporation. Acousto-ultrasonics has also been applied to the problem of determining the physical properties of human bones for the Hadassah Medical Center in Jerusalem, Israel.

Lewis contact: Harold E. Kautz, (216) 433–6015

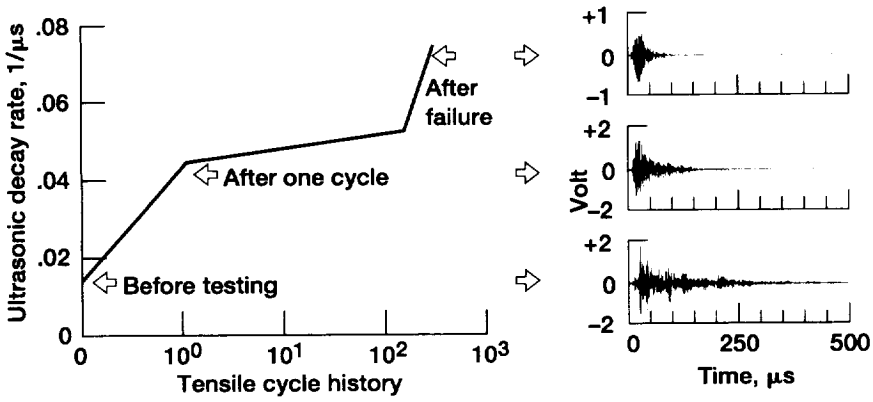

Figure 1.—Acousto-ultrasonic decay rate monitors tensile cycle fatigue in SiC/SiC specimens.

Award-Winning CARES/Life Ceramics Durability Evaluation Software: Making Advanced Technology Accessible

Products made from advanced ceramics show great promise for revolutionizing aerospace and terrestrial propulsion and power generation. However, ceramic components are difficult to design because brittle materials in general have widely varying strength values. The CARES (Ceramics Analysis and Reliability Evaluation of Structures)/Life software eases this task by providing a tool to optimize the design and manufacture of brittle material components by using probabilistic reliability analysis techniques.

CARES/Life is an integrated package that predicts the probability of a monolithic ceramic component's failure as a function of time in service. It couples commercial finite element programs, which resolve a component's temperature and stress distribution, to reliability evaluation and fracture mechanics routines for modeling strength-limiting defects. These routines are based on calculations of the probabilistic nature of the brittle material's strength.

The program has many features and options for materials evaluation and component design. The capability, flexibility, and uniqueness of CARES/Life has attracted much interest. To maintain this interest as well as to keep abreast with fast-changing operating systems and applications software, CARES/Life has been upgraded with graphic templates for common business presentation software such as Lotus Freelance Graphics. Additionally, an interactive input preparation program has been prepared and guides the user through various program control options and the specific data input formats. A grinding damage module has been added to account for flaws introduced from finishing (grinding) operations and specimen rupture data (fig. 1). This grinding damage module, in conjunction with finite element analysis, can now be used to characterize the material fracture behavior.

CARES/Life has been in high demand worldwide although present technology transfer efforts are entirely focused on U.S.-based organizations. Success stories can be cited in numerous industrial sectors including aerospace, automotive, biomedical (fig. 2), electronic, glass, nuclear, and conventional

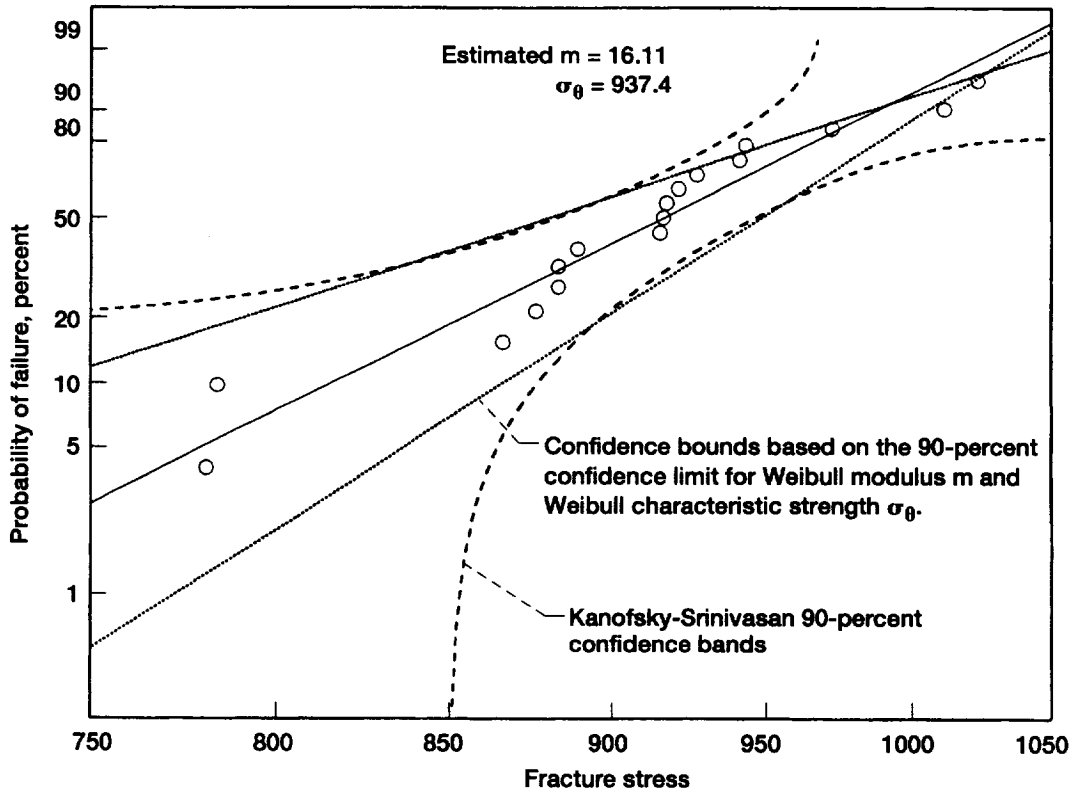

Figure 1.—Specimen rupture data depicted using common business presentation graphics packages that significantly enhance utility of CARES/Life for design engineers.

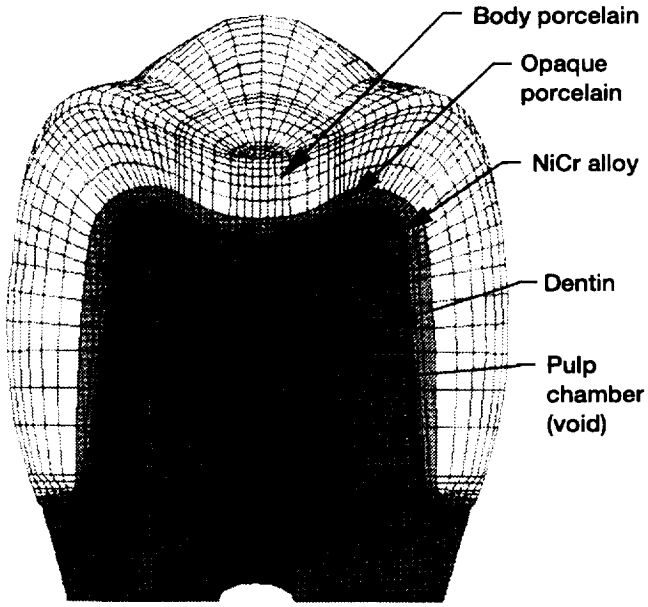

Figure 2.—Tilted view of cross section and top of finite element model of porcelain-fused-to-metal molar crown analyzed with CARES/Life.

power generation. In 1995 Lewis Research Center in partnership with Philips Display Components Company (PDCC) won a prestigious R&D 100 Award from R&D Magazine for the development of CARES/Life (by Lewis) and its application to the design and manufacture of an improved television picture tube (by PDCC) for the U.S. consumer market. The exceptional technical accomplishments and efforts of the CARES/Life development team were also recognized with the Lewis Research Center's 1995 Steven V. Szabo Engineering Excellence Award.

Lewis contacts: Noel N. Nemeth, (216) 433–3215, Lynn M. Powers, (216) 433–8374, Lesley A. Janosik, (216) 433–5160

Integrated Design Software Predicts Creep Life of Monolithic Ceramic Components

Significant improvements in propulsion and power generation for the next century will require revolutionary advances in high temperature materials and structural design. Advanced ceramics are candidate materials for these elevated temperature applications. As design protocols emerge for these material systems, designers must be aware of several innate features, including the degrading ability of ceramics to carry a sustained load. Generally, time-dependent failure in ceramics occurs because of two different delayed failure mechanisms, slow crack growth (SCG) and creep rupture. Slow crack growth initiates at a preexisting flaw and continues until a critical crack length is reached, causing catastrophic failure. Creep rupture, on the other hand, occurs because of bulk damage in the material in the form of void nucleation and coalescence that eventually leads to macrocracks which then propagate to failure. Successful application of advanced ceramics depends on the proper characterization of material behavior and the use of an appropriate design methodology. The life of a ceramic component can be predicted with the CARES (Ceramics Analysis and Reliability Evaluation of Structures) integrated design programs. CARES/CREEP determines the expected life of a component under creep conditions and CARES/LIFE predicts the component life due to fast fracture and subcritical crack growth. CARES/LIFE was previously developed and has been used in numerous industrial and government applications.

The advent of new techniques in ceramic processing technology has yielded a new class of ceramics that are highly resistant to creep at high temperatures. Such desirable properties have generated interest in using ceramics for turbine engine component applications where the design lives for such systems are on the order of 10 000 to 30 000 hr. These long life requirements necessitate subjecting the components to relatively low stresses. The combination of high temperatures and low stresses typically places failure for monolithic ceramics in the creep and creep rupture region of a time-temperature-failure-mechanism map.

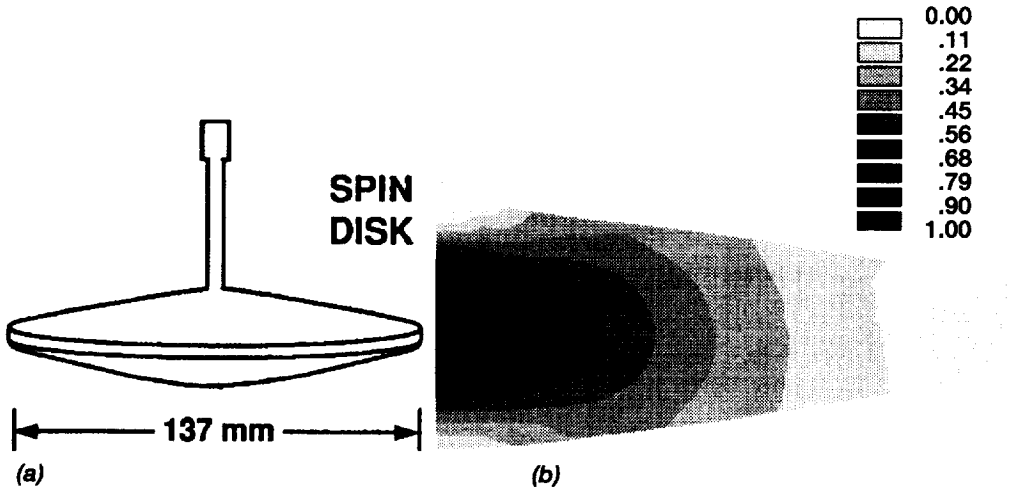

Figure 1.—Silicon nitride spin disk (AlliedSignal Engines) and analyzed to determine creep life. (a) Spin disk. (b) Damage map.

An analytical methodology in the form of an integrated design program (CARES/CREEP) has been developed for the life prediction of ceramic structural components subjected to creep-rupture conditions. This methodology utilizes commercially available finite element packages and takes into account the transient state of stress and creep strain distributions (stress relaxation). The creep life of a component is discretized into short time steps, during which the stress distribution is assumed constant. The damage is calculated for each time step based on a modified Monkman-Grant (MMG) creep-rupture criterion. In a manner similar to Miner's rule for cyclic fatigue loading, the cumulative damage is subsequently calculated as time elapses. Failure is assumed to occur when the normalized cumulative damage at any point in the component reaches unity. The corresponding time will be the creep-rupture life for that component.

CARES/CREEP has been distributed for beta testing. The first test site is Solar Turbines for their work in the development of industrial gas turbines of the 5.5-MW size. The code will also be disseminated to other engine companies such as Allison and AlliedSignal Engines. Benchmark examples from AlliedSignal have been used to validate the code as shown in figure 1.

Lewis contacts: Lynn M. Powers, (216) 433–8374, Lesley A. Janosik, (216) 433–5160, Noel N. Nemeth, (216) 433–3215

Thermomechanical Analysis of Ceramic Matrix Composite Components

Ceramic matrix composite material systems for use in the High-Speed Civil Transport (HSCT) combustor are currently being developed and evaluated. In addition, model development is also underway to allow accurate predictive capabilities for these new materials. Thermomechanical analyses were provided to support both the material and model development issues.

Damage mechanics models being developed under the Enabeling Propulsion Materials (EPM) program are being included in the finite element code CSTEM. Various test specimens are being analyzed to validate the models and to implement them in the code (fig. 1).

At the NASA Lewis Research Center, finite element analysis support is being provided for EPM-related testing, and at times is being used to explain unexpected material responses observed in the laboratory. A case in point is a high-temperature tensile endurance test where measured lifetimes were orders of magnitude lower than expected. A finite element analysis (FEA) revealed a pesty temperature problem. At other times, FEA support has been used before testing to establish run parameters necessary to achieve desired stress levels, an example of which is the work being done for cylindrically shaped CMC combustor liners. Analysis issues have been primarily focused on the complicated thermal boundary conditions: backside impingement cooling, hotside film cooling, and cold

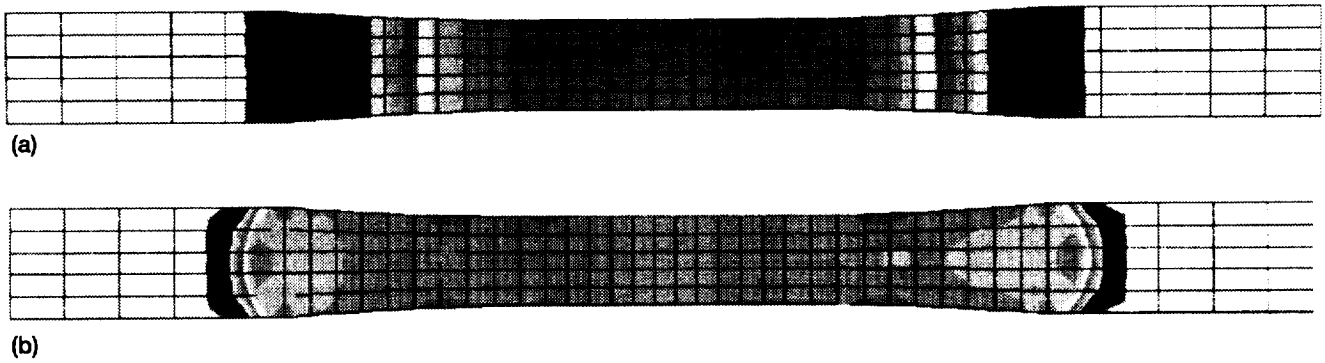

Figure 1.—Thermomechanically induced axial stresses and temperature profile for EPM tensile specimen. (a) Heated gage section and cold grips. (b) High-stress regions outside gage section.

contact regions. Initial analysis showed that the stress levels were far below the desired test levels. By modifying the impingement cooling, it is hoped that stresses can be raised locally to the desired levels.

Support is also being provided to NASA's Marshall Space Flight Center for designing and analyzing a CMC nozzle being considered for future use on the space shuttle main engine. Preliminary work has been done to establish baseline material requirements.

Lewis contact: David J. Thomas (216) 433–5664

Modeling the Effective Elastic Behavior of Transversely Cracked Laminated Composite

During loading, composite materials typically experience damage in the form of transverse matrix cracking (i.e., through-the-thickness cracks that run parallel to the fibers and are caused by the presence of the in-plane transverse stress).This form of damage may be noncatastrophic; it does not necessarily result in the immediate failure of the laminate. However, transverse matrix cracking does adversely affect the mechanical response of the material and is often a precursor to additional modes of failure. As such, a significant body of research has been devoted to modeling the effects of progressive transverse cracking. Continuum damage models as well as many shear-lag approaches have been proposed for analyzing cross-ply laminates. Shear-lag models implicitly assume that transverse matrix cracks occur at regularly spaced intervals. This assumption allows the solution of the stress state for the damaged laminate to be reduced to the solution for a characteristic volume element bounded by two transverse cracks and having a length equal to the average crack spacing. Thus, the effective elastic constants can be calculated. In this work, the validity of this assumption was investigated qualitatively by examining the probability density function for transverse crack location. The work proceeded to extend the method of Lee and Daniel for determining the shear-lag parameters to a general symmetric multilayer system. The elasticity problem for the region of the laminate between two parallel matrix cracks having an arbitrary off-axis orientation was established from equilibrium considerations in terms of the average (through-the-thickness) stresses and was solved using the newly developed generalized shear-lag (GSL) relation and the appropriate boundary conditions. Modeling of the effective elastic properties that result from the

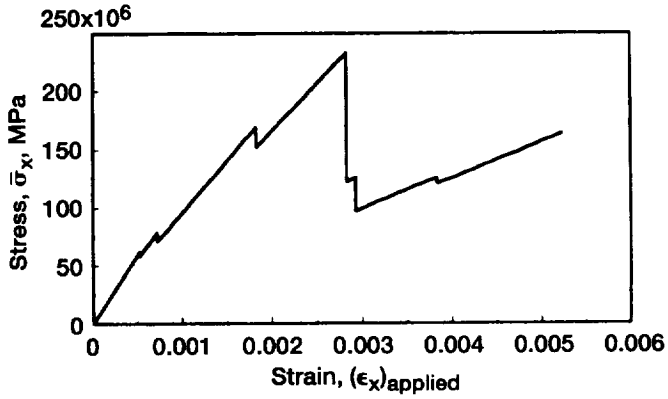

Figure 1.—Predicted average through-the-thickness laminate stress σ_x versus applied axial strain $(\epsilon_x)_{applied}$ for $[0/30/60/-30/-60]_s$ laminate using GSL model.

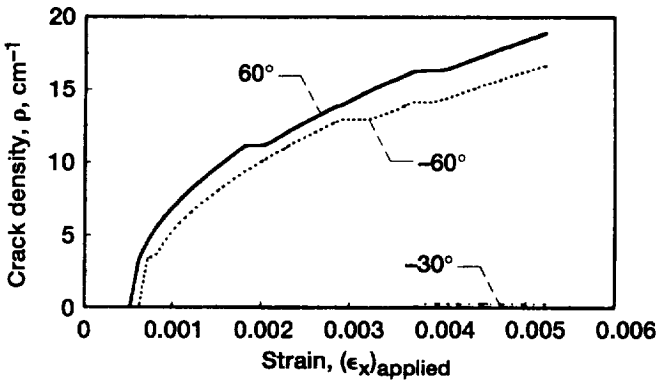

Figure 2.—Predicted evolution of crack densities in $[0/30/60/-30/-60]_s$ laminate as function of applied axial strain $(\epsilon_x)_{applied}$.

damaged layer was detailed. The analysis method was benchmarked against published results for a cross-ply laminate, and the advanced modeling capabilities of the model were demonstrated for a $[0/30/60/-30/-60]_s$ laminate (figs. 1 and 2).

Lewis contact: David J. Thomas, (216) 433–5664

Capability of Thermographic Imaging Defined for Detection of Defects in High-Temperature Composite Materials

The ability of a single-sided thermograhic imaging technique (fig. 1) to detect flat-bottom-hole defects of various diameters and depths was evaluated in four composite systems (two types of ceramic matrix composites (CMC's), one metal matrix composite (MMC), and one polymer matrix composite (PMC)) of interest as high-temperature structural materials. The holes ranged from 1 to 13 mm in diameter and from 0.1 to 2.5 mm in depth in samples approximately 2 to 3 mm thick. The thermographic imaging system utilized a scanning mirror optical system and an infrared (IR) focusing lens in conjunction with a Mercury-Cadmium-Telluride infrared detector element to obtain high-resolution infrared images. High-intensity flash lamps located on the same side as the infrared camera were used to heat the samples. After heating, up to 30 images were sequentially acquired at 70- to 150-msec intervals.

Limits of detectability based on the depth and diameter of the flat-bottom holes were observed for each composite material. For the SiC/CAS CMC

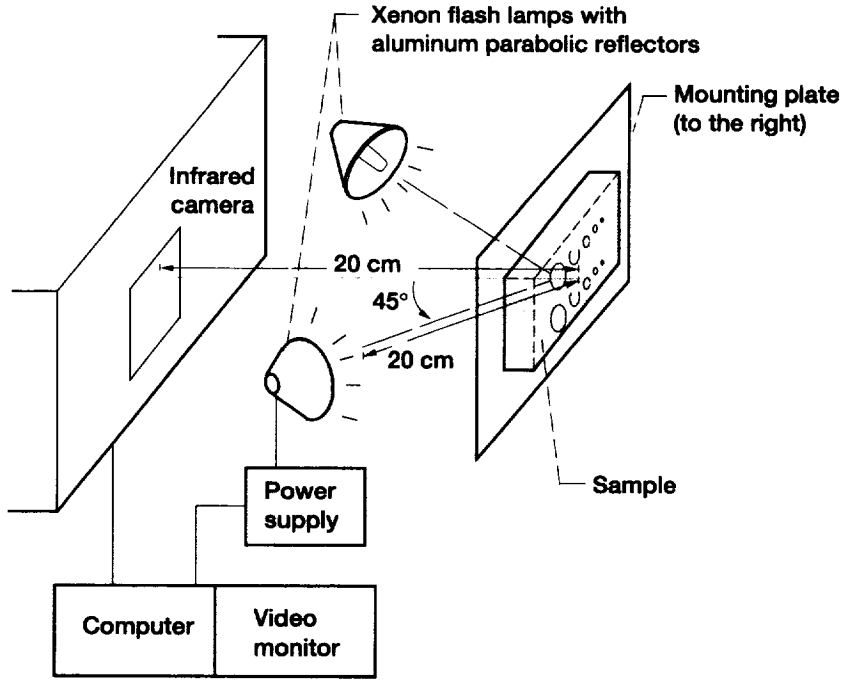

• Defect boundaries inside material slow down diffusion of thermal front as it propagates, resulting in different temperatures near defects as compared with good areas.

Figure 1.—Experimental thermography technique description.

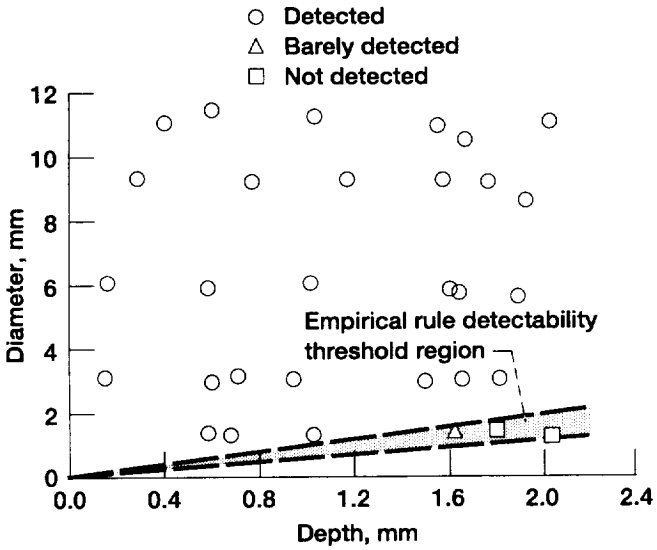

Figure 2.—Thermography detectability for SiC/CAS CMC results. (Defects ≤1.8 mm deep with diam ≥1.6 mm will be detected.)

samples, defects of depth less than or equal to 1.8 mm having diameters greater than or equal to 1.6 mm probably will be detected with the thermography methodology used in this study (fig. 2). For the SiC/SiC CMC samples, defects of depth less than or equal to 1.8 mm having diameters greater than or equal to 2.6 mm probably will be detected. For the SiC/Ti MMC samples, defects of depth less than or equal to 1.6 mm having diameters greater than or equal to 3.2 mm probably will be detected. For the graphite/polyimide PMC samples, defects approximately 3 to 12 mm in diameter and less than or equal to 1.8 mm in depth probably will be detected. Depth appears to be the limiting variable with regard to detectability in the PMC system. The thermography imaging results were consistent with the empirical rule which states that defects of diameter less than or equal to 0.5 to $1.0 \times d$ (where d is the depth below the surface) probably will not be detected.

The thermographic images were compared with ultrasonic and conventional film radiographic images. Radiographic images clearly revealed all flat-bottom holes and provided the highest quality images of the three imaging methods. The ultrasonic imaging results were material dependent. For the SiC/CAS CMC material, thermographic imaging revealed defects as clearly as or more clearly than the ultrasonic imaging did. For the SiC/SiC CMC material, pulse-echo ultrasonic imaging had difficulty clearly revealing all defects whereas through-transmission ultrasonic imaging enabled the visualization of all defects; thermographic images revealed the shallowest and intermediate-depth defects but could not reveal the deepest defects (those at depths ≥ ~ 2.0 mm below the surface). For the SiC/Ti MMC material, ultrasonic imaging revealed all defects while thermographic images did not reveal the smallest, deepest defects (those 1 to 3 mm in diam at depths of 1.6 to 1.7 mm below the surface). For the graphite/polyimide PMC material, ultrasonic images barely revealed indications of the deepest defects (≥1.8 mm below the surface, ~1 to 12 mm in diameter) whereas thermographic images did not reveal any of the deepest defects.

Lewis contact: Don J. Roth (216) 433–6017

Crack Extension Measurement in Brittle Materials

Ceramics are of great interest as structural components in engines because of their low density and high-temperature load-bearing capabilities. However, ceramics and glasses are brittle and exhibit time-dependent crack growth. A simple technique was developed to monitor crack extension in brittle materials such as ceramics and glasses.

A variety of specimens with sharp cracks have been used to monitor crack extension in glasses and ceramics; however, many of them are complicated or use grooves to guide the cracks. Measurements using the simple beam specimen with a straight-through precrack were improved by placing a strain gage on the backface after precracking, as shown in figure 1. Finite element analysis was used to

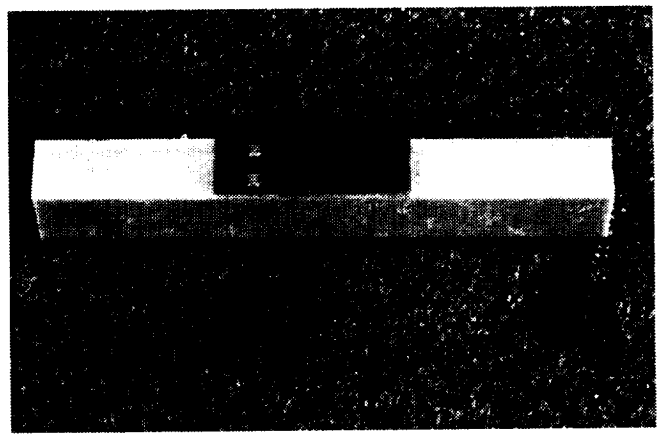

Figure 1.—Simple beam specimen.

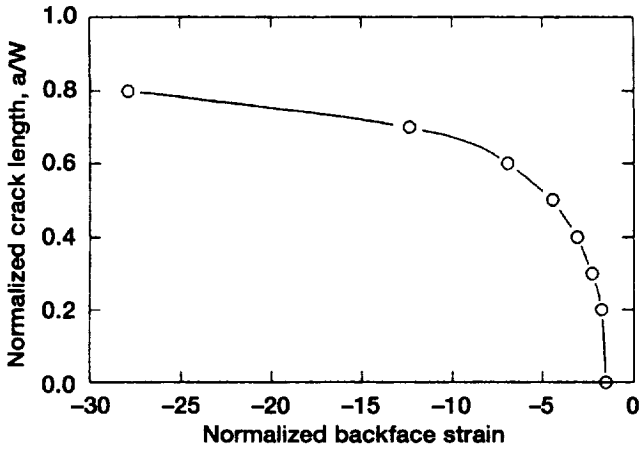

Figure 2.—Backface strain as function of crack length.

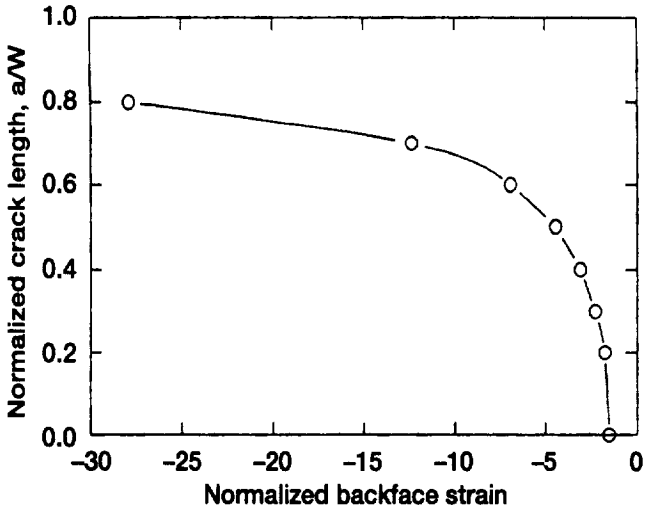

Figure 2.—Backface strain as function of crack length.

calibrate the backface strain as a function of crack length (fig. 2). The finite element modeling (FEM) results were verified by conducting an experimental calibration in which saw-notched specimens were used to simulate cracks. The results are shown in figure 3, and experimental load versus backface strain is shown in figure 4.

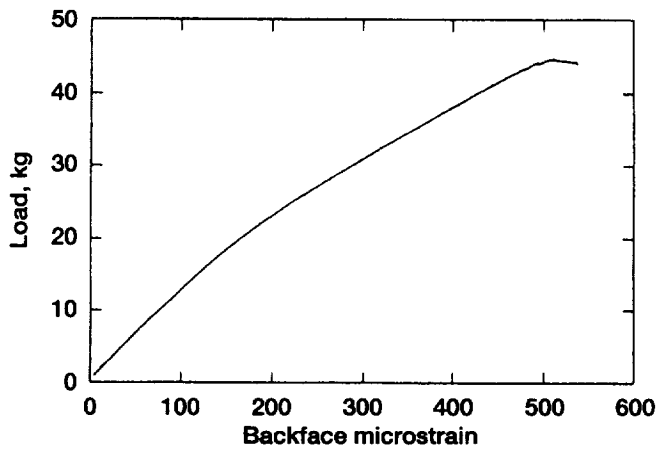

Figure 4.—Experimental load as function of backface strain.

The results allow simple, inexpensive monitoring of stable crack extension, crack growth resistance, and fatigue crack growth in brittle materials.

Customers include Oak Ridge National Laboratory, which funded the research, and members of the American Society for Testing Materials Committee C28 fracture task group, such as the National Institute of Standards and Technology, AlliedSignal, and Allison Gas Turbine.

Lewis contacts: Jon Salem, (216) 433–3313, Sung Choi, (216) 433–8366, Louis Ghosn, (216) 433–3249, and Ralph Pawlik, (216) 433–8563

Experimental Verification of Crack Growth Models for Ceramics

Because of their low density and high-temperature load-bearing capabilities, ceramics are of great interest as structural components in engines. However, ceramics and glasses are brittle and exhibit time-dependent crack growth.

A variety of models for room- and elevated-temperature crack growth exist and have been incorporated in the CARES (Ceramics Analysis and Reliability Evaluation of Structures)/Life design code. The code allows designers to analyze and

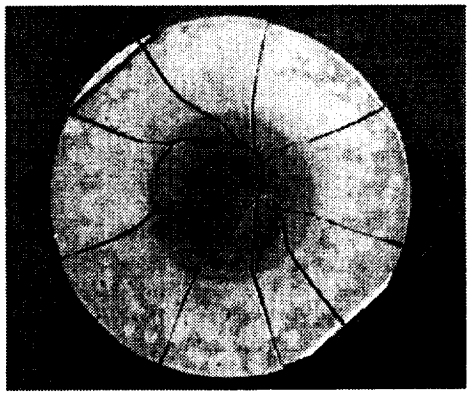

Figure 1.—Failed biaxial flexure specimen.

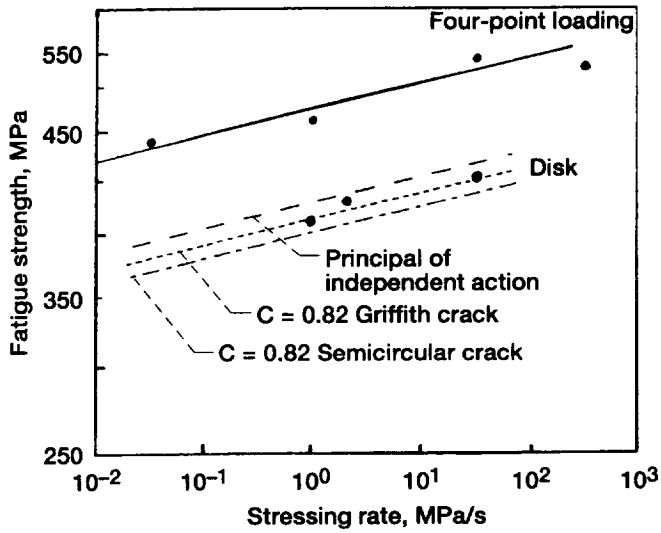

Figure 2.—Silicon nitride test in air at 1300 °C.

predict the probability of failure of structural components made from brittle materials over their lifetime. Experimental verification of the CARES/Life crack growth code was undertaken by testing silicon nitride, a structural ceramic of industrial interest, at 1300 °C in air. Four-point flexure loading was used to generate simple specimen (design) data, and biaxial flexure of plates was used to simulate a larger test volume with a multiaxial stress state.

A failed biaxial flexure specimen is shown in figure 1 and the test results are shown in figure 2. Agreement was good for most of the failure criteria used in the predictions, indicating that the code can predict failure probabilities of multiaxial stress states when the governing mechanism is slow crack growth.

Customers included ORNL, which funded the research, and other participants in the Ceramic Technology Program: AlliedSignal, Allison Gas Turbine, and Solar Turbine.

Lewis contacts: Jon Salem, (216) 433–3313, Sung Choi, (216) 433–8366, Ralph Pawlik, (216) 433–8563

Bibliography

Abdul-Aziz, A., et al.: An Experimental and Analytical Investigation of Stirling Space Power Converter Heater Head. NASA TM–107013, 1995.

Aboudi, J.; Pindera, M.-J.; and Arnold, S.M.: A Coupled Higher-Order Theory for Functionally Graded Composites with Partial Homogenization. Compos. Eng., vol. 5, no. 7, 1995, pp. 771–792.

Aboudi, J.; Pindera, M.-J.; and Arnold, S.M.: HOTFGM-2D: A Higher-Order Theory for Metal Matrix Composites Functionally Graded in Two Directions. HITEMP Review 1995, vol. II, NASA CP–10178, pp. 33–1 to 33–12.

Aboudi, J.; Pindera, M.-J.; and Arnold, S.M.: Thermoelastic Theory for the Response of Materials Functionally Graded in Two Directions. Int. J. Solids Struct., vol. 33, no. 7, 1996, pp. 931–966.

Aboudi, J.; Pindera, M.-J.; and Arnold, S.M.: Thermo-Inelastic Response of Functionally Graded Composites. Int. J. Solids Structures, vol. 32, no. 12, 1995, pp. 1675–1710.

Abumeri, G.H.; Chamis, C.C.; and Generazio, E.R.: Insertion and Benefits of Processing Technology in Composite Structures. Proceedings of the 40th International SAMPE Symposium and Exhibition, 1995, pp. 838–848.

Abumeri, G.H.; Chamis, C.C.; and Generazio, E.R.: T/BEST: Technology Benefit Estimator Select Features and Applications. NASA TM–106960, 1995.

Addy, H.E., et al.: Preliminary Results of Silicon Carbide Brush Seal Testing at NASA Lewis Research Center. AIAA Paper 95–2763. 1995.

Arnold, S.M.; Aboudi, J.; and Pindera, M.-J.: Thermally-Induced Interlaminar Stresses in TBC-Protected Plate: A Material and Geometric Parametric Study. HITEMP Review 1995, vol. II, NASA CP–10178, pp. 34–1 to 34–14.

Arnold, S.M.; and Castelli, M.G.: What Constitutes a Model Material? A LeRC Structural Fatigue Branch Perspective. HITEMP Review 1995, vol. II, NASA CP–10178, pp. 35–1 to 35–18.

Arnold, S.M.; Saleeb, A.F.; and Castelli, M.G.: A Fully Associative, Nonisothermal Nonlinear Kinematic, Unified Viscoplastic Model for Titanium Alloys. NASA TM–106926, 1995.

Arnold, S.M.; Saleeb, A.F.; and Wilt, T.E.: A Modeling Investigation of Thermal and Strain Recovery and Nonlinear Hardening in Potential Based Viscoplasticity. J. Eng. Mater. Technol., vol. 117, no. 2, 1995, pp. 157–167.

Arnold, S.M.; Pindera, M.-J.; and Wilt, T.E.: Influence of Fiber Architecture on the Elastic and Inelastic Response of Metal Matrix Composites. NASA TM–106705, 1995.

Arya, Vinod K.; and Halford, Gary R.: Analyses of Oxide Layer Cracking Patterns of MA956 and MA956/Sapphire Composite Systems. Contemporary Research in Engineering Science, Romesh C. Batra, ed., Springer, New York, 1995, pp. 41–54.

Arya, V.K.; and Halford, G.R.: Finite Element Analysis of Structural Engineering Problems Using a Viscoplastic Model Incorporating Two Back Stresses. J. Eng. Gas Turbines Power, vol. 117, no. 2, 1995, pp. 377–383.

Arya, V.K.; and Halford, G.R.: Large Displacement Structural Durability Analysis of Simple Bend Specimen Emulating Rocket Nozzle Liners. NASA TM–106521, 1995.

Arya, V.K.; Halford, G.R.; and Westfall, L.J.: Large-Displacement Structural Durability Analyses of Simple Specimens Emulating Rocket Chambers. J. Propul. P., vol. 12, no.1, 1996, pp 55–60,

Athavale, M.M., et al.: Numerical Analysis of Intra-Cavity and Power-Stream Flow Interaction in Multiple Gas-Turbine Disk Cavities. ASME International Congress, 1995.

Athavale, M.M., et al.: Simulation of Secondary Flow in Gas Turbine Disk Cavities and Interaction With the Main Flow Path. AIAA Paper 95–2620, 1995.

Athavale, M.M.; Hendricks, R.C.; and Steinetz, B.M.: Numerical Simulation of Flow in a Whirling Annular Seal and Comparison With Experiments. NASA TM–106961, 1995.

Baaklini, G.Y.: CT for Reducing Development Cycle Time of Composites. NDE: Your Best Bet for the 21st Century (Including the Proceedings of the ASNT Spring Conference), American Society for Nondestructive Testing, 1995.

Baaklini, G.Y.: NASA HITEMP Program—NDE Accomplishments and Plans. Invited paper to the Research Symposium on NDE of Composites and Composite Structures held in conjunction with the 1995 Spring ASNT Conference, Las Vegas, NV, March 27–31, 1995.

Baaklini, G.Y., et al.: X-Ray Microtomography of Ceramic and Metal Matrix Composites. Mater. Eval., vol. 53, no. 9, 1995, pp. 1040–1044.

Bakhle, M. A.: FPCAS3D User's Guide: A Three Dimensional Full Potential Aeroelastic Program, Version 1.0. NASA CR–198367, 1995.

Belegundu, A.; Berke, L.; and Patnaik, S.N.: An Optimization Algorithm Based on the Methods of Feasible Directions. Struct. Optimization, vol. 9, no. 2, 1995, pp. 83–88.

Binienda, W.K.; and Arnold, S.M.: Driving Force Analysis in an Infinite Anisotropic Plate With Multiple Crack Interactions. Int. J. Fract., vol. 71, no. 3, pp. 213–245.

Birman, V.; Saravanos, D.A.; and Hopkins, D.A.: Micromechanics of Composites With Shape Memory Alloy Fibers in Uniform Thermal Fields. AIAA Paper 95–1210 (NASA TM–107011), 1995.

Bonacuse, P.J.; and Kalluri, S.: Axial-Torsional, Thermomechanical Fatigue Behavior of Haynes 188 Superalloy. Presented at the Structures and Materials Panel, AGARD CP-569, 1996.

Bonacuse, P.J.; and Kalluri, S.: Elevated Temperature Axial and Torsional Fatigue Behavior of Haynes 188. J. Eng. Mat. Tech., vol. 117, no. 2, 1995, pp. 191–199.

Bowman, R.R.; Misra, A.J.; and Arnold, S.M.: Processing and Mechanical Properties of Al_2O_3 Fiber-Reinforced NiAl Composites. Metall. T-A, vol. 26, no. 3, 1995, pp. 615–628.

Boyce, L.; and Chamis, C.C.: Probabilistic Constitutive Relationships for Cyclic Material Strength Models. AIAA Paper 88–2376, 1988, pp. 1299–1306.

Brewer, D., et al.: Measurement of Mechanical Damage in SiC/SiC Composites Using Vibration, Acousto-Ultrasonic, and Thermographic NDE. HITEMP Review 1995, vol. II, NASA CP–10178, 1995, pp. 36–1 to 36–12.

Brown, G.V.; DiRusso, E.; and Provenza, A.J.: An Active Homopolar Magnetic Bearing With High Temperature Superconductor Coils and Ferromagnetic Cores. NASA TM–106916, 1995.

Brown, G.V.; DiRusso, E.; and Provenza, A.J.: An Active Magnetic Bearing With High T_c Superconducting Coils and Ferromagnetic Cores. NASA TM–106995, 1995.

Castelli, M.G.: A Summary of Damage Mechanisms and Mechanical Property Degradation in Titanium Matrix Composites Subjected to TMF Loadings. Presented at the Structures and Materials Panel, AGARD CP–569, 1996.

Castelli, M.G.: Mechanical Property Degradation During Thermomechanical Fatigue of Titanium Matrix Composites. Proceedings of Second International Conference on Composites Engineering (ICCE/2), 1995, pp. 107–108.

Castelli, M.G., et al.: Thermomechanical Fatigue Deformation Behavior of the Cobalt Base Superalloy Haynes 199. HITEMP Review 1995, vol. II, NASA CP–10178, pp. 31–1 to 31–14.

Castelli, M.G., Rao, K.B.S.; and Ellis, J.R.: Micromechanisms Influencing High Temperature Fatigue Deformation in Haynes 188 Superalloy. Proceedings of the Symposium on Micromechanics of Advanced Materials, Minerals, Metals and Materials Society, Warrendale, PA,1995, pp. 197–203.

Chamis, C.C.; and Minnetyan, L.: Progressive Fracture of Composite Offshore Risers. Materials, Design and Analysis Symposium; Energy-Sources Technology Conference, ASME, New York, 1995, pp. 39–46.

Chamis, C.C. and Minnetyan, L: Progressive Fracture of Composite Structures. The Composites Institute, The Society of the Plastic Industry 50th Annual Conference, 1995, pp. 11–C–1.

Chamis, C.C.; and Shah, A.R.: Probabilistic Sizing of Laminates With Uncertainties. Published in High Technology Composites in Modern Applications by the University of Patras, Sept. 1995, pp. 498–506.

Chamis, C.C.; and Shiao, M.C.: Probabilistic Composite Analysis Design. Composite Institute, The Society of the Plastic Industry 50th Annual Conference, 1995, pp. 11–D–1 to 11–D–6.

Chamis, C.C.; and Singhal, S.N.: Quantification of Uncertainties of Hot-Wet Composite Long Term Behavior. Published by AIAA in Aerospace Thermal Structures and Materials for a New Era, 1995, pp. 259–272.

Chen, A.S.; and Matthews, F.L.: A Review of Multiaxial/Biaxial Loading Tests for Composite Materials. CPSOA, vol. 24, no. 5, July 1993, pp. 395–406.

Choi, et al.: High-Temperature Slow Crack Growth of Si_3N_4 Specimens Subjected to Uniaxial and Biaxial Dynamic Fatigue Loading Conditions. Ceram. Eng. Sci. Proc., vol. 16, no. 4, 1995, pp. 509–518.

Choi, S.R.; and Salem, J.A.: Dynamic, Static, and Cyclic Fatigue of Alumina With Indentation-Induced Flaws. J. Mater. Sci. Lett., vol. 14, 1995, pp. 1286–1288.

Choi, S.R.; and Salem, J.A.: Effect of Preloading on Fatigue Strength in Dynamic Fatigue Testing of Ceramic Materials at Elevated Temperatures. Ceram. Eng. Sci. Proc., vol. 16, no. 4, 1995, pp. 87–94.

Cios, J.K.; Baaklini, G.Y.; and Vary, A.: Soft Computing in Design and Manufacturing of Advanced Materials. J. Eng. Gas Turbines Power, vol. 117, no. 1, Jan. 1995, pp. 161–165.

Covey, S.J.; Lerch, B.A.; and Jayaraman, N.: Fiber Volume Fraction Effects on Fatigue Crack Growth in SiC/Ti–15–3 Composites. Mater. Sci. Eng., vol. 200, no. 1-2, 1995, pp. 68–77.

dos Reis, H.L.M.: Acousto-Ultrasonics: Theory and Application. John C. Duke, ed., Plenum Press, New York, NY, 1988, pp. 283–299.

Ellis, J.R.; and Castelli, M.G.: Characterization of Titanium Matrix Composites. NASP TM–1199, vol. XII, NASA Lewis Research Center, Cleveland, OH, June 1995.

Gendy, A.S., et al.: Design Optimization of a Spacer Structure for Space Station Freedom. Comput. Struct., vol. 54, no. 2, 1995, pp. 355–363.

Gendy, A.S., et al.: Issues in Substructure Optimization. Proceedings of First World Congress of Structural and Multidisciplinary Optimization, 1995, pp. 857–862.

Gendy, A.S., et al.: Parallel Computational Environment for Substructure Optimization. NASA TM–4680, 1995.

Generazio, E.R.; and Chamis, C.C.: Benefits Estimation of New Engine Technology. Published by AIAA in Aerospace Thermal Structures and Materials for a New Era, Washington DC, 1995, pp. 384–400.

Generazio, E.R.; and Chamis, C.C.: Benefits of Inserting Composite Technology in Engine Structures. Materials, Design and Analysis Symposium; Energy-Sources Technology Conference, ASME, New York, 1995, pp. 217–227.

Generazio, E.R.; and Chamis, C.C.: Technology Benefits Estimation (T/BEST) for Aerospace Engine Technology Propulsion Systems—Life and Maintenance. ASME International Congress, 1995.

Goldberg, R.K.; and Hopkins, D.A.: Application of the Boundary Element Method to the Micromechanical Analysis of Composite Materials. Comput. Struct., vol. 56, no. 5, 1995, pp. 721–731.

Goldberg, R.K.; and Hopkins, D.A.: Thermal Analysis of a Functionally Graded Material Subject to a Thermal Gradient Using the Boundary Element Method. Compos. Eng., vol. 5, no. 7, 1995, pp. 793–806.

Gotsis, P.K.: Computational Simulation of Fiber Composite Thin Shell Structures in a Hygrothermal Environment. High Technology Composites in Modern Applications—Advanced Composites in Emerging Technologies (Including the Proceedings of the 4th International Symposium on Composite Materials), The University of Patras, 1995, pp. 507–518.

Gotsis, P.K.: Structural Optimization of Shell Structures. Comput. Struct., vol. 50, no. 4, 1994, pp. 499–507.

Gotsis, P.K; Chamis, C.C.; and Minnetyan, L.: Effect of Combined Loads on the Durability of a Stiffened Adhesively Bonded Composite Structure. Adaptive Structures Forum, ASME, New York, 1995, pp. 1083–1092.

Gotsis, P.K.; and Guptill, J.D.: Fiber Composite Thin Shells Subjected to Thermal Buckling Loads. Comput. Struct., vol.53, no. 6, 1994, pp. 1263–1274.

Gotsis, P.K.; and Guptill, J.D.: Free Vibration of Fiber Composite Thin Shells in a Hot Environment. J. Reinf. Plast. Comp., vol. 14, no. 2, 1995, pp. 143–163.

Gotsis, P.K.; and Guptill, J.D.: Laminated Thin Shell Structures Subjected to Free Vibration in a Hygrothermal Environment. NASA TM–106600, 1994.

Guptill, et al.: CometBoards Users Manual, NASA TM–4537, 1996.

Gyekenyesi, A.L.; and Castelli, M.G.: A Study of Elevated Temperature Testing Techniques for the Fatigue Behavior of PMC's. HITEMP Review 1995, vol. I, NASA CP–10178, 1995, pp. 13–1 to 13–13.

Gyekenyesi, A.L., et al.: A Study of Elevated Temperature Testing Techniques for the Fatigue Behavior of PMC's: Application to T650–35/AMB–21. NASA TM–106927, 1995.

Hendricks, R.C., et al.: Interactive Development of Seals, Bearings, and Secondary Flow Systems with the Power Stream. Int. J. Rotating Mach., vol. 0., no. 1, 1995, pp. 153–185.

Jankovsky, R.S., et al.: Structurally-Compliant Rocket Engine Combustion Chamber—Experimental and Analytical Validation. J. Spacecr. Rock., vol. 32, no. 4, 1995, pp. 645–652.

Janosik, L.A., et al.: NASA CARES Dual-Use Ceramic Technology Spinoff Applications. Proceedings of the 32nd Space Congress, 1995, pp. 7–18 to 7–27.

Jansen, R.; and DiRusso, E.: Passive Magnetic Bearing with Ferrofluid Stabilization. NASA TM–107154, 1996.

Johnson, D.: Alternative Operating Modes for Magnetic Bearing Control. Ph.D. Dissertation, State University of New York at Buffalo, 1995.

Kalluri, S.; Halford, G.R.; and McGaw, M.A.: Prestraining and Its Influence on Subsequent Fatigue Life. Advances in Fatigue Lifetime Predictive Techniques: 3rd Volume, vol. 1292, M.R. Mitchell and R.W. Landgraf, eds., American Society for Testing and Materials, 1996, pp. 328–341.

Kautz, H.E.: Determination of Plate Wave Velocities and Diffuse Field Decay Rates With Broad-Band Acousto-Ultrasonic Signals. NASA TM–106158, 1993.

Kautz, H.E., et al.: Vibration and Acousto-Ultrasonic NDE for Monitoring Mechanical Damage in Ceramic Matrix Composites. NDE: Your Best Bet for the 21st Century (Including the Proceedings from the ASNT Spring Conference), American Society for Nondestructive Testing, 1995.

Klann, J.L.; and Snyder, C.A.: NEPP Programmers Manual, NASA TM–106575, 1994.

Kurkov, A.P.; and Lucci, B.L.: Measurement of Gust Response on a Turbine Cascade. ASME International Congress, 1995.

Lee, G.W.; and Daniels, I.M.: Progressive Transverse Cracking of Crossply Composite Laminates. J. Compos. Mater., vol. 24, no. 11, 1990, pp. 1225–1243.

Lee, H.-J. and Saravanos, D.A.: A Coupled Layerwise Analysis of the Thermopiezoelectric Response of Smart Composite Beams. AIAA Paper 95–1101 (NASA TM–106889), 1995.

Lee, H.-J.; and Saravanos, D.A.: On the Response of Smart Piezoelectric Composite Structures in Thermal Environments. Adaptive Structures Forum, ASME, New York, 1995, pp. 2876–2885.

Lei, J-F., et al.: Comparison Testings Between a High Temperature Extensometer and a Resistance Strain Gage With Multiple Installation Techniques. Proceedings of the SEM Spring Conference on Experimental Mechanics, Society of Experimental Mechanics, 1995, pp. 471–478.

Lerch, B.A., et al.: Bending Properties of Nickel Electrodes for Nickel-Hydrogen Batteries. NASA TM–106756, 1995.

Lerch, B.A.; and Halford, G.R.: Effects of Control Mode and R-Ratio on the Fatigue Behavior of a Metal Matrix Composite. Mater. Sci. Eng. vol. A200, nos. 1-2, 1995, pp. 47–54.

Lerch, B.A.; and Halford, G.R.: Fatigue Mean Stress Modeling in a [0]32 Titanium Matrix Composite. HITEMP Review 1995, vol. II, NASA CP–10178, 1995, pp. 21–1 to 21–10.

Lin, Y., et al.: Modelling and Fuzzy Logic Control of an Active Reaction Compensating Platform System. J. Shock Vib., vol. 2, no. 6, 1995, pp. 493–506.

Lissenden, C.J.; Lerch, B.A.; and Ellis, J.R.: Inelastic Surfaces at High Temperature Under Axial-Torsional Loading. HITEMP Review 1995, vol. II, NASA CP-10178, 1995, pp. 23-1 to 23-10.

Merrick, H.F., et al.: Multiaxial Deformation of a SCS-6/Ti-6-4 Composite Ring. HITEMP Review 1995, vol. II, NASA CP-10178, 1995, pp. 35-1 to 35-9.

Minnetyan, L.; and Chamis, C.C.: Pressure Vessel Fracture Simulation. Fracture Mechanics: New Trends in Fracture Mechanics, vol. 1220, 1995, pp. 671-684.

Minnetyan, L.; and Chamis, C.C.: Progressive Damage and Fracture of Graphite/Epoxy Composites Subject to Biaxial Stress States. High Technology Composites in Modern Applications—Advanced Composites in Emerging Technologies (Including the Proceedings of the 4th International Symposium on Composite Materials), The University of Patras, 1995, pp. 507-518.

Minnetyan, L., et al.: Discontinuously Stiffened Composite Panel Under Compressive Loading. J. Reinf. Plast. Comp. vol. 14, no. 1, 1995, pp. 85-98.

Minnetyan, L.; and Gotsis, P.K.: Progressive Fracture in Adhesively Bonded Concentric Cylinders. Proceedings of the 40th International SAMPE Symposium and Exhibition, vol. 40, book 1, 1995, pp. 849-860.

Mital, S.K.; and Chamis, C.C.: Microfracture in Toughened Epoxy Composites. Proceedings of the 40th International SAMPE Symposium and Exhibition, 1995, pp. 1330-40.

Mital, S.K.; Chamis, C.C.; and Gotsis, P.K.: Micro-Fracture in High-Temperature Metal-Matrix Laminates. Comp. Sci. T., vol. 50, 1994, pp. 59-70.

Mital, S.K.; Murthy, P.L.N.; and Chamis, C.C.: Micromechanics for Ceramic Matrix Composites Via Fiber Substructuring. J. Compos. Mater., vol. 29, no. 5, 1995, pp. 614-633.

Mital, S.K.; Murthy, P.L.N.; and Chamis, C.C.: Micromechanics for Woven Composites. HITEMP Review 1995, vol. III, NASA CP-10178, pp. 52-1 to 52-12.

Mital, S.K.; Murthy, P.L.N.; and Chamis, C.C.: Simplified Micromechanics of Two-Dimensional Plain Woven Fabric Composites. ASME International Congress, 1995, pp. 829-840.

Mital, S.K.; Murthy, P.L.N.; and Chamis, C.C.: Simulation of Ceramic Matrix Composites Behavior Including Progressive Fracture and Load Redistribution. AIAA Paper 95-1215-CP, 1995.

Mittelman, A., et al.: Acousto-Ultrasonic Characterization of Physical Properties of Human Bones. Acousto-Ultrasonics: Theory and Application, J.C. Duke, ed., Plenum Press, New York, NY, 1988, pp. 305-309.

Morales, W., et al.: A New Antiwear Additive/Surface Pretreatment for PFPE Liquid Lubricants. NASA TM-107038, 1995.

Murray, S.F.; and Heshmat, H.: Accelerated Testing of Space Mechanisms. NASA CR-198437, 1995.

Murthy, P.L.N.; and Chamis, C.C: Integrated Composite Analyzer (ICAN): Users and Programmers Manual, NASA TP-2515,1986.

Nemeth, N.N., et al.: Designing Ceramic Components for Durability. Am. Ceram. Soc. Bull., vol. 72, no. 12, Dec. 1993, pp. 59-66.

Nemeth, N.N., et al.: Durability Evaluation of Ceramic Components Using CARES/Life. ASME Paper 94-GT-362, 1994.

Nemeth, N.N., et al.: Lifetime Reliability Evaluation of Structural Ceramic Parts With the CARES/Life Computer Program. AIAA paper 93-1497-CP, 1993, pp. 1634-1646.

Nemeth, N.N., et al.: Time-Dependent Reliability Analysis of Monolithic Ceramic Components Using the CARES/Life Integrated Design Program. ASTM Special Technical Publication, Proceedings of the Symposium on Life Prediction Methodologies and Data for Ceramic Materials, ASTM STP-1201, C.R. Brinkman and S.F. Duffy, eds., American Society for Testing and Materials, Philadelphia, PA, 1994, pp. 390-408.

Noebe, R.D.; Lerch, B.A.; and Rao, K.B.S.: Assessment of Microalloying Effects on the High Temperature Fatigue Behavior of NiAl. High-Temperature Ordered Intermetallic Alloys VI Symposium, part 1, Materials Research Society, Pittsburgh, PA, 1995, pp. 291-296.

Pai, S.S.; and Chamis, C.C.: Probabilistic Assessment of Combustor Liner Design. ASME International Congress, 1995.

Patnaik, S., et al.: Completed Beltrami-Michell Formulation for Analyzing Mixed Boundary Value Problems in Elasticity. AIAA Journal, vol. 34, no. 1, Jan. 1996, pp. 143-148.

Patnaik, S.N.; Guptill, J.D.; and Berke, L.: Merits and Limitations of Optimality Criteria Method for Structural Optimization. Int. J. Numer. Methods Eng., vol. 38, no. 18, 1995, pp. 3087-3120.

Pindera, M.-J.; Aboudi, J.; and Arnold, S.M.: Limitations of the Uncoupled, RVE-Based Micromechanical Approach in the Analysis of Functionally Graded Composites. Mech. Mater., vol. 20, no. 1, 1995, pp. 77-94.

Portlock, L.E.; Schetky, L. McD; and Steinetz, B.M.: Shape Memory Alloy Adaptive Control of Gas Turbine Engine Blade Clearance. AIAA Paper 95-2762, 1995.

Powers, L.M., et al.: Lifetime Reliability Evaluation of Structural Ceramic Parts With the CARES/Life Computer Program. Collection of Technical Papers from the 34th Structures, Structural Dynamics and Materials Conference. AIAA, Washington, DC, part. 3, 1993, pp. 1634-1646.

Powers, L.M.; Jadaan, O.M.; and Gyekenyesi, J.P.: Creep Life of Ceramic Components Using a Finite Element Based Integrated Design Program (CARES/CREEP). ASME Paper 96-GT-369, 1996.

Rao, K.B.S.; Castelli, M.G.; and Ellis, J.R.: On the Low Cycle Fatigue Deformation of Haynes 188 Superalloy in the Dynamic Strain Aging Regime. Scrip. Metal. et Materialia, vol. 33, no. 6, 1995, pp. 1005-1012.

Rao, K.B.S., et al.: Temperature Dependent Cyclic Deformation Mechanisms in Haynes 188 Superalloy. NASA TM–107016, 1995.

Rao, K.B.S.; Lerch, B.A.; and Noebe, R.D.: Effect of Processing Route on Strain Controlled Low Cycle Fatigue Behavior of Polycrystalline NiAl. Proceedings of the Fatigue and Fracture of Ordered Intermetallic Materials II Symposium, W.O. Soboyejo, T.S. Srivatsan, and R.O. Ritchie, eds., TMS, Warrendale, PA, 1996, pp. 245–271.

Rao, K.B.S., et al.: Temperature and Strain-Rate Effects on Low-Cycle Fatigue Behavior of Alloy 800H. Metall T-A, vol. 27A, no. 2, 1995, pp. 255–267.

Reddy, T.S.R.: User's Guide for ECAP2D: An Euler Unsteady Aerodynamic and Aeroelastic Analysis Program for Two Dimensional Oscillating Cascades. NASA CR–189146, 1995.

Roberts, G.D, et al.: Adhesively Bonded Strain Gages for Extended Use on PMR–15 at 316 °C. HITEMP Review 1995, vol. I, NASA CP–10178, 1995.

Rokhlin, S.I.; Chu, Y.C.; and Baaklini, G.Y.: Assessment of Damage in Ceramics and Ceramic Matrix Composites Using Ultrasonic Techniques. J. Eng. Gas Turbines Power, vol. 117, no. 3, 1995, pp. 417–423.

Roth, D.J.; Bodis, J.R.; and Bishop, C.: Thermographic Imaging for High-Temperature Composite Materials: A Defect Detection Study. NASA TM–106950, 1995.

Roth, D.J., et al.: An NDE Approach for Characterizing Quality Problems in Polymer Matrix Composites. NASA TM–106807, 1995.

Salem, J.A., et al.: Reliability Analysis of Uniaxially Ground Brittle Materials. 95–GT–31, Proceedings of ASME International Congress, 1995.

Saravanos, D.A.; and Hopkins, D.A.: Local Stresses in Composite Plates with Piezoelectric Actuators and Sensors Using a Discrete-Layer Theory. Proceedings of ASME International Congress, 1995.

Shah, A.R.; and Chamis, C.C.: Cyclic Load Effects on Long Term Behavior of Polymer Matrix Composites. NASA TM–107007, 1995.

Shah, A.R.; Murthy, P.L.N.; and Chamis, C.C.: Effect of Cyclic Thermo-Mechanical Loads on Fatigue Reliability in Polymer Matrix Composites. NASA TM–107091, 1996.

Shapiro, W., et al.: Space Mechanisms Lessons Learned Study. Volume I: Summary. NASA TM–107046, 1995.

Shapiro, W., et al.: Space Mechanisms Lessons Learned Study. Volume II: Literature Review. NASA TM–107047, 1995.

Shiao, M.C.; Singhal, S.N.; and Chamis, C.C.: Network Based Parallelism of Probabilistic Composite Structural Analysis. AIAA Paper 95–1259–CP, 1995, pp. 889–899.

Shiao, M.C.; Singhal, S.N.; and Chamis, C.C.: Reliability, Risk and Cost Trade-Offs for Composite Designs. Proceedings of the 40th International SAMPE Symposium and Exhibition, 1995, pp. 881–891.

Srivastava, R.; and Reddy, T.S.R.: Aeroelastic Analysis of Ducted Rotors. ASME 1995 International Congress, 1995.

Steinetz, B. M.: Aerospace Seal Requirements. Proceedings of the Seals Code Development Workshop, 1995, pp. 41–53.

Steinetz, B.M. and Kren, L.A.: Resilient Braided Rope Seal. Lew 16, 231–1, Invention Disclosure, January 1995.

Sutjahjo, E.; and Chamis, C.C.: Multidisciplinary Finite Elements for Coupled Analysis of Fluid Mechanics, Heat Transfer, and Solid Mechanics. AIAA Paper 95–1309–CP, 1995, pp. 1318–1327.

Verrilli, M.J., et al.: Standardization Activities in TMF Test Methodologies. Presented at the Structures and Materials Panel, AGARD CP–569, 1996.

Weaver, R.L.: Diffuse Field Decay Rates For Material Characterization. Solid Mechanics Research for Quantitative Non-Destructive Evaluation, J.D. Achenbach and Y. Rajapaskie, eds., Martinus Nijhoff Publishers, Hingham, MA, 1987, pp. 425–434.

Zaretsky, E.V.; August, R.; and Coe, H.H.: Effect of Hoop Stress on Ball Bearing Life Prediction. NASA TM–106874, 1995.

Zaretsky, E.V.; Poplawski, J.V.; and Peters, S.M.: Comparison of Life Theories for Rolling-Element Bearings. NASA TM–106585, 1995.

Zaretsky, E.V.: STLE Life Factors for Rolling Bearings. STLE SP–34, 1992.

REPORT DOCUMENTATION PAGE

Form Approved
OMB No. 0704-0188

1. AGENCY USE ONLY (*Leave blank*)	2. REPORT DATE	3. REPORT TYPE AND DATES COVERED
	July 1997	Technical Memorandum

4. TITLE AND SUBTITLE

Structures Division 1995 Annual Report

5. FUNDING NUMBERS

WU-505-63-5B

6. AUTHOR(S)

7. PERFORMING ORGANIZATION NAME(S) AND ADDRESS(ES)

National Aeronautics and Space Administration
Lewis Research Center
Cleveland, Ohio 44135-3191

8. PERFORMING ORGANIZATION REPORT NUMBER

E-10385

9. SPONSORING/MONITORING AGENCY NAME(S) AND ADDRESS(ES)

National Aeronautics and Space Administration
Washington, D.C. 20546-0001

10. SPONSORING/MONITORING AGENCY REPORT NUMBER

NASA TM-107300

11. SUPPLEMENTARY NOTES

Responsible person, Cynthia Acquaviva, organization code 5900, (216) 433-3306.

12a. DISTRIBUTION/AVAILABILITY STATEMENT

Unclassified - Unlimited
Subject Categories 39 and 24

This publication is available from the NASA Center for AeroSpace Information, (301) 621-0390.

12b. DISTRIBUTION CODE

13. ABSTRACT ***(Maximum 200 words)***

The NASA Lewis Research Center Structures Division is an international leader and pioneer in developing new structural analysis, life prediction, and failure analysis related to rotating machinery and more specifically to hot section components in air-breathing aircraft engines and spacecraft propulsion systems. The research consists of both deterministic and probabilistic methodology. Studies include, but are not limited to, high-cycle and low-cycle fatigue as well as material creep. Studies of structural failure are at both the micro- and macrolevels. Nondestructive evaluation methods related to structural reliability are developed, applied, and evaluated. Materials from which structural components are made, studied, and tested are monolithics and metal-matrix, polymer-matrix, and ceramic-matrix composites. Aeroelastic models are developed and used to determine the cyclic loading and life of fan and turbine blades. Life models are developed and tested for bearings, seals, and other mechanical components, such as magnetic suspensions. Results of these studies are published in NASA technical papers and reference publication as well as in technical society journal articles. The results of the work of the Structures Division and the bibliography of its publications for calendar year 1995 are presented.

14. SUBJECT TERMS	15. NUMBER OF PAGES
Structural mechanics; Structural fatigue; Structural dynamics; Structural integrity	70
	16. PRICE CODE: A04

17. SECURITY CLASSIFICATION OF REPORT	18. SECURITY CLASSIFICATION OF THIS PAGE	19. SECURITY CLASSIFICATION OF ABSTRACT	20. LIMITATION OF ABSTRACT
Unclassified	Unclassified	Unclassified	